

## Article

# A Comparative Study of Load Frequency Regulation for Multi-Area Interconnected Grids Using Integral Controller

Awadh Ba Wazir <sup>1,2,\*</sup>, Ahmed Althobiti <sup>2,3</sup>, Abdullah A. Alhussainy <sup>1,2</sup>, Sultan Alghamdi <sup>1,2</sup>, Mahendiran Vellingiri <sup>1,2</sup>, Thangam Palaniswamy <sup>1,2</sup> and Muhyaddin Rawa <sup>1,2,\*</sup>

<sup>1</sup> Department of Electrical and Computer Engineering, Faculty of Engineering, King Abdulaziz University, Jeddah 21589, Saudi Arabia; aalhussainy0001@stu.kau.edu.sa (A.A.A.); smalgamdi1@kau.edu.sa (S.A.); mvellingiri@kau.edu.sa (M.V.); tswamy@kau.edu.sa (T.P.)

<sup>2</sup> Smart Grids Research Group, Center of Research Excellence in Renewable Energy and Power Systems, King Abdulaziz University, Jeddah 21589, Saudi Arabia; asleemalthobiti@stu.kau.edu.sa

<sup>3</sup> Department of Electrical and Computer Engineering, Faculty of Engineering, K. A. CARE Energy Research and Innovation Center, King Abdulaziz University, Jeddah 21589, Saudi Arabia

\* Correspondence: aawadhbaawazir@stu.kau.edu.sa (A.B.W.); mrawa@kau.edu.sa (M.R.)

**Abstract:** The present paper provides an optimal design for load frequency control (LFC) in the interconnected power system. To obtain an adequate LFC response alongside shortening implementation time and minimizing costs, an integral (I) controller is used. A deep analysis of the I controller-based LFC is presented. At first, a two-area interconnected power system is used, and to enhance the LFC response, the I controller and frequency bias parameters are optimized using three novel optimization algorithms, which are the incomprehensible but intelligible-in-time logic algorithm (ILA), the coati optimization algorithm (COA), and the brown-bear optimization algorithm (BOA). Also, five well-known techniques, namely, particle swarm optimization (PSO), genetic algorithm (GA), simulated annealing (SA), pattern search (PS), and nonlinear programming (NP), are used. A new objective function utilizing the integral of squared error (ISE), settling time, settling-max, and settling-min of the dynamic response is used to increase the efficacy of estimating the parameters. The presented results in this paper showed that the optimized I controller outperforms the classic I controller. After considering a load change in one area by 18.75%, the optimized I controller achieved the lowest ISE values. ISE values were: 0.00582, 0.00179, 0.00176, 0.00178, 0.00321, 0.00304, 0.00179, 0.00185, and 0.00181, for classic I, PSO-I, GA-I, SA-I, PS-I, NP-I, ILA-I, COA-I, and BOA-I. Then, the proposed method is applied to a nonlinear two-area system, demonstrating that the proposed strategies can deal with nonlinearity. As the purpose of the hybrid power system is to create a robust energy infrastructure that adheres to sustainability standards, the proposed algorithms are analyzed in a three-area multi-source power system comprising renewable energy sources (RESs) such as photovoltaic (PV) and wind turbine (WT), a battery energy storage system (BESS), and an electric vehicle (EV).



**Citation:** Ba Wazir, A.; Althobiti, A.; Alhussainy, A.A.; Alghamdi, S.; Vellingiri, M.; Palaniswamy, T.; Rawa, M. A Comparative Study of Load Frequency Regulation for Multi-Area Interconnected Grids Using Integral Controller. *Sustainability* **2024**, *16*, 3808. <https://doi.org/10.3390/su16093808>

Academic Editor: Bowen Zhou

Received: 30 January 2024

Revised: 19 April 2024

Accepted: 29 April 2024

Published: 1 May 2024

**Keywords:** load frequency control; integral controller; parameter estimation; optimization technique; renewable energy



**Copyright:** © 2024 by the authors. Licensee MDPI, Basel, Switzerland. This article is an open access article distributed under the terms and conditions of the Creative Commons Attribution (CC BY) license (<https://creativecommons.org/licenses/by/4.0/>).

## 1. Introduction

### 1.1. Background and Challenges

The control strategy aims to generate and distribute power in an interconnected system as efficiently and reliably as possible [1]. So, several aspects can be taken into account when examining the stability of the system. One of the most significant aspects of power system stability is frequency stability, which refers to the power system's capacity to maintain an acceptable frequency in the entire system during normal operating conditions and after being subjected to disturbances. Load disturbances cause frequency instability. Therefore, when the load is suddenly increased, the system frequency falls. As a consequence of

the frequency fall, power generation is reduced, so the generation does not meet the load demand. Also, in interconnected systems, frequency deviation affects the exchange of power between group members. Hence, frequency deviation as well as exchange power deviation must be zero for balancing the generated power and the demand at the load side and to maintain the stability of the system. Load frequency control (LFC) is the most common solution for frequency deviation. By modifying the generation system, LFC has shown to be very successful in controlling system frequency. LFC employs a control approach that can cope with the erratic changes in load demand and keep the frequency and exchange power in the desired values. LFC has two loops, designated as the primary and secondary loops. The core loop is responsive. Then, the secondary loop operates at a slower rate to eliminate the minor frequency variations. With the secondary loop, as the system load changes continuously, the generation is adjusted automatically to restore the frequency to the nominal value. Thus, the secondary loop must have a sufficient speed of response to adjust any changes in frequency and tie-line power. Because of its importance, the secondary loop is a fascinating subject for scholars. It has become more crucial as the scale of the systems and the extent to which they are interconnected have grown while taking into account the economic aspects and grid reliability. So, to face these challenges throughout the previous several decades and up to now, several works have developed a number of LFC problem-controlling solutions.

### 1.2. Literature Review

LFC was used in an electric power system as a part of the automatic generation control scheme (AGC). The flywheel governor was the initial method used by AGC to control the synchronous machine's frequency (primary control), but it was subsequently discovered that this method was inadequate and needed to be improved. The improvement was a secondary control supported by a signal that was directly proportional to the variation in frequency plus its integral (secondary control) [2]. The size of electrical networks has recently grown, and renewable resources and nonlinear components have been added, increasing the system's complexity and the requirement to keep the frequency at its nominal value.

The proper design of LFC relies on the exchange of information between different areas and the control center including the frequency deviation and tie-power. However, this communication technology can introduce vulnerabilities to the system known as communication delays. These delays can lead to inaccurate frequency detection and coordination problems among frequency regulating devices, resulting in significant system frequency oscillations, extending the settling time of the frequency response [3]. In extreme cases, it can even cause instability [4]. Therefore, this issue has been thoroughly studied in many works [4–6].

In order to obtain an optimal response from the LFC, various strategies and control techniques have been suggested for the LFC design. A critical literature review of LFCs in traditional and modern power system networks is accessible in [7,8], where different control strategies for the LFC problem were reviewed. Some of these strategies use optimization techniques to determine the parameters of the secondary loop controller such as particle swarm optimization (PSO), memetic algorithm (MA), simulated annealing (SA), genetic algorithm (GA), harmony search algorithm (HSA), sine-cosine algorithm (SCA), salp swarm algorithm (SSA), grasshopper optimization algorithm (GOA), gradient-based optimizer (GBO), wild horse optimizer (WHO), artificial ecosystem-based optimization (AEO), non-dominated sorting genetic algorithm-II (NSGA-II), bees Algorithm (BA), etc.

As mentioned, researchers frequently employ optimization strategies for efficient LFC by optimizing the controller. In this regard, Mansour et al. [9] used equilibrium optimization (EO) to initialize a fuzzy proportional–integral (FPI) controller to improve the AGC in a single-area system. Comparing the suggested controller against a classic, optimized PI controller demonstrated its superiority. The suggested fuzzy proportional–integral–derivative (FPID) controller optimized by EO also showed its superiority compared to an

optimal PIDA controller in the two-area system. Also, Chen et al. [10] proposed an FPID controller enhanced by the improved ant colony optimization (IACO) algorithm for LFC in a two-area thermal system. The optimization was expanded to incorporate a two-area, four-source hydro-thermal power system. The optimization was also extended to a two-area power system with nonlinearity in the governor's dead band (GDB), and the IACO-FPID handled nonlinearity effectively. On the other hand, Magzoub and Alquthami [11] used the SA approach to fine-tune another structure of the FPID controller, which is PID plus fuzzy controller AGC in a two-area thermal power system. The results of the simulation for the AGC based on SA using a hybrid PID-fuzzy controller demonstrated better performance than a conventional PID controller.

Optimization strategies were also used to optimize the classic PI and PID controllers for LFC. For instance, Rout et al. [12] used the differential evolution algorithm (DE) to modify the PI controller parameters for AGC of an interconnected two-area thermal power system. The superiority of DE optimization was proved by comparing the results to those of other previously published modern heuristic optimization techniques, such as the bacteria foraging optimization algorithm (BFOA). Moreover, Rathor et al. [13] utilized the artificial bee colony (ABC) algorithm to tune a modified PI controller LFC for a two-area thermal power system. Also, Ali and Abd-Elazim [14] used the BFOA to update the PI controller for the LFC in a two-area thermal power system. In addition, Padhan et al. [15] used the firefly algorithm (FA)-based PI and PID controllers for the LFC of a two-area thermal power system. The authors extended the optimization to three unequal-area power systems with generation rate constraint (GRC) and GDB nonlinearity to highlight the ability of the FA optimization to deal with the unequal-area power system. Nahas et al. [16] employed a nonlinear threshold-accepting algorithm (NLTA) to design a combination of LFC and automatic voltage regulation (AVR) for multi-area power systems using a PID controller. The results demonstrated the NLTA's powerful ability to adjust its performance under various operating scenarios. El-Sehiemy et al. [17] suggested a PID controller for LFC in multi-area power systems of two-area non-reheat thermal systems optimally designed using a novel artificial rabbits algorithm (ARA). The results obtained with the ARA-PID controller were compared to those obtained with other published techniques such as PSO, DE, JAYA optimizer, and self-adaptive multi-population elitist (SAMPE) JAYA. The comparisons revealed that the ARA-PID controller handles LFC issues effectively and successfully.

In recent years, hybrid algorithms have gained popularity and are used in many different fields, such as LFC issues. For instance, Sahu et al. [18] updated PI and PID with filtered derivative (PIDF) controllers based on a hybrid gravitational search algorithm and pattern search (hGSA-PS) technique for LFC in an integrated two-area thermal power system. The proposed technique was expanded to a two-area reheat thermal power system by accounting for physical constraints such as GRC, reheat turbine nonlinearity, and GDB nonlinearity. Extending the study to a nonlinear three unequal-area power system demonstrated the ability of the hGSA-PS technique to deal with nonlinear and unequal interconnected areas. Panwar et al. [19] proposed a hybrid optimization algorithm created by combining PSO-oriented BFOA (HBFO) in a novel way to fine-tune the PID controller for LFC in a hybrid power system with photovoltaic (PV) and thermal generators. The hybrid system was evaluated for step load change and the results were compared to different powerful optimization algorithms such as BFOA, PSO, and flower pollination algorithm (FPA)-based PID. The results demonstrated the superiority of HBFO-PID over PSO-PID, BFO-PID, and FPA-PID. Gupta et al. [20] designed a PI controller using a hybrid gravitational search with a firefly algorithm (hGFA) for LFC in two-area hydrothermal power systems. To determine the efficacy of the hGFA, its performance was compared to that of several well-known optimization techniques. The hGFA outperformed PSO, GA, GSA, and FA techniques.

Additionally, optimization strategies based on fractional order (FO) controllers attracted the interest of academics. As an example, Shouran and Anayi [21] proposed the teaching-learning-based optimization (TLBO) approach for modifying the parameters of

the new suggested I controller plus a fuzzy cascade fractional-order proportional–integral and fractional order proportional–derivative (I + F C FOPI-FOPD) controller. Also, Shouran and Alsseid [22] used the PSO approach to find the best values for the parameters of the proposed fuzzy cascade fractional-order proportional–integral and fractional order proportional–derivative (FC FOPI-FOPD) controller. Using a tilt-integral-derivative (TID) controller and Harris hawk optimization (HHO) technique, Bhuyan et al. [23] designed an LFC in a unique independent double area-interconnected hybrid microgrid system (IHM) that includes a novel, combined solar gas turbine (CSGT), biodiesel generator (BDG), wind turbine generator (WTG), energy storage units, and DC link (DCL). The dynamic performance of the TID, PID, and PI controllers was compared to the gains acquired by tuning with various techniques. The results demonstrated the superiority of the HHO-optimized TID controller. Alharbi et al. [24] used the dandelion optimizer (DO) algorithm to design fractional-order proportional–integral and proportional–integral–derivative plus double derivative (FOPI-PIDD<sup>2</sup>) controller for both LFC and AVR in a multi-area power system encompassing electric vehicles (EV) and renewable energy sources (RESs).

The optimal controller parameters have actually been found using a variety of optimization techniques to improve LFC performance. However, we have only touched on a few of them. Since the controller design needs to be robust enough to deal with disturbances and changes in the parameters of the power system, the adaptive methods for setting the gains of controllers are used by researchers to design robust LFC. Unlike conventional controllers with fixed parameter values, adaptive controllers alter their parameter values based on the system's current condition, which yields a better performance. For example, the conventional PI controller may fail to meet the required system requirements when the system's many characteristics change, particularly when the load changes [25]. The adaptive PI controller addresses the shortcomings of the conventional PI controller, which tunes continually in response to load fluctuations [25]. In addition, an adaptive fuzzy gain scheduling PID (FGPID) controller performed better than PID and FOPID controllers for the LFC of a three-area inter-connected modern power system [26]. Furthermore, an adaptive type 2 fuzzy PID (AT2PID) controller performed better than the type 1 fuzzy PID (T1PID) controller and the type 2 fuzzy PID (T2FPID) controller for the LFC of cutting-edge power systems [27].

On the other hand, in order to address LFC issues, the researchers also employed other control schemes. Gulzar et al. [28] proposed an advanced control method, namely an adaptive model predictive controller (AMPC), for the LFC of a series power system comprised of PV, wind, and thermal power. To demonstrate the effectiveness and competence of the proposed controller, AMPC was compared to other controllers such as GA-PI, FA-PI, and model predictive controller (MPC). Ali et al. [29] presented a recent multi-verse optimizer (MVO) metaheuristic optimization approach for designing LFC-based MPC embedded in a large multi-interconnected system. In the event of load disturbances, MVO is used to determine the optimal parameters of the MPC-LFC in order to achieve the desired output of the interconnected system. The proposed MPC optimized via MVO is compared to those designed via intelligent water drops (IWD) and GA. Ersdal et al. [30] presented MPC for LFC of an interconnected power system. Both descriptive examples and extensive simulation have demonstrated that applying MPC to LFC can result in improved control performance and a reduction in the use of reserves, reducing the costs associated with LFC. Oshnoei et al. [31] suggested a novel LFC model for an interconnected thermal two-area power system with wind turbine generation and a redox flow battery (RFB) using a two-degree of freedom (2DOF)-based controller called a 2DOF-hybrid controller. A FOPID controller and a TID controller are included in the hybrid controller. A modified sine-cosine algorithm (MSCA) is used to optimize the controller's parameters. The dynamic performance of the 2DOF-hybrid controller was compared to that of the integral-double-derivative (IDD), integral-tilt-derivative (I-TD), PID plus double-derivative (PID-DD), 2DOF-PID, 2DOF-TID, and 2DOF-FOPID controllers. Furthermore, RFB modeling based on the 2DOF-hybrid controller outperformed conventional RFB modeling in terms of reducing oscillation ampli-

tude. Zaid et al. [32] suggested a novel optimized intelligent fractional-order integral (iFOI) controller with the implementation of virtual inertia control (VIC) for the LFC of a two-area interconnected modern power system. The gray wolf optimization (GWO) algorithm was used to optimize the iFOI controller.

These studies which implemented the optimized controller using different optimization techniques for the LFC are summarized in Table 1.

**Table 1.** Summarized literature review.

Ref.	Case Study	Non-Linearities Considered	Control Scheme	Optimizer	Surpassed (Controller-Optimizer)
[9]	Single-area system	-	FPI	EO	PI-GA, PI-GSA, and PI-HSA
[16]	Single-area system	-	PID	NLTA	PID-BFOA
[9]	Two-area system	-	FPID	EO	PIDA-HSA, PIDA-SCA, and PIDA-TLBO
[10]	Two-area system	-	FPID	IACO	PI-BFOA, PI-DE, PI-(hBFOA-PSO), FPI-PSO, FPI-PS, FPI-(hPSO-PS), and FPID-ACO
[10]	Two-area system	GDB	FPID	IACO	PI-(hBFOA-PSO) and PI-CRAZYPSO
[11]	Two-area system	-	PID + Fuzzy	SA	PID-SA
[12]	Two-area system	-	PI	DE	PI-GA and PI-BFOA
[13]	Two-area system	-	PI	ABC	-
[14]	Two-area system	-	PI	BFOA	PI-GA
[15]	Two-area system	-	PID	FA	PI-GA, PI-BFOA, PI-DE, PI-PS, PI-(hBFOA-PSO), and PI-FA
[16]	Two-area system with AVR	-	PID	NLTA	-
[17]	Two-area system	-	PIDF	ARA	PID-FA, PIDF-(SAMPE-JAYA), PIDF-JAYA, PIDF-DE and PIDF-PSO
[18]	Two-area system	-	PIDF	hGSA-PS	PI-GA, PI-BFOA, PI-DE, PI-FA, PI-PSO, PI-(hBFOA-PSO), PI-NSGA-II, and PI-(hGSA-PS)
[18]	Two-area system	GDB and GRC	PIDF	hGSA-PS	PI-GSA and PI-(hGSA-PS)
[19]	Two-area system	GDB and GRC	PID	HBFO	PID-BFO, PID-PSO and PID-FPA
[20]	Two-area system	-	PI	hGFA	PI-PSO, PI-GA, PI-GSA and PI-FA
[21]	Two-area system	-	I + F C FOPI-FOPD	TLBO	PI-FA
[22]	Two-area system	-	FC FOPI-FOPD	PSO	PID-LCOA, FPID-TLBO, and FPIDF-PSO
[10]	Two-area Multi sources system	-	FPID	IACO	PI-GA, FPI-PSO, FPI-(hPSO-PS), and PID-ACO
[23]	Two-area Multi sources system	-	TID	HHO	HHO-PI, HHO-PID, TID-GA, TID-PSO, TID-SSA, TID-SCA and TID-GOA
[24]	Two-area Multi sources system with AVR	-	FOPI-PIDD2	DO	(FOPI-PIDD2)-WHO, (FOPI-PIDD2)-GBO, (FOPI-PIDD2)-AEO, (PD-PIDD2)-DO, and (TD-TI)-DO
[24]	Two-area Multi sources system with AVR	Communication Time Delay (CTD)	FOPI-PIDD2	DO	(PD-PIDD2)-DO and (TD-TI)-DO
[31]	Two-area Multi sources system with AVR	GDB and GRC	2DOF-hybrid (Hybrid FOPID and TID based on 2DOF)	MSCA	(2DOF-PID)-MSCA, (2DOF-TID)-MSCA, (2DOF-FOPID)-MSCA, (2DOF-hybrid)-SCA, (2DOF-hybrid)-GA, (2DOF-hybrid)-DE and (2DOF-hybrid)-PSO.
[32]	Two-area Multi sources system	Rate Limiter and GRC	iFOI	GWO	FOI-GWO
[15]	Three-area system	GDB and GRC	PID	FA	I-GA, I-FA, and PI-FA
[18]	Three-area system	GDB and GRC	PIDF	hGSA-PS	PI-(hGSA-PS)
[31]	Three-area system	GDB and GRC	2DOF-hybrid (Hybrid FOPID and TID based on 2DOF)	MSCA	(2DOF-FOPID)-MSCA, (2DOF-hybrid)-SCA, (2DOF-hybrid)-GA, (2DOF-hybrid)-DE and (2DOF-hybrid)-PSO.
[29]	Six-area Multi sources system	GDB and GRC	MPC	MVO	MPC-GA and MPC-IWD

As a summary of the results of the literature review, we observed that enhancing the controller results in significant performance improvements. The more powerful the controller, the greater the performance and stability. Optimization approaches are also critical, although not in the same manner that the sort of controller is. For instance, the

performance between FPID-ACO and FPID-IACO was somewhat close, but the performance between PID-ACO and FPID-IACO was vastly different, where FPID demonstrated its superiority. Moreover, the objective function plays an essential role in the parameter estimation process. Most authors have used integral time absolute error (ITAE) as an objective function, and some have proposed new objective functions that contain ITAE and the characteristics of the dynamic response, such as the settling time. So, choosing a robust controller, powerful optimization software, and suitable objective function is critical to attaining optimal performance.

### 1.3. Motivation and Scopes

Based on the survey of the above-mentioned literature, it is observed that, most authors used a PID controller to solve LFC problems, comprising of controllers such as fuzzy plus PID controller which contain many parameters, complex controllers such as fractional-order PID controller, etc. So, when the system has many interconnected areas, these controllers may make the system complex, increasing the controllers' parameters and thus requiring more time to find their best values. Since the controller performance depends on its parameters, a huge number of parameters need powerful optimizer algorithms and super-computing. Furthermore, it is observed that the majority of researchers merely tune the controller parameters to their optimum values. However, it is also important to tune the optimal values of the frequency bias parameters since they have an impact on the LFC's response. In recent years, the size of power grids has increased, and renewable resources and nonlinear components have been included, raising system complexity and the necessity for maintaining frequency at its nominal value. The challenge is to find a controller that improves LFC's response while reducing implementation time and costs. Although various controllers have been tested extensively, it is observed that the integral controller has not been deeply tested. This motivated the authors to use this control structure with optimal tuning for frequency bias parameters. This paper examines the design and analysis of a two-area non-reheat thermal system with integral controllers. The two-area thermal system parameters are shown in Appendix A. In order to achieve the optimal response, PS, nonlinear programming (NP), incomprehensible but intelligible-in-time logics algorithm (ILA), coati optimization algorithm (COA), brown-bear optimization algorithm (BOA), SA, GA, and PSO are the eight optimization techniques utilized to improve the settings of the integral controller and frequency bias for the secondary loop of the LFC. LFC action is provided through different techniques, and a comparison between the proposed controller and the base system controller is described below. The settling time and the peak amplitude of frequency deviations are taken as performance indices (transient analysis). The work is also extended to a two-area power system with a GRC and a GDB nonlinearity to assess the suggested approach's capability to deal with nonlinearity. Moreover, the work is extended to a three-area power system to test the proposed approach's ability to deal with multi-areas interconnected power systems. Finally, to test the suitability of the suggested approach for contemporary power systems, the work is extended to a three-area multi-source power system that includes RESs like PV and wind turbine (WT), battery energy storage system (BESS), and EV.

### 1.4. Contribution and Paper Organization

This paper's contribution is succinctly described as follows:

1. Designing an optimal LFC for a two-area, non-reheat thermal power system using an integral controller. The present work proposes an objective function and eight optimization techniques, including PSO, GA, SA, PS, NP, ILA, COA, and BOA, to optimize the parameters of the integral controller and frequency bias of the secondary loop in LFC.
2. Providing deep analysis for LFC based on the integral controller. Different cases are used to describe the behavior of frequency and tie-line power flow deviations in the presence of load perturbation. Also, the system's robustness to changes in the loading

conditions and system parameters is analyzed. Furthermore, real-time simulation for the frequency and power deviations is provided.

3. Assessing the effectiveness of the proposed approach in a two-area power system with GRC and GDB nonlinearity and a three-area power system.
4. Evaluating the proposed approach in a three-area hybrid power system involving PV, WT, BESS, and EV.

The rest of this paper is structured as follows. The LFC power system model for two areas is described in Section 2. Section 3 explains the control strategy. This work's methodology is explained in Section 4. Section 5 describes the suggested objective function. The eight optimization strategies are listed in Section 6. The results and discussion are shown in Section 7 and the work's conclusion is presented in Section 8.

## 2. Load Frequency Control (LFC) Mathematical Model

LFC is the common name for active power control and frequency control. The primary roles of LFC are to keep the desired output power of a generator in sync with the changing load, to support managing the frequency of larger interconnection, and to keep the net exchange power between group members at the set values. This is accomplished by the use of two loops, primary and secondary. The primary loop responds fairly quickly. Afterward, the secondary loop runs slowly in order to eliminate the minor frequency variations. While the turbine's response time tightens the primary loop's time response, the secondary loop's time response can be modified by properly tuning its controller. With the secondary loop, as the system load changes continuously, the generation is adjusted automatically to restore the frequency to the nominal value. Figure 1 below depicts the conventional model for the LFC of the two-area interconnected power system. The components of each area are the controller, speed governing system, turbine, generator, and load. Transfer functions are employed to model each component of the areas, which simplifies the frequency domain analyses.

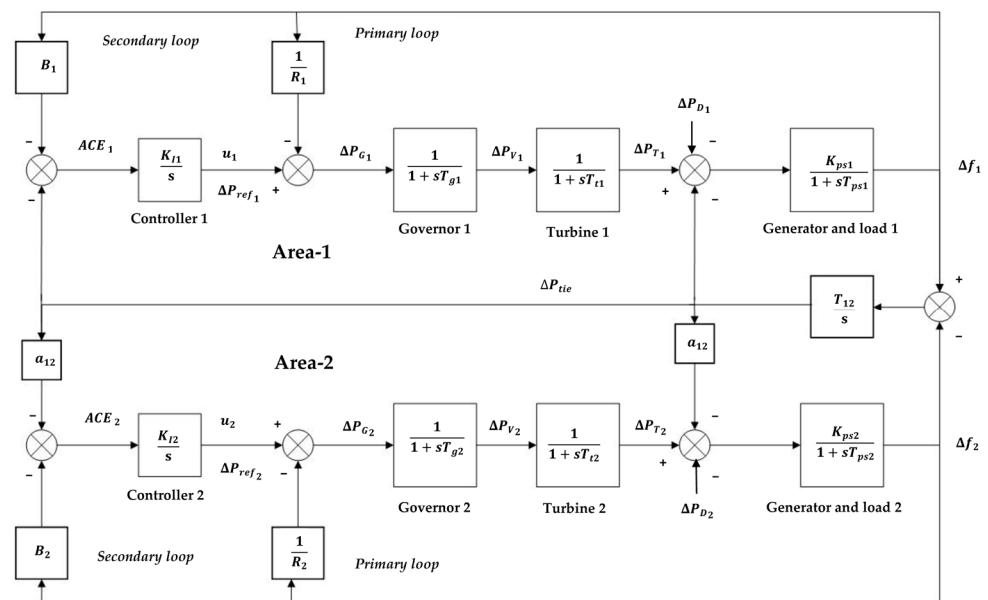


**Figure 1.** Block diagram of linear LFC model for two-area power system.

In Figure 1,  $ACE_1$  and  $ACE_2$  are area control errors.  $B_1$  and  $B_2$  are the frequency bias parameters. The governor speed regulation settings (Hz/p.u.) are  $R_1$  and  $R_2$ .  $u_1$  and  $u_2$  or  $\Delta P_{ref1}$  and  $\Delta P_{ref2}$  are the outputs from the integral controller (the reference power setting). The speed governor time constants in seconds are denoted by  $T_{g1}$  and  $T_{g2}$ .  $T_{t1}$  and  $T_{t2}$  are the turbine time constants in seconds.  $K_{ps1}$  and  $K_{ps2}$  denote the generator and load gains.  $T_{ps1}$  and  $T_{ps2}$  denote the generator and load time constants in seconds.

The governor output command (p.u.) is represented by  $\Delta P_{G1}$  and  $\Delta P_{G2}$ . The steam valve position command (p.u.) is represented by  $\Delta P_{V1}$  and  $\Delta P_{V2}$ . The change in turbine output powers is represented by  $\Delta P_{T1}$  and  $\Delta P_{T2}$ . Changes in load demand are represented by  $\Delta P_{D1}$  and  $\Delta P_{D2}$ . The synchronizing coefficient is denoted by  $T_{12}$ . The incremental change in tie-line power (p.u.) is denoted by  $\Delta P_{tie}$ .  $\Delta f_1$  and  $\Delta f_2$  denotes the frequency variations in the system in hertz [1].

The speed governor mechanism acts as a comparator whose  $\Delta P_G$  is the difference between  $\Delta P_{ref}$  and the power  $\frac{1}{R}\Delta f$ . The hydraulic amplifier of the speed governor converts the command  $\Delta P_G$  (the error to be corrected) into the steam valve position command  $\Delta P_V$ . The governor's transfer function is shown in Equation (1) [1].

$$G_G(s) = \frac{\Delta P_V(s)}{\Delta P_G(s)} = \frac{1}{1 + sT_g} \quad (1)$$

The turbine or the prime mover is the source of mechanical power. The turbine model relates changes in mechanical power output  $\Delta P_T$  to changes in steam valve position  $\Delta P_V$ . The transfer function of the turbine is shown in Equation (2) [1].

$$G_T(s) = \frac{\Delta P_T(s)}{\Delta P_V(s)} = \frac{1}{1 + sT_t} \quad (2)$$

The swing equation has been used to obtain the generator equation, as indicated in (3) [1]. The power system's load is made up of several electrical devices, so the speed load characteristic of this composite load is given by (4) [1].

$$\Delta f(s) = \frac{1}{2Hs} (\Delta P_T(s) - \Delta P_e(s)) \quad (3)$$

$$\Delta P_e = \Delta P_D + D\Delta f \quad (4)$$

where  $H$  is the constant of inertia;  $\Delta P_D$  is the non-frequency-sensitive load change; and  $D\Delta f$  is the frequency-sensitive load change.  $D$  is expressed as percent change in load divided by percent change in frequency. Thus, the generator and load transfer function will be as shown in Equation (5) [1]:

$$G_{GL}(s) = \frac{1}{D + s2H} \text{ or } G_{GL}(s) = \frac{K_{ps}}{1 + sT_{ps}} \quad (5)$$

$K_{ps} = \frac{1}{D}$  and  $T_{ps} = \frac{2H}{f^\circ D}$ .  $D = \frac{\Delta P_D}{\Delta f^\circ}$ .  $P_D$  is the normal load and  $f^\circ$  is the steady state frequency [10].

### 3. Control Strategy

When the load is suddenly increased, the system frequency falls. As a consequence of the frequency falling, power generation is reduced, so the generation does not meet the load demand. LFC must have a fast enough response time to adjust any changes in frequency and tie-line power; thus, the integral controllers are introduced in both areas to eliminate the deviations in frequency and tie lines. The respective ACEs are the error inputs to the controllers, denoted by Equations (6) and (7) [1]:

$$e_1(t) = ACE_1 = \Delta P_{tie,12} + B_1\Delta f_1 \quad (6)$$

$$e_2(t) = ACE_2 = \Delta P_{tie,21} + B_2\Delta f_2 \quad (7)$$

ACE monitors the area load variation and provides effective control. When ACE is less than zero, the generation must be increased, when ACE is greater than zero, the generation must be decreased, and when ACE is equal to zero, the system is in the steady stable

state [33].  $u_1$  ( $\Delta P_{ref1}$ ) and  $u_2$  ( $\Delta P_{ref2}$ ) are the control inputs of the power system being the outputs of the controllers, as shown in Equations (8) and (9) [12]:

$$\Delta P_{ref1} = K_{I1} \int ACE_1 dt \quad (8)$$

$$\Delta P_{ref2} = K_{I2} \int ACE_2 dt \quad (9)$$

$K_{I1}$ ,  $K_{I2}$  are the integral controller parameters;  $B_1$ ,  $B_2$  are the frequency bias parameters. These parameters must be chosen carefully for a satisfactory response.

#### 4. Methodology

As stated in the preceding section, the integral controller is introduced to act on the load reference setting to eliminate the error between the new load demand and generation. Since the controller performance depends on its parameters, thus the parameters  $K_{I1}$ ,  $K_{I2}$ ,  $B_1$ , and  $B_2$  in Equations (6)–(9) should be chosen so that their values provide a stable system and should be adjusted to acquire the best response. In this study, eight optimization approaches, PSO, GA, SA, PS, NP, ILA, COA, and BOA, are utilized to obtain the optimal values of  $K_{I1}$ ,  $K_{I2}$ ,  $B_1$ , and  $B_2$  that improve the LFC response, with the help of a proposed objective function. The objective function is chosen to assess the dynamic responsiveness of the LFC, on which optimization techniques rely when determining appropriate parameters.

#### 5. Objective Function

Optimization techniques rely on minimizing the objective function in each iteration until it reaches its minimum value where the desired requirements have been met. So, based on the intended requirements and limitations, the objective function is established [10]. The system is considered to have an optimum control strategy if the controller settings are changed so that the goal function approaches a minimum value. So, the minimum value of objective function gives the best values of controller's gains if the objective function carefully established. The performance of LFC is evaluated based on the performance criteria in the time domain such as the settling time, overshoot, undershoot, and steady-state error. Minimizing these criteria ensure that the frequency of the system and tie-line exchange power return to its nominal value quickly under a step load change. Preferably, these criteria are included in the selected objective function. Based on what has already been stated, the proposed objective function of this work is shown in Equation (10):

$$J = ISE + (SS_{max} + |SS_{min}|) + ST_s \quad (10)$$

$ISE$  is given by Equation (11) [10].

$$ISE = \int_0^t (|\Delta f_1|^2 + |\Delta f_2|^2 + |\Delta P_{tie}|^2) dt \quad (11)$$

Integral of squared error ( $ISE$ ) reduced the overshoot since it penalizes the larger error quickly [34].  $SS_{max}$  is the sum of the settling-max of  $\Delta f_1$ ,  $\Delta f_2$ , and  $\Delta P_{tie}$ . Settling-max ( $S_{max}$ ) is the maximum value of  $\Delta f_1$ ,  $\Delta f_2$ , and  $\Delta P_{tie}$  once the response has risen.  $SS_{min}$  is the sum of the settling-min of  $\Delta f_1$ ,  $\Delta f_2$ , and  $\Delta P_{tie}$ . Settling-min ( $S_{min}$ ) is the minimum value of  $\Delta f_1$ ,  $\Delta f_2$ , and  $\Delta P_{tie}$  once the response has risen.  $ST_s$  is the sum of settling times of  $\Delta f_1$ ,  $\Delta f_2$ , and  $\Delta P_{tie}$ . Settling time ( $T_s$ ) is defined as the first time for transients to decay within a specified small percentage of final steady-state and stay in that range. Minimizing  $ISE$ ,  $S_{min}$ ,  $S_{max}$ , and  $T_s$  ensure that the frequency of the system and tie-line exchange power return to its nominal. Figure 2 illustrates the  $S_{min}$ ,  $S_{max}$ , and  $T_s$ .

The researchers have chosen different objective functions for LFC and ITAE error criteria are the basis of the objective function for most of them because ITAE is utilized to reduce peak overshoot and the length of settling time [34]. In order to show the effectiveness

of the proposed objective function, the optimization will be repeated based on ITAE, and the comparison between proposed objective function and ITAE will be performed. ITAE is given by Equation (12) [10].

$$ITAE = \int_0^t (|\Delta f_1| + |\Delta f_2| + |\Delta P_{tie}|) \cdot t \cdot dt \quad (12)$$

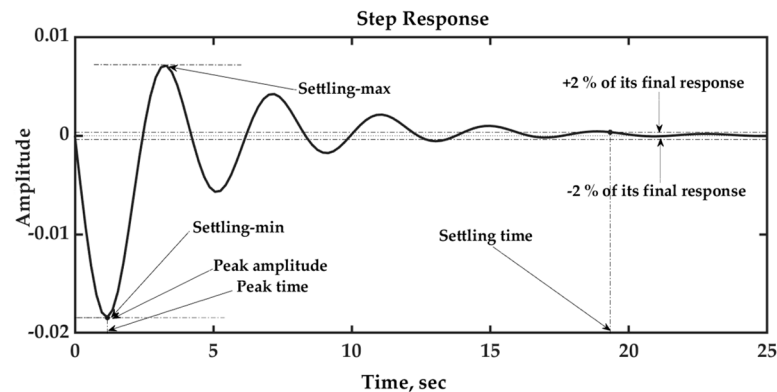


Figure 2. Specifications of transient response.

## 6. Optimization Techniques

For the optimal LFC, researchers frequently employ optimization techniques. These methods are designed for optimization, and the system's performance is enhanced by the adoption of these algorithms [34]. As mentioned earlier, eight optimization techniques, which are PSO, GA, SA, PS, NP, ILA, COA, and BOA, are utilized to obtain the optimal values of  $K_{I1}$ ,  $K_{I2}$ ,  $B_1$ , and  $B_2$  in order to improve the LFC response by minimizing the objective function.

### 6.1. Nonlinear Programming

This paper employs the MATLAB optimization toolbox's `fmincon` function as a nonlinear programming solver. The goal of the `fmincon` algorithm is to determine the minimum of a restricted nonlinear multivariable function [35]. The `fmincon` function offers several optimization algorithms such as interior point (IP), trust region reflective (TRR), and successive quadratic programming (SQP). In this paper, IP is used which is used to find the best solution to a mathematical optimization problem by moving from one point on the objective function to another within the feasible region. More specifically, this method typically follows a two-phase approach, with the first phase identifying a feasible solution and the second phase refining the solution to optimality. The reasons behind the selection of this algorithm are IP methods are commonly used to solve linear programming problems but can also be applied to nonlinear programming problems and the algorithm is typically more powerful and efficient than traditional methods like the simplex algorithm [36]. More information is provided in [35] on the `fmincon` function. The flow chart in Figure 3 represents the main steps of the NP algorithm, where  $x$  is a vector of the variables that need to be estimated, and  $J$  is the objective function. Here,  $x = [K_{I1}, K_{I2}, B_1, \text{ and } B_2]$ .

### 6.2. Genetic Algorithms

The notion of evolutionary biology observation and genetics of natural selection is the basis for the strong tools known as genetic algorithms (GAs) which can handle a variety of optimization problems in a variety of sectors [38]. This method generates subsequent points from the first generation by selection crossover and mutation. It begins with an initial generation of potential solutions that were examined against an objective function [39]. The stages involved in implementing and developing a genetic algorithm are as follows:

- Create a random population.
- Evaluate population fitness.
- Choose the population's fittest members.
- Implement crossover operations.
- Put low-probability mutation operations into action.
- Continue performing the fitness analysis until the convergence condition is satisfied.

The flow chart in Figure 4 represents the main steps of the GA.

### 6.3. Particle Swarm Optimization

Kennedy and Eberhart created the PSO algorithm in 1995. In their approach, they applied optimization methods that were inspired by nature. In this algorithm, particles are flown through the search space and adjust their position and speed at each time step [40,41]. Each particle searches for the ideal solution in the search space, which is indicated as the particle's optimal value. The individual optimal values of each particle in the particle swarm are shared, and the optimal individual optimal value obtained is designated as the global optimal value. PSO is a common swarm intelligence optimization technique that is extensively utilized in various fields because of its easy programming, limited number of parameters, and minimal computational complexity [42]. The flow chart in Figure 5 represents the main steps of the PSO algorithm, where  $pbest$  denotes the best position (best value of  $x$ ) of each particle until the current iteration, and  $gbest$  denotes the best position of the group until the current iteration.

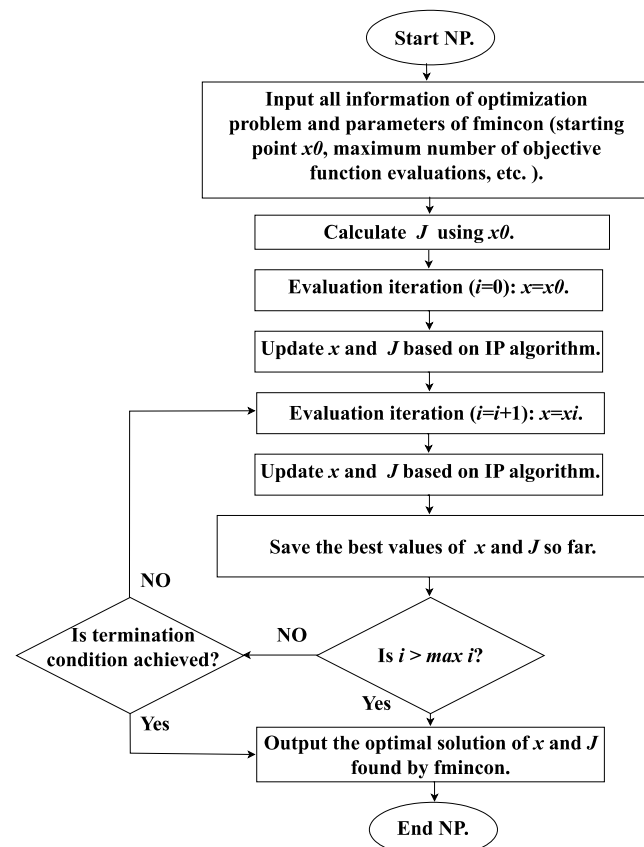


Figure 3. Flow chart of NP optimization [37].

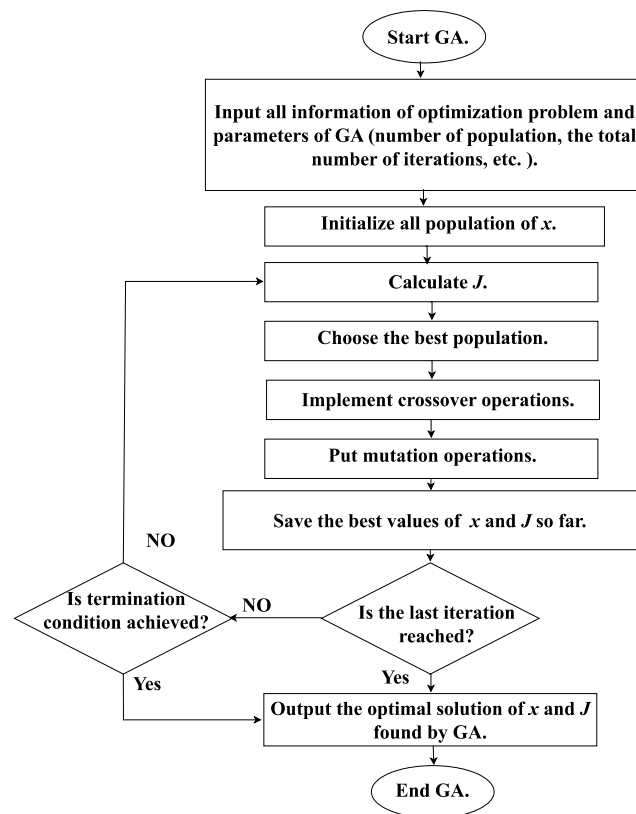


Figure 4. Flow chart of GA optimization [2].

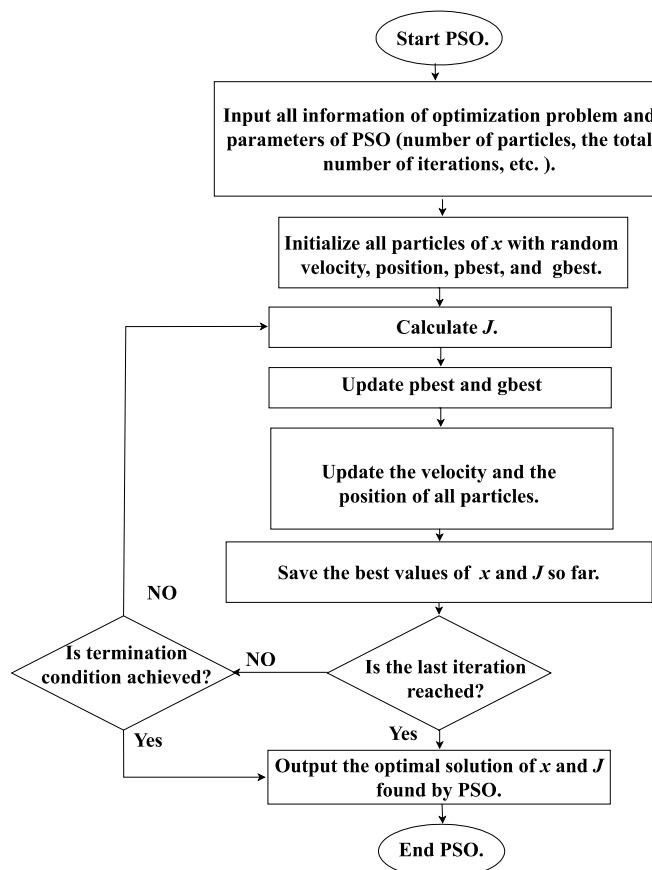


Figure 5. Flow chart of PSO optimization [41].

#### 6.4. Simulated Annealing

SA is a powerful, practical approach for resolving optimization issues. Simulated annealing is a probabilistic method for resolving combinatorial problems that was first introduced in 1983 by “S. Kirkpatrick”, “C. D. Gelatt”, “Jr.”, and “M. P. Vecchi”, and independently developed by “Cerny” in 1985. Its goal was to find the global minimum for a cost function that had numerous local minima. SA resolves this problem simulating the physical process in which a solid is gradually cooled until its structure is eventually frozen, and that takes place when the least amount of energy is created [43]. The flow chart in Figure 6 represents the main steps of the SA algorithm.

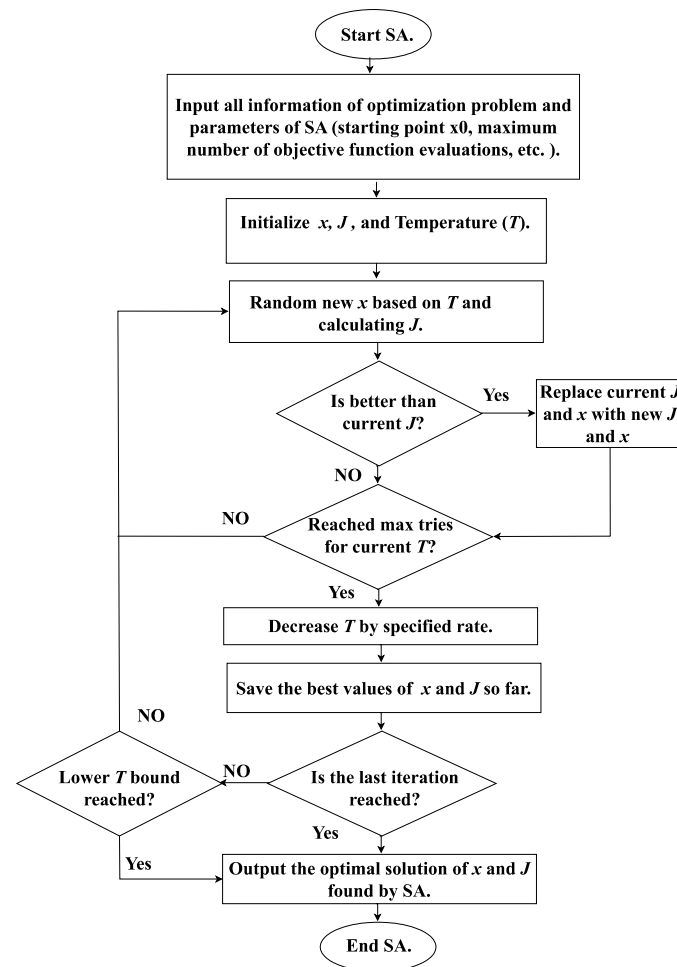


Figure 6. Flow chart of SA optimization [11].

#### 6.5. Pattern Search

PS techniques are a type of direct search method for tackling nonlinear optimization problems [44]. The direct search algorithms described by Hooke and Jeeves include pattern direct search techniques as a subset. The algorithms were employed in their work to handle curve fitting difficulties and they were promising since they either offered answers to some issues that had not been addressed by conventional approaches or expedited the resolution of issues that could be resolved by conventional methods [45]. PS generates a sequence of points that may or may not be close to the optimal point. PS begins with a set of points called mesh that surrounds the initial points. The current point is added to a scalar multiple of a set of vectors known as a pattern to create the mesh. If a point in the mesh has a better objective function value, it becomes the current point during the next iteration. PS consists of a sequence of polls [18]. The flow chart in Figure 7 represents the main steps of PS algorithm.

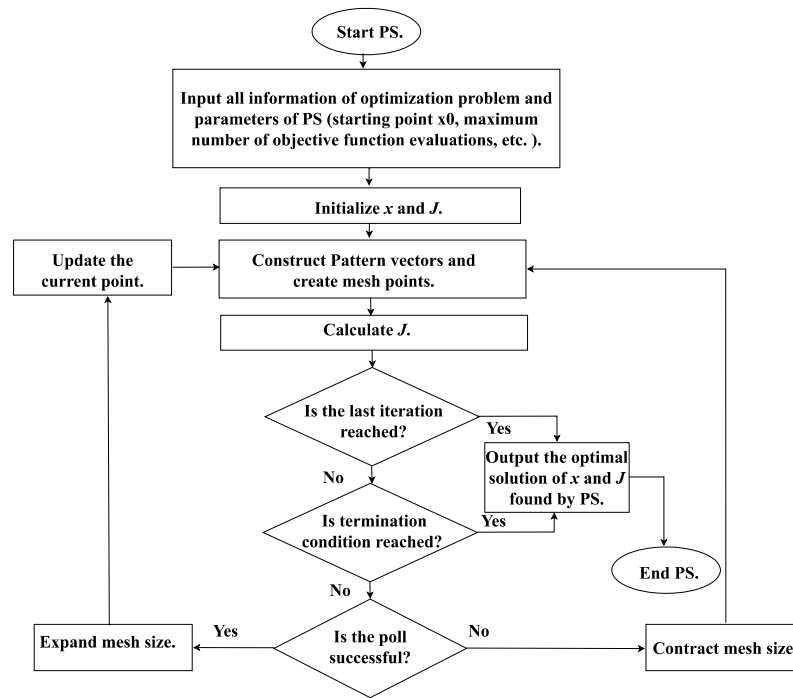


Figure 7. Flow chart of PS optimization [18].

6.6. Incomprehensible but Intelligible-in-Time Logics Algorithm

The ILA is a novel optimization technique based on the concept of incomprehensible but intelligible-in-time (IbI) logic introduced by Mirrashid and Naderpour [46]. The ILA is divided into three stages: exploration, integration, and exploitation. Each of the three ILA stages has a distinct function. The exploration phase is in charge of discovering new solutions in the search space. The integration phase is in charge of integrating the new and old solutions. The exploitation phase is in charge of discovering the optimal solution in the search space. The flow chart in Figure 8 represents the main steps of the ILA.

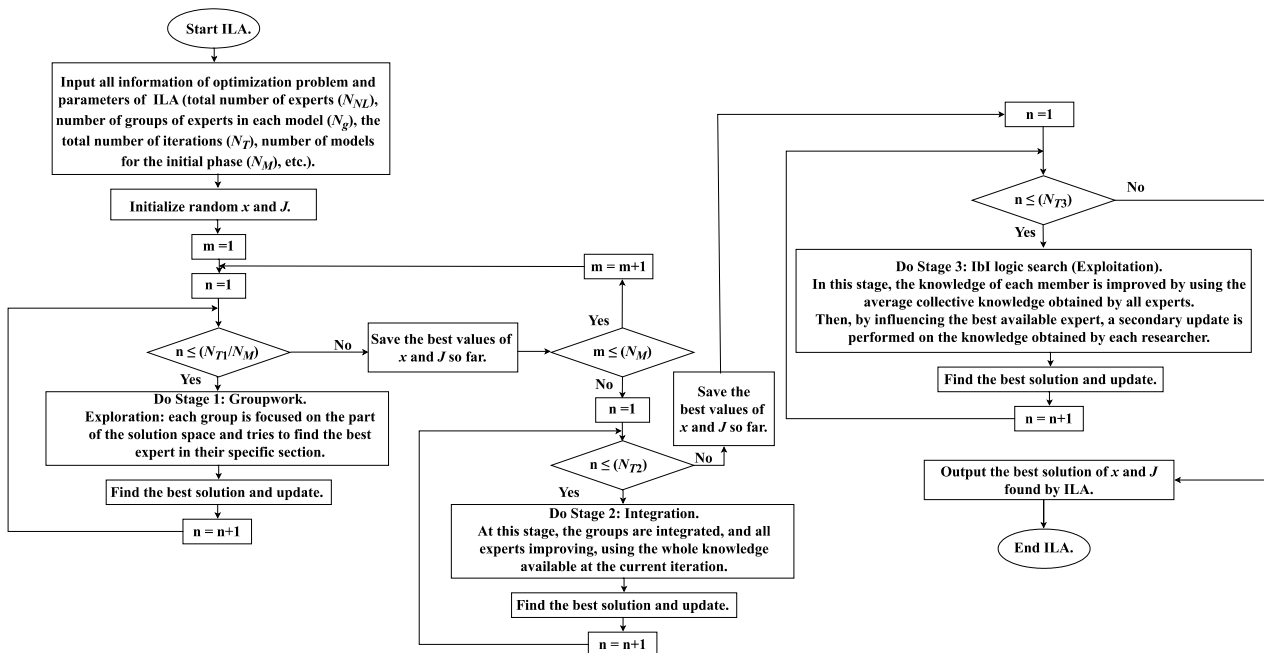


Figure 8. Flow chart of ILA optimization [46].

### 6.7. Coati Optimization Algorithm

The COA is a novel metaheuristic algorithm that was published by Dehghani et al. [47] and it is designed to replicate coati behavior in the wild. The basic idea of COA is to simulate two natural coati behaviors: (i) attacking and hunting iguanas and (ii) escaping from predators. These behaviors are mathematically represented in two phases: exploration and exploitation. The flow chart in Figure 9 represents the main steps of the COA.

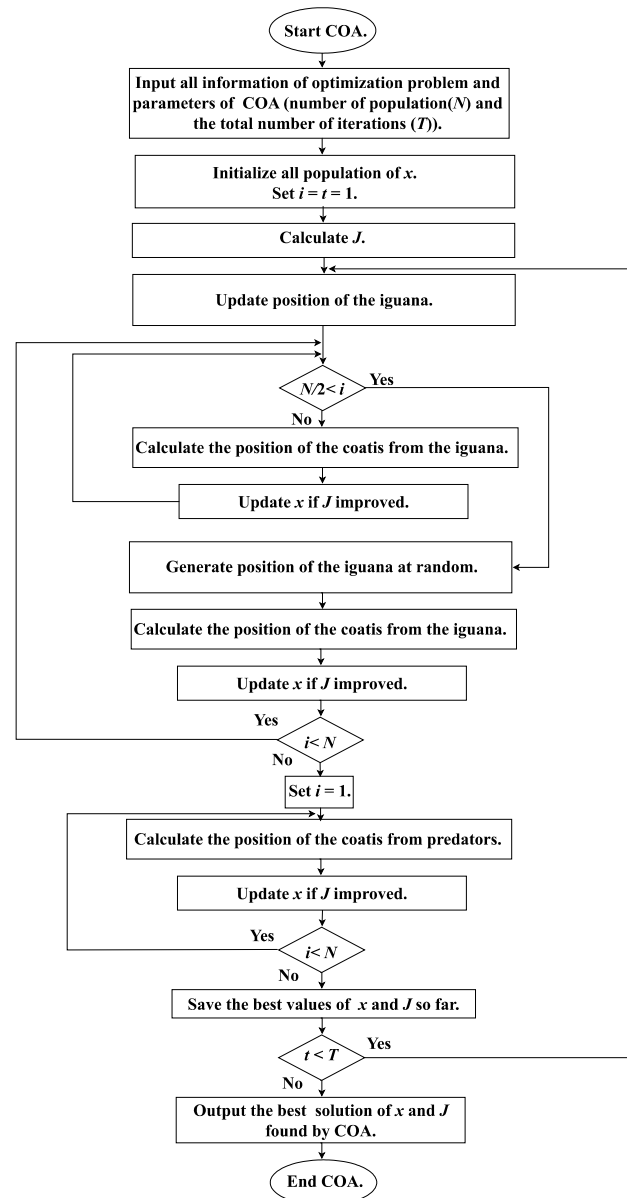


Figure 9. Flow chart of COA optimization [47].

### 6.8. Brown-Bear Optimization Algorithm

BOA is a new optimizer proposed by Prakash et al. [48] to tackle the economic dispatch problem (EDP), which is a major problem of optimum power-system management. It is based on the means of communication between brown bears and features pedal scent marking and sniffing activities. Bears' pedal scent marking activity, which is a basic way of communication between them, is distinguished by several characteristics such as walking with a distinctive stride, cautious stepping on pedal markings, and twisting of feet on depressions produced on the ground. Their sniffing action boosts their communication even further. BOA is formed by developing a mathematical model that includes the

mentioned bear behaviors. The algorithm strikes a balance between exploration and exploitation and is devoid of algorithm-specific parameters. The flow chart in Figure 10 represents the main steps of the BOA.

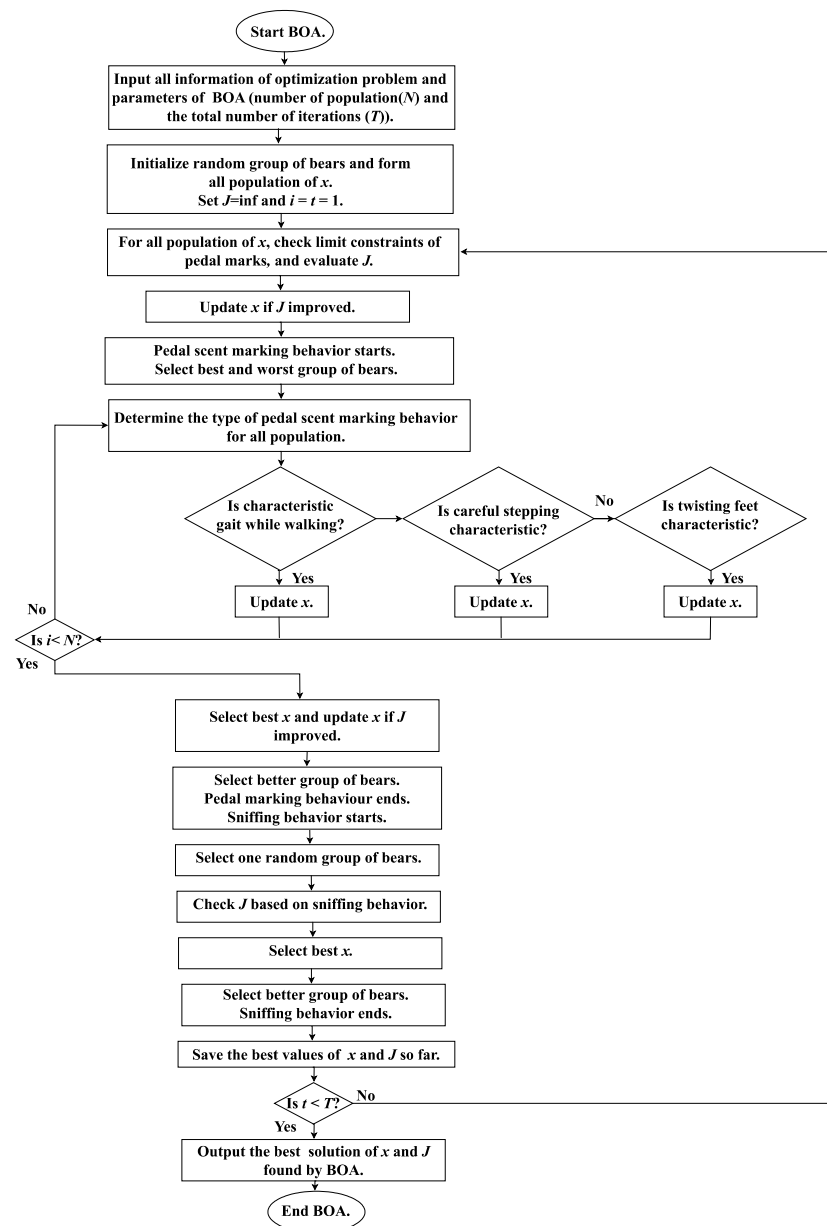


Figure 10. Flow chart of BOA optimization [48].

### 6.9. Work Procedures Using the Selected Techniques

It is worth mentioning that the optimization algorithm is just a tool to solve the problem; therefore, we will not go into detail about each technique's procedure. The references which were previously mentioned in the text include a detailed explanation of how each technique works. As previously stated, the eight optimization techniques are applied in this work to find best value of  $K_{I1}$ ,  $K_{I2}$ ,  $B_1$ , and  $B_2$ , as shown in Figure 11. First, the tested system's model, which is depicted in Figure 1, was created in the MATLAB/Simulink environment and the programs of the eight optimization techniques were written in script file format. The developed model was simulated in a separate program considering a 0.1875 (p.u) (18.75%) step load change in area 1 at  $t = 0$  s. Then, the objective function was calculated in script file format based on the simulation model output. The parameters  $K_{I1}$ ,  $K_{I2}$ ,  $B_1$ , and  $B_2$  were used throughout the optimisation process and updated with the

optimization techniques based on the value of the objective function in each iteration until the end of the iterations; the optimization processing was then stopped and the parameters that achieved the lowest value of the objective function were selected as the best parameters. Constraints on the decision variable's range were applied to the optimization in the manner described in Equations (13) and (14).

$$0 \leq K_{I1} \leq K_{I1max}, 0 \leq K_{I2} \leq K_{I2max} \quad (13)$$

$$0 \leq B_1 \leq B_{1max}, 0 \leq B_2 \leq B_{2max} \quad (14)$$

where  $K_{I1max}$ ,  $K_{I2max}$  are maximum integral gain values for areas 1 and 2;  $B_{1max}$ ,  $B_{2max}$  are the maximum values of the frequency bias for areas 1 and 2. For specifying the range of the optimization variables, the maximum values of the integral gain  $K_{I1max}$ ,  $K_{I2max}$  were chosen to be 2, and the maximum values of the frequency bias  $B_{1max}$ ,  $B_{2max}$  were chosen to be  $2\beta_1$  and  $2\beta_2$ , where  $\beta$  was the area frequency response characteristic (AFRC) and is given by Equation (15) [1]:

$$\beta_i = \frac{1}{R_i} + D_i \quad (15)$$

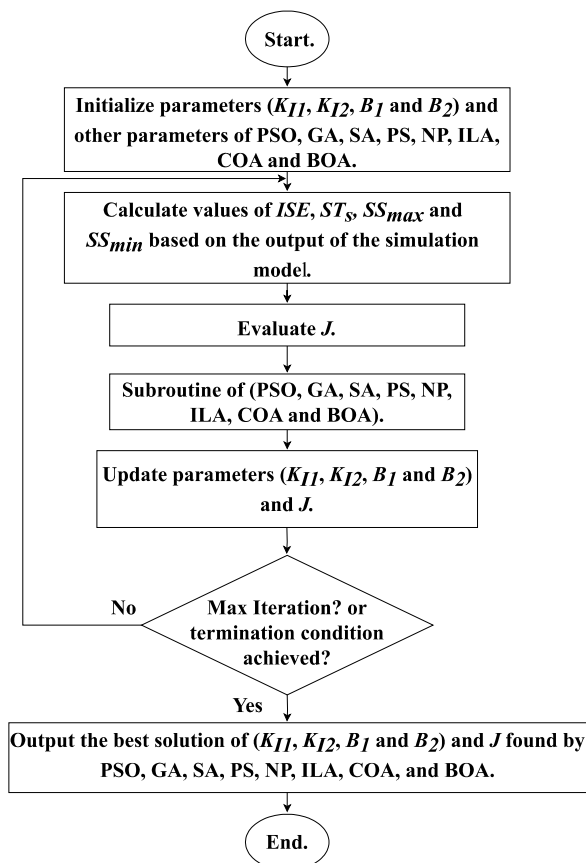


**Figure 11.** Flow chart of optimization procedure used with PSO, GA, SA, PS, NP, ILA, COA, and BOA algorithms and proposed objective function to find the best value of  $K_{I1}$ ,  $K_{I2}$ ,  $B_1$ , and  $B_2$ .

Also, the optimization is repeated and the ITAE is used as objective function, in order to show the effectiveness of the proposed objective function. In this paper, the maximum number of objective function evaluations allowed is set to 8100 for all algorithms. Simulations were run in the MATLAB (R2020a) environment on an Intel Core i5-3317U CPU with 1.7 GHz and 12 GB RAM. The optimization procedure was performed numerous times, and the best answer from these runs picked as the ideal  $K_{I1}$ ,  $K_{I2}$ ,  $B_1$ , and  $B_2$  values. It is worth mentioning that the MATLAB optimization toolbox was used for performing the

optimization by PSO, SA, GA, PS, and NP techniques. The code of ILA was taken from [49], COA's code was taken from [50], and the BOA code was obtained from [51].

## 7. Results and Discussion

### 7.1. Optimization Techniques Results

The parameters of controller and frequency bias that are selected by the eight optimization techniques and the parameters of the base system are shown in Tables 2 and 3. As seen in Table 2, the parameters which are obtained by optimization techniques have a lower value of ISE, total settling time, and objective function than the parameters of the base system (nominal parameters). So, these parameters improved the control effect and the PSO technique established its superiority over the others. The PSO technique achieved a minimum value of total settling time which is equal to 39.799 s and a lowest value of objective function which is equal to 39.86. However, the lowest value of ISE was achieved with the GA technique and its value is 0.001755. On the other hand, based on the total settling time, Table 3 demonstrates the superiority of the proposed objective function over ITAE.

**Table 2.** Optimization results for the eight methods using proposed objective function ( $J_1$ ).

Technique	$K_{i1}$	$K_{i2}$	$B_1$	$B_2$	ISE	$TT_s$ (s) <sup>1</sup>	$J_1$
Base System [1]	0.3	0.3	20.6	16.9	0.005816	61.925	61.98
PSO	1.77350	1.77350	4.7464460	3.3639450	0.001792	<b>39.799</b> *	<b>39.86</b>
SA	1.72160	1.72160	4.9996200	3.3580300	0.001781	40.009	40.07
GA	1.63920	1.63920	5.3745400	3.6335000	<b>0.001755</b>	40.206	40.27
NP	0.44061	0.44061	19.155740	10.282129	0.003035	44.661	44.72
PS	0.33125	0.33125	26.595424	10.554219	0.003205	44.008	44.06
ILA	1.76550	1.76550	4.772300	3.3600000	0.001793	39.838	39.90
COA	1.74690	1.74690	4.485200	3.4862000	0.001845	40.087	40.15
BOA	1.74530	1.74530	4.711800	3.3760000	0.001814	39.977	40.04

<sup>1</sup>  $TT_s$ : Total settling time of  $\Delta f_1$ ,  $\Delta f_2$ , and  $\Delta P_{tie}$ . \* The figures in bold are the best.

**Table 3.** Optimization results for the eight methods using ITAE ( $J_2$ ).

Technique	$K_{i1}$	$K_{i2}$	$B_1$	$B_2$	ISE	$TT_s$ (s)	$J_2$
Base System [1]	0.3	0.3	20.6	16.9	0.005816	61.925	2.263258
PSO	1.5447	1.5447	5.5805400	4.2537300	0.001767	46.308	<b>0.482199</b>
SA	1.5396	1.5396	5.5290400	4.2233100	0.001780	<b>46.065</b>	0.482690
GA	1.5400	1.5400	5.6217400	4.2520400	0.001764	46.332	0.482240
NP	1.5449	1.5449	5.5784800	4.2537300	0.001767	46.306	<b>0.482199</b>
PS	1.5447	1.5447	5.5805400	4.2537300	0.001767	46.308	<b>0.482199</b>
ILA	1.5445	1.5445	5.58030	4.25470	0.001767	46.310	<b>0.482199</b>
COA	1.5264	1.5264	5.74250	4.22370	<b>0.001758</b>	46.328	0.482760
BOA	1.5433	1.5433	5.6079	4.2501	0.001764	46.386	0.482216

The figures in bold are the best.

It is noted from Tables 2 and 3 that the performance of the eight optimization techniques was different for  $J_1$  and  $J_2$ , which proves that the selection of the objective function influences the performance of the optimization techniques. Although four techniques obtained the minimum value of the  $J_2$ , the lowest values of ISE and TTs were achieved when  $J_1$  used. Therefore, it is best to include the required specifications in the objective function while designing it. Also, it is noted that the approaches which have small  $K_I$  and large  $B$  achieved large ISE. Thus, it is necessary to select the proper values of  $K_I$  and  $B$ .

It is worth noting that the issue of the time complexity is also important in the optimization especially in the case of on-line tuning. What the time complexity problem has in common among the optimization techniques is the selection of random initial values of the variables that need to tune and the upper and lower bounds of these variables. The techniques will yield random initial values that are closer to the desired variables the more precisely the upper and lower values of these variables are defined. In order to reduce

the time of finding the desired solutions with optimization techniques, we recommend increasing the population size and reducing the number of iterations. Furthermore, the elapsed time of the optimization process is important. The elapsed time is determined by the PC specifications, optimization technique's code complexity, and code layers' size.

## 7.2. Simulation Results

Four scenarios of the input disturbance were investigated to analyze the system's dynamic response using the same values of  $K_{I1}$ ,  $K_{I2}$ ,  $B_1$ , and  $B_2$ , which are obtained in the case of a 0.1875 (p.u.) input disturbance applied in area 1 at  $t = 0$  s. The four scenarios of the change in load powers have been examined as:

1. Case 1: the load changes interpreted as  $\Delta P_{D1} = 0.1875$  (p.u.) and  $\Delta P_{D2} = 0.0$  (p.u.);
2. Case 2: the load changes interpreted as  $\Delta P_{D1} = 0.0$  (p.u.) and  $\Delta P_{D2} = 0.1875$  (p.u.);
3. Case 3: the load changes interpreted as  $\Delta P_{D1} = 0.1875$  (p.u.) and  $\Delta P_{D2} = 0.1875$  (p.u.);
4. Case 4: the load changes interpreted as  $\Delta P_{D1} = 0.1$  (p.u.) and  $\Delta P_{D2} = -0.2$  (p.u.).

### 7.2.1. Case 1: Step Load Change in Area 1

A 0.1875 (p.u.) step load change is applied in area 1 at  $t = 0$  s, to exhibit the dynamic reaction of the system with the suggested parameters derived by the proposed objective function. The settling time and peak amplitude of frequency and tie-line power deviations are listed in Table 4.  $J_1$  is used as the performance index to compare between the techniques. It is noted from Table 4 that the proposed parameters (optimized:  $K_{I1}$ ,  $K_{I2}$ ,  $B_1$ , and  $B_2$ ) obtained by the eight techniques achieved better transient performances compared to the base system parameters (nominal:  $K_{I1}$ ,  $K_{I2}$ ,  $B_1$ , and  $B_2$ ). Therefore, the results indicated that the proposed parameters are effective. For this case, the PSO technique achieved a minimum value of  $J_1$  which is equal to 39.86. Also, the value of  $J_1$  of ILA is very close to the  $J_1$  value of PSO. It is noted that the peak values of  $\Delta f_2$  for PSO, SA, GA, ILA, COA, and BOA are a little bigger than the other methods. NP and PS performed better than the base system, but not better than PSO, SA, GA, ILA, COA, and BOA based on value of  $J_1$ .

**Table 4.** Dynamic performance characteristic of various methods for case 1.

Technique	$T_s$ (s) <sup>1</sup>			$M_p$ (p.u.) <sup>2</sup>			$J_1$
	$\Delta f_1$	$\Delta f_2$	$\Delta P_{tie}$	$\Delta f_1$	$\Delta f_2$	$\Delta P_{tie}$	
Base System	14.3546	22.9294	24.6405	-0.0128	<b>-0.0030</b>	-0.0328	61.98
PSO	9.93450	<b>15.8378</b>	14.0266	<b>-0.0126</b>	-0.0049	-0.0302	<b>39.86</b>
SA	9.92370	15.8607	14.2244	<b>-0.0126</b>	-0.0048	-0.0301	40.07
GA	<b>9.88270</b>	15.8683	14.4551	<b>-0.0126</b>	-0.0046	<b>-0.0300</b>	40.27
NP	10.9160	20.0391	<b>13.7063</b>	-0.0127	-0.0031	-0.0312	44.72
PS	10.8743	18.7568	14.3770	-0.0127	<b>-0.0030</b>	-0.0311	44.06
ILA	9.9360	15.8422	14.0597	<b>-0.0126</b>	-0.0049	-0.0302	39.90
COA	10.0197	15.9110	14.1563	-0.0127	-0.0049	-0.0304	40.15
BOA	9.9692	15.8709	14.1367	-0.0127	-0.0049	-0.0303	40.04

<sup>1</sup>  $T_s$ : settling time; <sup>2</sup>  $M_p$ : peak amplitude. The figures in bold are the best.

Table 4 shows that no approach achieves the best values of all performance characteristics. Therefore, the comparison between methods is often performed using  $J_1$  to determine the superiority of one over the other. Figure 12 confirms what is shown in Table 4, which depicts the dynamic response of the base system as well as the dynamic response achieved by the eight techniques. Based on the response curves shown in Figure 12, it is clear that the transient dynamics die off quickly when the eight techniques used than the base system. So, the most observed enhancement from the curves is in the settling time of the responses. Also, the curves of PSO, GA, SA, ILA, COA, and BOA are almost same. On the other hand, the curves of NP and PS are very similar, because the values of KI and B that are selected by the NP and PS methods are close, and the situation is the same with PSO, GA, SA, ILA, COA, and BOA. Also, it is observed that to obtain optimal settling time, either bigger

settling-max or bigger settling-min must be accepted, or both. However, the settling time is very important, because it measures how quickly the transient dynamics die off.

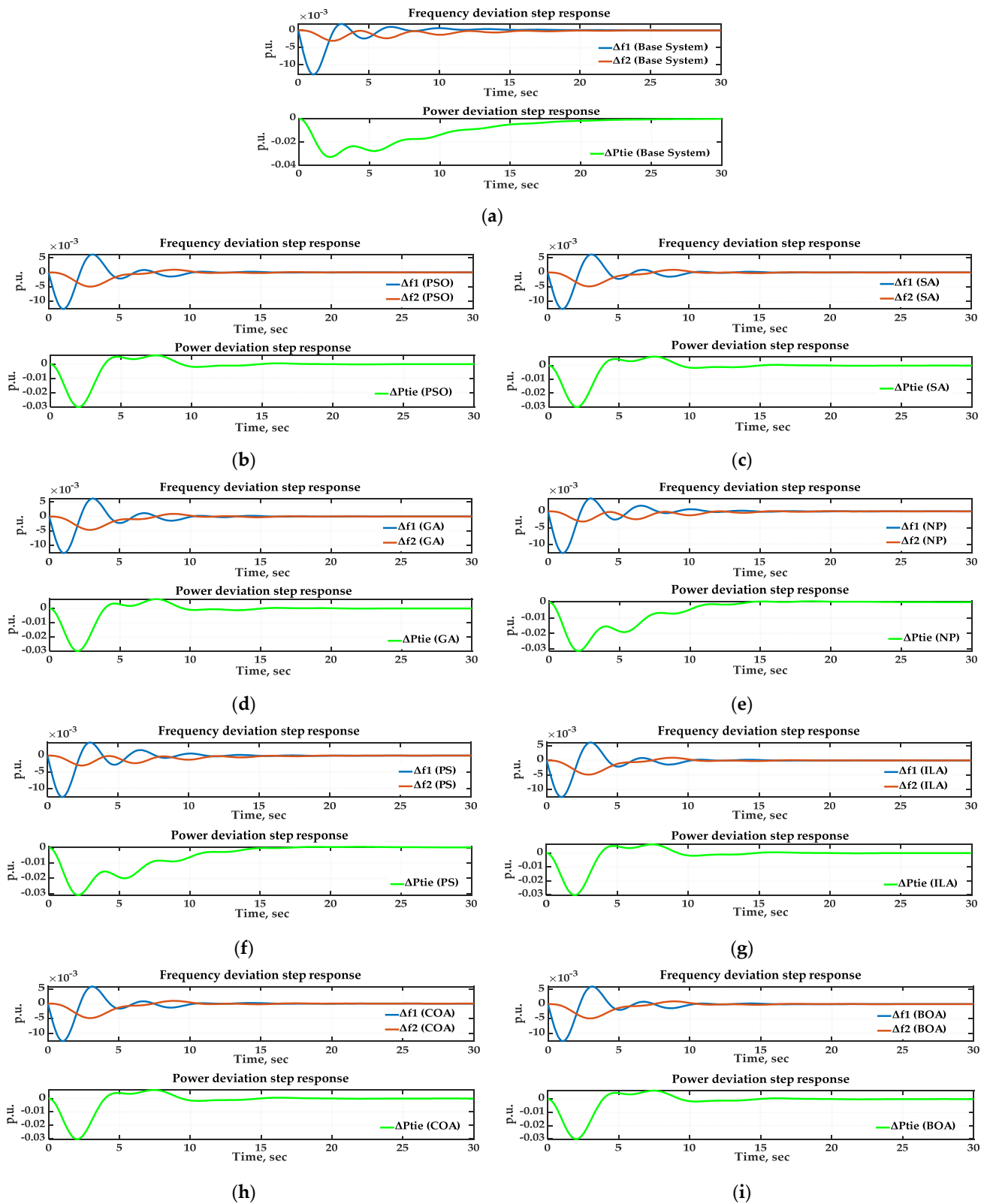


**Figure 12.** Frequency and tie-line power deviation response of the system under case 1: (a) base system; (b) using PSO; (c) using SA; (d) using GA; (e) using NP; (f) using PS; (g) using ILA; (h) using COA; (i) using BOA.

As shown in Figure 12 above, the settling time of  $\Delta f_1$ ,  $\Delta f_2$ , and  $\Delta P_{tie}$  are reduced when the proposed approach is applied. PSO achieved the minimum value of total settling time which equals to 39.799 s. The minimum settling time of  $\Delta f_1$  was 9.88270 s and it was obtained by GA. The lowest settling time of  $\Delta f_2$  was achieved by PSO and it equals to 15.8378 s. NP achieved the minimum settling time of  $\Delta P_{tie}$  which equals to 13.7063 s. Minimum peak amplitude of  $\Delta f_1$  is  $-0.0126$  (p.u.) and it was obtained by PSO, SA, ILA, and GA. However, the minimum peak amplitude of  $\Delta f_2$  was  $-0.0030$  (p.u.) which was achieved by PS and the base system. Minimum peak amplitude of  $\Delta P_{tie}$  was obtained by GA and it is equal to  $-0.0300$  (p.u.).

### 7.2.2. Case 2: Step Load Change in Area 2

The point of this scenario is to show how the proposed parameters will perform when the disturbance position changes. Table 5 shows the dynamic responses of the system for a 0.1875 (p.u.) step load increase in area 2 at  $t = 0$  s. As indicated in Table 5, the NP approach obtained the minimum value of  $J_1$  equal to 51.55.

**Table 5.** Dynamic performance characteristic of various methods for case 2.

Technique	$T_s$ (s)			$M_p$ (p.u.)			$J_1$
	$\Delta f_1$	$\Delta f_2$	$\Delta P_{tie}$	$\Delta f_1$	$\Delta f_2$	$\Delta P_{tie}$	
Base System	22.8332	19.3138	23.2464	<b>-0.0031</b>	-0.0172	0.0464	65.48
PSO	18.2038	20.1464	17.5901	-0.0056	<b>-0.0171</b>	0.0434	56.04
SA	18.0107	18.4381	17.5266	-0.0054	<b>-0.0171</b>	0.0436	54.07
GA	<b>17.7894</b>	20.0450	17.4248	-0.0052	<b>-0.0171</b>	0.0435	55.35
NP	20.1255	<b>15.8993</b>	<b>15.4425</b>	-0.0032	-0.0173	0.0468	<b>51.55</b>
PS	18.6762	19.5340	20.7193	<b>-0.0031</b>	-0.0174	0.0483	59.02
ILA	18.1828	20.1036	17.5840	-0.0055	<b>-0.0171</b>	0.0434	55.97
COA	18.2249	20.2440	17.6315	-0.0056	<b>-0.0171</b>	<b>0.0433</b>	56.20
BOA	18.1446	19.9780	17.5851	-0.0055	<b>-0.0171</b>	0.0435	55.80

The figures in bold are the best.

In Table 5 above, the settling time of  $\Delta f_1$ ,  $\Delta f_2$ , and  $\Delta P_{tie}$  are decreased when using the proposed approach. NP achieved a minimum value of a total settling time equal to 51.467 s. The base system and PS technique achieved the minimum peak amplitude of  $\Delta f_1$  and it was equal to  $-0.0031$  (p.u.). Minimum peak amplitude of  $\Delta f_2$  was achieved by PSO, SA, ILA, COA, BOA, and GA algorithms and its value was  $-0.0171$  (p.u.). Minimum peak amplitude of  $\Delta P_{tie}$  was 0.0433 (p.u.) and was obtained by the COA algorithm. It is noted that the total settling time for case 2 was bigger than case 1, so the system takes more time to be stable, thus the changes in the disturbance position affect the system performance. The previous proper selection of  $K_I$  and  $B$  lessens this issue. Figures 13–15 show the dynamic response of the base system and the dynamic response using the eight techniques.

As shown in Figures 13 and 14, due to the rising load in area 2, which exceeds the capacity of the existing power generation, the frequency in areas 1 and 2 will drop. Hence, the frequency deviation peak amplitude is a negative value. According to Figures 13 and 14, the frequency deviation peak amplitude of region 2 is bigger than that of area 1, since the frequency in area 1 drops due to the load shift, which occurs in area 2 and has a stronger influence there. The electricity flows from area 1 to area 2 to mitigate the impact of the increased demand in area 2, which simultaneously lowers the frequency in area 1. This occurs because the load in area 2 increases while the load in area 1 remains the same. As a result, in Figure 15, the tie-line power from region 1 to area 2 is positive. However, in scenario 1, the tie-line power from area 1 to area 2 is negative due to an increase in step load in area 1.

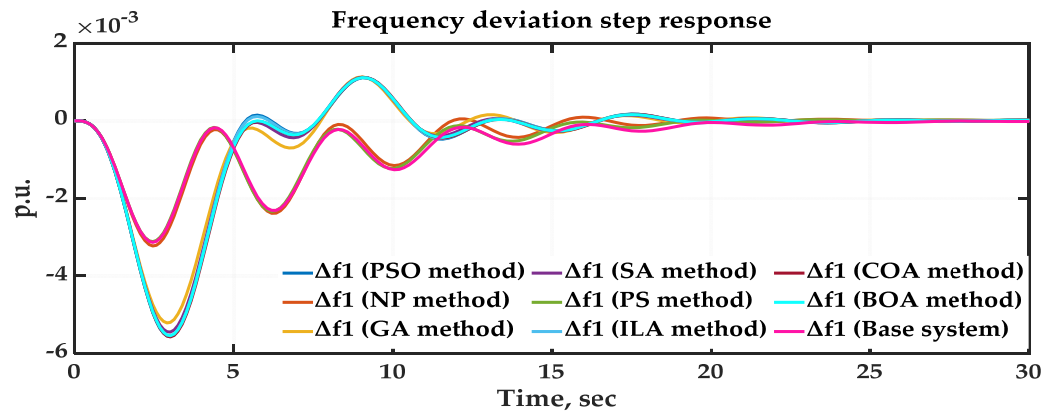


Figure 13. Area 1 frequency deviation response of the base system and using the eight methods for case 2.

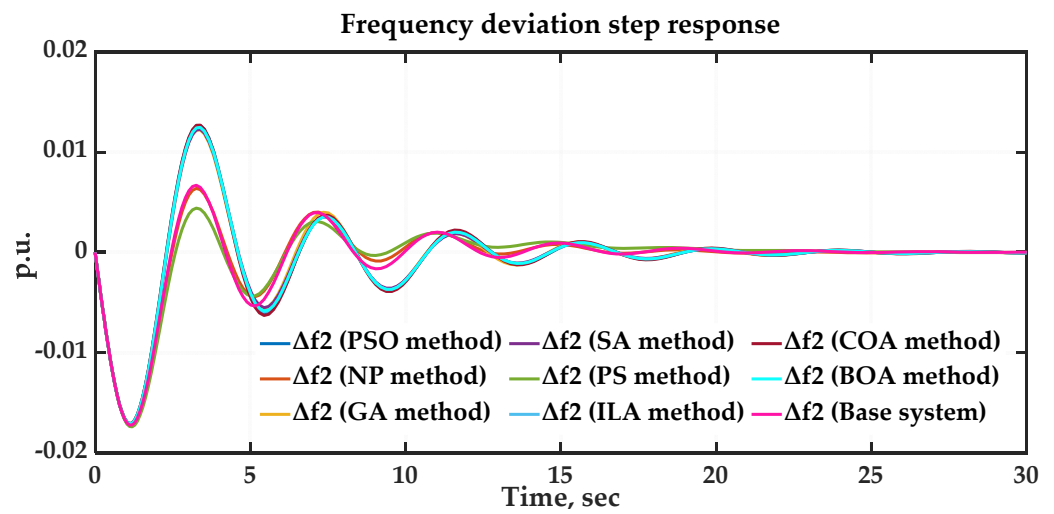


Figure 14. Area 2 frequency deviation response of the base system and using the eight methods for case 2.

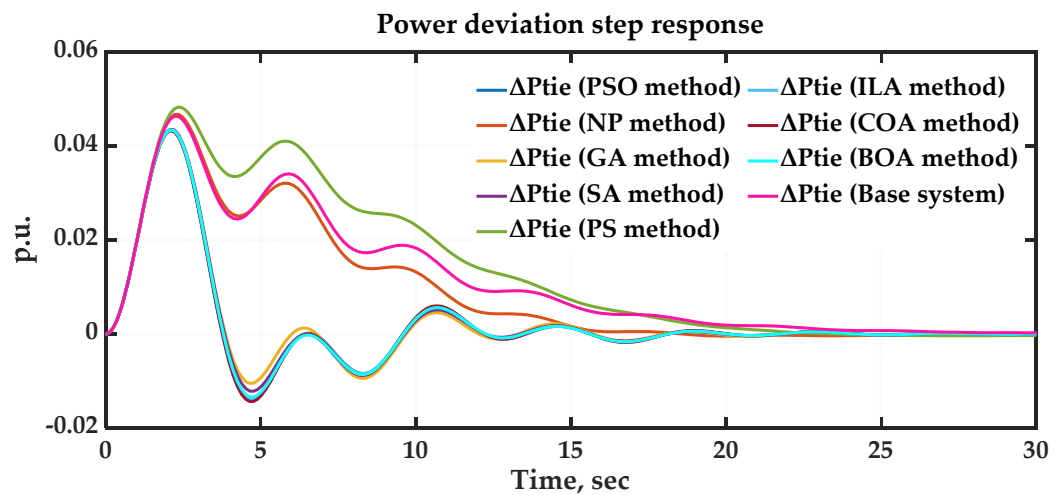


Figure 15. Tie-line power deviation response of the base system and using the eight methods for case 2.

### 7.2.3. Case 3: Step Load Change in Both Areas

In this case, a 0.1875 (p.u.) step load increase occurred in area 1 and area 2 at  $t = 0$  s. Table 6 shows that the proposed parameters have better robustness and dynamic performance when the position and size of disturbance changes. The NP technique achieved a

minimum value of  $J_1$  which equals to 46.66. And unexpectedly, PSO, GA, ILA, COA, BOA, and PS techniques did not perform superior to the base system in this case based on value of  $J_1$ . The PS technique achieved a maximum value of  $J_1$  which was equal to 57.69.

**Table 6.** Dynamic performance characteristics of various methods for case 3.

Technique	$T_s(s)$			$M_p(p.u.)$			$J_1$
	$\Delta f_1$	$\Delta f_2$	$\Delta P_{tie}$	$\Delta f_1$	$\Delta f_2$	$\Delta P_{tie}$	
Base System	14.5663	17.3265	22.5093	-0.0137	-0.0182	0.0137	54.45
PSO	12.4536	20.1537	23.4316	<b>-0.0135</b>	<b>-0.0180</b>	0.0139	56.10
SA	12.3803	18.3716	23.2157	<b>-0.0135</b>	-0.0181	0.0144	54.03
GA	12.2511	20.1072	23.3405	<b>-0.0135</b>	<b>-0.0180</b>	0.0144	55.76
NP	<b>11.6314</b>	<b>15.9851</b>	<b>18.9893</b>	<b>-0.0135</b>	-0.0183	0.0173	<b>46.66</b>
PS	15.0072	19.4044	23.2109	<b>-0.0135</b>	-0.0184	0.0238	57.69
ILA	12.4442	20.0982	23.4091	<b>-0.0135</b>	<b>-0.0180</b>	0.0140	56.02
COA	12.4128	20.2749	23.5322	-0.0136	<b>-0.0180</b>	<b>0.0133</b>	56.28
BOA	12.4111	20.0011	23.3721	<b>-0.0135</b>	<b>-0.0180</b>	0.0139	55.85

The figures in bold are the best.

As shown in Figures 16–18, the settling time of  $\Delta f_1$ ,  $\Delta f_2$ , and  $\Delta P_{tie}$  are decreased when NP and SA techniques are used. NP achieved the minimum value of total settling time which equals to 46.61 s. The peak amplitude of  $\Delta f_1$  is the same for the PSO, SA, GA, NP, PS, ILA, and BOA methods which equals to -0.0135 (p.u.). PSO, ILA, COA, BOA, and GA algorithms achieved the lowest peak amplitude of  $\Delta f_2$  that equals -0.0180 (p.u.), and the minimum peak amplitude of  $\Delta P_{tie}$  was 0.0133 (p.u.) which was obtained when COA was used. It is noted that the parameters  $K_{I1}$ ,  $K_{I2}$ ,  $B_1$ , and  $B_2$ , which NP obtained in the case of a 0.1875 (p.u.) input disturbance applied in area 1 at  $t = 0$  s, perform well in this case and do not need to be reset. Also, the performance of the other techniques is acceptable. The dynamic response which is achieved by the eight technique and the base system dynamic response are shown in Figures 16–18.

As shown in Figures 16–18 above, as a result of greater step load disruptions in both areas than in cases 1 and 2, in case 3, the frequency deviations were increased. Thus, both areas increase their generation in order to meet the increase in load demand on both areas. Also, the power peak amplitude was less than in case 1 and case 2 because both areas tended to absorb their own load.

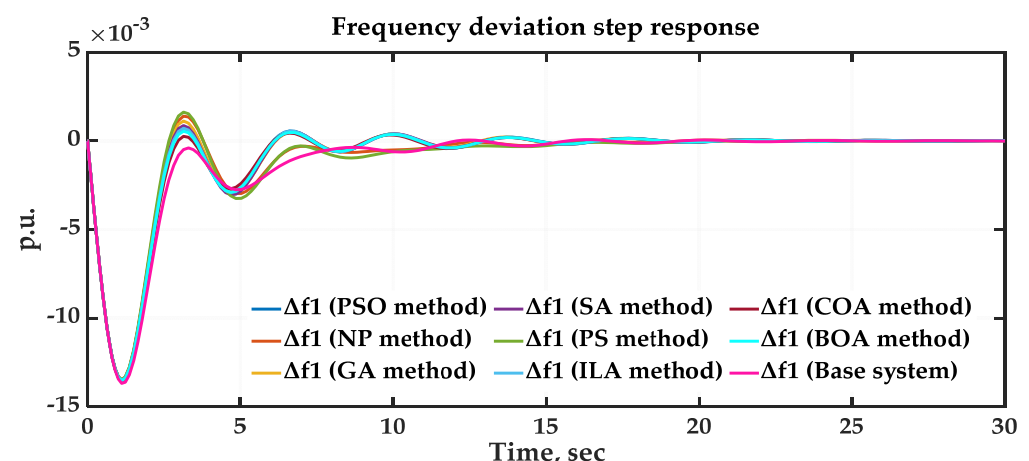


**Figure 16.** Area 1 frequency deviation response of the base system and using the eight methods for case 3.

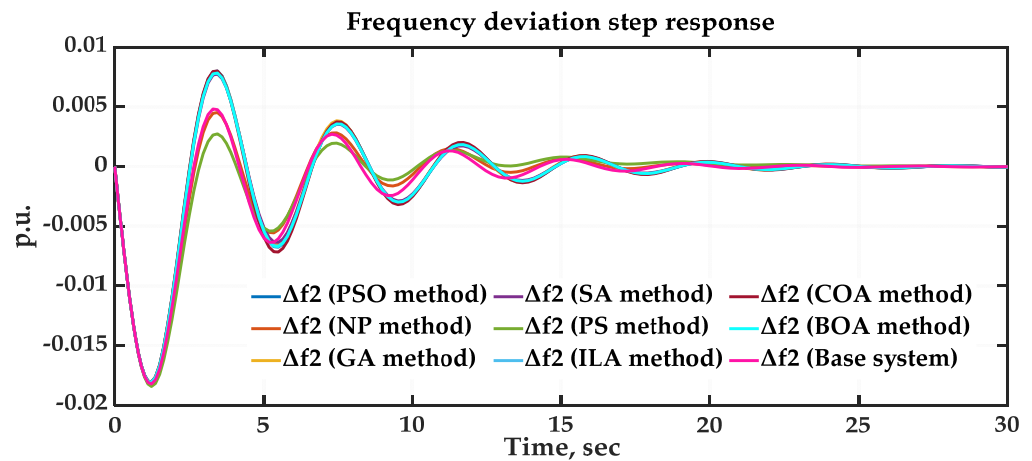


Figure 17. Area 2 frequency deviation response of the base system and using the eight methods for case 3.

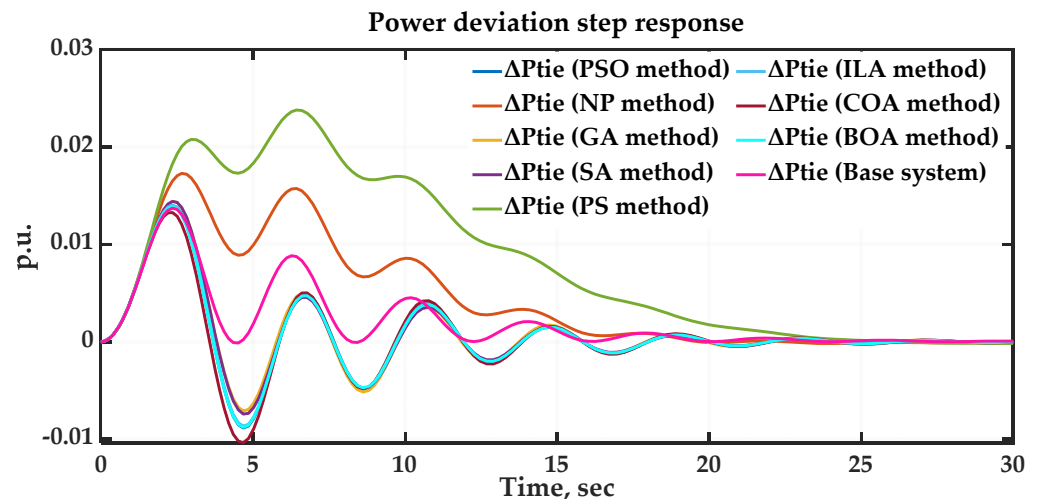


Figure 18. Tie-line power deviation response of the base system and using the eight methods for case 3.

#### 7.2.4. Case 4: Step Load Increment in Area 1 and Decrement on Area 2

In this case, the load changing occurred as a 0.1 (p.u.) step load increase in area 1 and a 0.2 (p.u.) step load decrease in area 2 at  $t = 0$  s. The point of this scenario is to show how the fallibility changes in the system if it can handle variation. Table 7 shows that when the position, magnitude, and sign of the disturbance vary, the proposed parameters have greater resilience and dynamic performance. In this situation, the NP approach obtained a minimum value of  $J_1$  of 49.10.

As shown in Table 7 above, the settling time of  $\Delta f_1$ ,  $\Delta f_2$ , and  $\Delta P_{tie}$  are reduced when using the eight optimization techniques. NP achieved the lowest value of total settling time that equals 48.98 s. The best settling time of  $\Delta f_1$  was 15.8344 s and it was obtained by the SA algorithm. Minimum settling time of  $\Delta f_2$  was achieved by the NP technique and it is equal to 15.8582 s. Furthermore, NP achieved the lowest settling time of  $\Delta P_{tie}$  which equals 15.0639 s. Base system, NP, and PS achieved the minimum peak amplitude of  $\Delta f_1$  and its value was  $-0.0061$  (p.u.). However, the minimum peak amplitude of  $\Delta f_2$  was 0.0177 (p.u.) and it was obtained by the PSO, ILA, and COA algorithms. Also, PSO and ILA algorithms achieved the minimum peak amplitude of  $\Delta P_{tie}$  with value equal to  $-0.0623$  (p.u.). Although, the parameters  $K_{I1}$ ,  $K_{I2}$ ,  $B_1$ , and  $B_2$  which obtained in a case of a 0.1875 (p.u.) input disturbance applied in area 1 are used in this case, however, the performance of the eight techniques is acceptable, and do not necessarily need to reset. The dynamic response which was achieved by the eight techniques and the base system dynamic response are shown in Figures 19–21.

**Table 7.** Dynamic performance characteristic of various methods for case 4.

Technique	$T_s(s)$			$M_p(p.u.)$			$J_1$
	$\Delta f_1$	$\Delta f_2$	$\Delta P_{tie}$	$\Delta f_1$	$\Delta f_2$	$\Delta P_{tie}$	
Base System	22.3529	19.4834	23.4830	−0.0061	0.0179	−0.0669	65.44
PSO	17.7870	20.1529	17.4934	0.0092	<b>0.0177</b>	− <b>0.0623</b>	55.57
SA	<b>15.8344</b>	18.4625	17.4141	0.0091	0.0178	−0.0625	51.85
GA	15.8676	20.0362	17.2725	0.0088	0.0178	−0.0624	53.30
NP	18.0546	<b>15.8582</b>	<b>15.0639</b>	− <b>0.0061</b>	0.0179	−0.0663	<b>49.10</b>
PS	18.2397	19.5765	19.6645	− <b>0.0061</b>	0.0180	−0.0677	57.69
ILA	17.7377	20.1159	17.4876	0.0092	<b>0.0177</b>	− <b>0.0623</b>	55.48
COA	17.8448	20.2425	17.5517	0.0090	<b>0.0177</b>	−0.0624	55.78
BOA	17.6181	19.9757	17.4958	0.0091	0.0178	−0.0625	55.22

The figures in bold are the best.

In Figures 19 and 20, because of the decrease in load in region 2, the frequency in area 2 will be increased. Area 2's total load demand is less than the present power generation. As a result, in Figure 19, the peaks of frequency deviation of region 2 are positive. Also, due to increased step load disturbances in site 1 and decreased in site 2, the tie-line power deviation in case 4 is greater than in cases 1, 2, and 3, as shown in Figure 21. Figure 22 depicts the best and worst objective function values for the four situations.

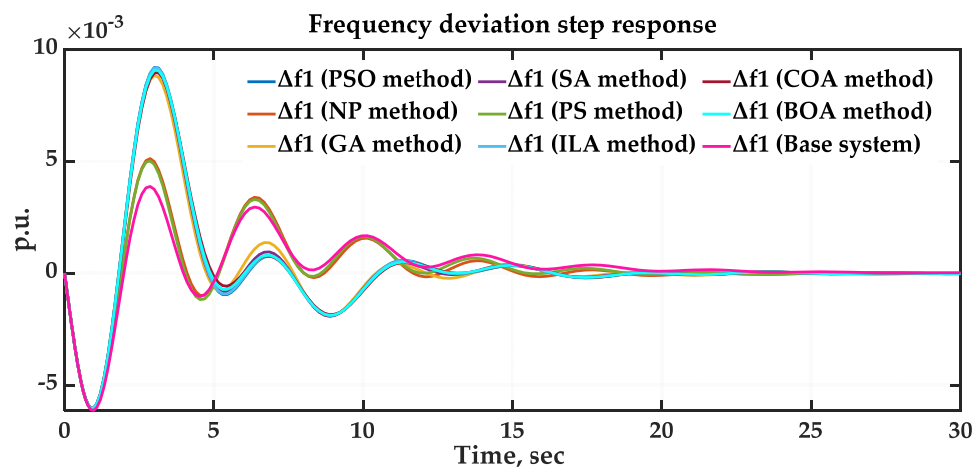


**Figure 19.** Area 1 frequency deviation response of the base system and using the eight methods for case 4.

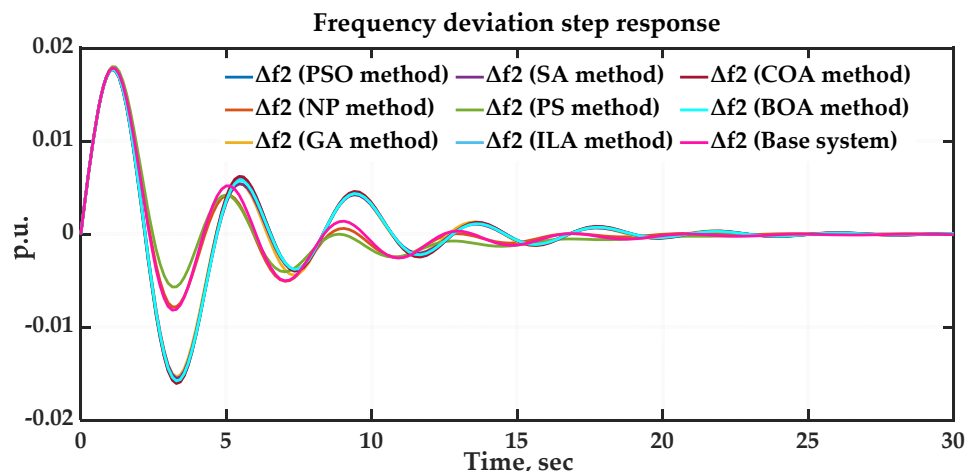


**Figure 20.** Area 2 frequency deviation response of the base system and using the eight methods for case 4.

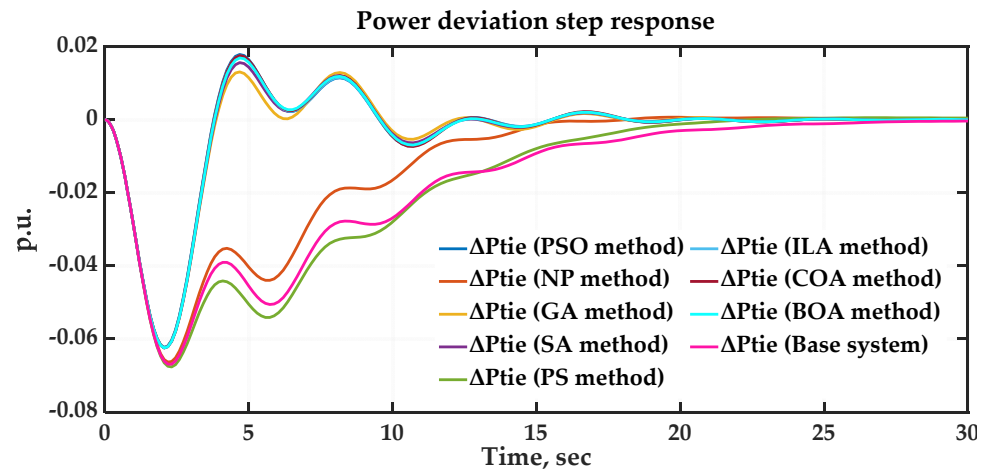


Figure 21. Tie-line power deviation response of the base system and using the eight methods for case 4.

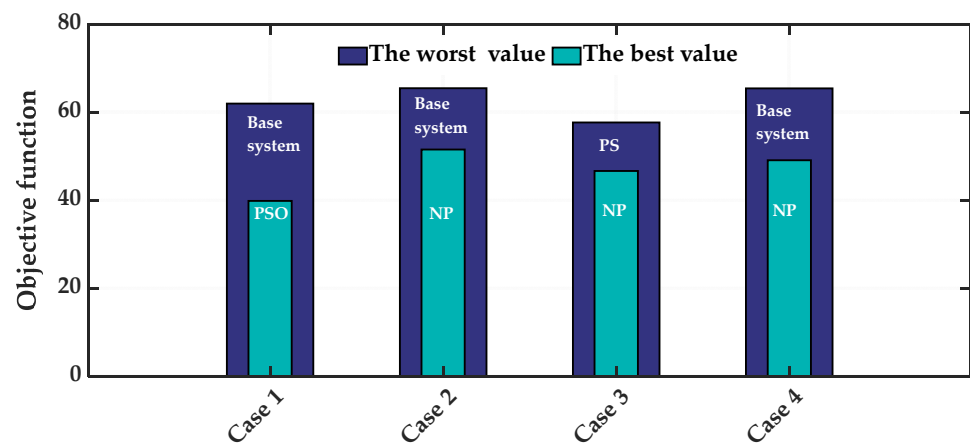


Figure 22. The best (lower) and worst (higher) value of the objective function for the four cases.

The parameters  $K_{I1}$ ,  $K_{I2}$ ,  $B_1$ , and  $B_2$  which were obtained by optimization techniques and so have a lower value of  $J_1$  than the parameters of the base system in the four previous cases, as shown in Figure 22. In case 1, the PSO technique achieved the minimum value of  $J_1$ , and the NP technique achieved the minimum value of  $J_1$  for case 2, case 3m and case 4. Base system parameters achieved the maximum value of  $J_1$  for all cases except case 3 where the max value was achieved by PS technique. Overall, we can state that the suggested parameters enhanced the control effect. Although, the parameters  $K_{I1}$ ,  $K_{I2}$ ,  $B_1$ , and  $B_2$  are obtained in a case of a 0.1875 (p.u.) input disturbance applied in area 1 at  $t = 0$  s, they performed well for different scenarios of load variations. In the extra three scenarios, the values of  $J_1$  obtained by the eight techniques were better than the value of  $J_1$  which the base system obtained in the main case, which proves that the proposed approach can guarantee the stability of the system regardless of the magnitude and location of the change in the load without reset parameters  $K_{I1}$ ,  $K_{I2}$ ,  $B_1$ , and  $B_2$ .

### 7.3. Sensitivity Analysis

Sensitivity analysis is used to verify the system's robustness when the loading circumstances and system parameters fluctuate within a tolerable range. It demonstrates whether the proposed approach maintains the system stability regardless of changeable system characteristics and loading conditions. In this work, the time constants of speed governor ( $T_g$ ), turbine ( $T_t$ ), and tie-line power ( $T_{12}$ ) are varied from their nominal values in the range of +20% to -20%. Table 8 proves that objective function, peak amplitude, and settling time

that have been achieved by proposed parameters are within acceptable change under the effect of sensitivity analysis.

**Table 8.** Robustness analysis.

Technique	Parameter Variation	Change %	$T_s$ (s)			$M_P$ (p.u.)			$J_1$
			$\Delta f_1$	$\Delta f_2$	$\Delta P_{tie}$	$\Delta f_1$	$\Delta f_2$	$\Delta P_{tie}$	
Base System	Nominal (case 1)		14.35	22.93	24.64	-0.0128	-0.0030	-0.0328	61.98
	Loading condition	+20	14.35	22.93	24.64	-0.0154	-0.0037	-0.0394	61.99
		-20	14.35	22.93	24.64	-0.0103	-0.0024	-0.0263	61.97
	$T_g$	+20	14.64	26.92	23.51	-0.0132	-0.0033	-0.0339	65.13
		-20	14.64	26.92	23.51	-0.0132	-0.0033	-0.0339	61.89
	$T_t$	+20	14.64	26.93	23.51	-0.0132	-0.0033	-0.0339	66.06
		-20	13.85	23.96	25.03	-0.0121	-0.0027	-0.0306	62.90
	$T_{12}$	+20	14.03	22.26	21.48	-0.0127	-0.0035	-0.0376	57.84
-20		14.87	27.12	29.17	-0.0130	-0.0025	-0.0276	71.20	
PSO	Nominal (case 1)		9.93450	15.8378	14.0266	-0.0126	-0.0049	-0.0302	39.86
	Loading condition	+20	10.8844	17.4138	16.1784	-0.0152	-0.0059	-0.0362	44.55
		-20	10.8837	17.4199	16.1870	-0.0101	-0.0039	-0.0241	44.54
	$T_g$	+20	15.1645	18.4055	16.9348	-0.0130	-0.0051	-0.0312	50.57
		-20	9.9930	15.5123	13.7873	-0.0122	-0.0047	-0.0290	39.35
	$T_t$	+20	15.8702	22.6956	17.5201	-0.0133	-0.0053	-0.0324	56.16
		-20	10.0375	15.3515	13.7493	-0.0119	-0.0045	-0.0278	39.20
	$T_{12}$	+20	11.5850	17.7453	16.2127	-0.0125	-0.0055	-0.0346	45.62
-20		12.3642	16.4515	15.0720	-0.0128	-0.0042	-0.0253	43.94	
SA	Nominal (case 1)		9.92370	15.8607	14.2244	-0.0126	-0.0048	-0.0301	40.07
	Loading condition	+20	10.7796	15.8611	14.2258	-0.0151	-0.0058	-0.0361	40.94
		-20	10.7845	15.8611	14.2262	-0.0101	-0.0039	-0.0241	40.92
	$T_g$	+20	15.2227	18.2229	16.8100	-0.0130	-0.0050	-0.0312	50.33
		-20	9.99520	15.6224	14.0030	-0.0122	-0.0046	-0.0290	39.68
	$T_t$	+20	17.5189	22.5773	17.4532	-0.0133	-0.0052	-0.0323	57.62
		-20	10.0701	15.4858	13.9353	-0.0119	-0.0044	-0.0278	39.55
	$T_{12}$	+20	11.5081	17.6523	16.2899	-0.0125	-0.0054	-0.0346	45.52
-20		12.6522	16.4102	15.1722	-0.0127	-0.0041	-0.0252	44.29	
GA	Nominal (case 1)		9.88270	15.8683	14.4551	-0.0126	-0.0046	-0.0300	40.27
	Loading condition	+20	14.3419	15.8664	14.4538	-0.0151	-0.0056	-0.0361	44.74
		-20	14.3362	15.8665	14.4539	-0.0101	-0.0037	-0.0240	44.71
	$T_g$	+20	15.2529	21.9710	16.5494	-0.0130	-0.0048	-0.0312	53.84
		-20	9.94110	15.6589	14.2582	-0.0122	-0.0044	-0.0289	39.92
	$T_t$	+20	17.5794	24.7061	17.3350	-0.0132	-0.0050	-0.0322	59.70
		-20	9.95830	15.4721	14.1572	-0.0119	-0.0042	-0.0277	39.64
	$T_{12}$	+20	11.3496	17.5491	16.2472	-0.0125	-0.0052	-0.0345	45.22
-20		12.8664	16.1050	15.1589	-0.0127	-0.0040	-0.0252	44.19	
NP	Nominal (case 1)		10.9160	20.0391	13.7063	-0.0127	-0.0031	-0.0312	44.72
	Loading condition	+20	10.9164	20.0233	18.6898	-0.0152	-0.0037	-0.0374	49.70
		-20	10.9165	20.0244	18.6910	-0.0101	-0.0025	-0.0249	49.68
	$T_g$	+20	16.0300	24.6622	19.6857	-0.0131	-0.0033	-0.0323	60.44
		-20	10.6599	17.8717	13.5006	-0.0123	-0.0029	-0.0301	42.08
	$T_t$	+20	16.7806	25.4125	20.3262	-0.0133	-0.0035	-0.0335	62.58
		-20	10.1794	17.4258	13.3589	-0.0120	-0.0027	-0.0289	41.01
	$T_{12}$	+20	12.1324	20.1141	18.9450	-0.0126	-0.0036	-0.0359	51.25
-20		11.1303	19.0998	15.2101	-0.0128	-0.0026	-0.0261	45.49	
PS	Nominal (case 1)		10.8743	18.7568	14.3770	-0.0127	-0.0030	-0.0311	44.06
	Loading condition	+20	10.8750	18.7506	14.3802	-0.0152	-0.0036	-0.0372	44.07
		-20	10.8749	18.7502	14.3803	-0.0101	-0.0024	-0.0248	44.05
	$T_g$	+20	16.0414	22.3617	22.8000	-0.0131	-0.0032	-0.0322	61.26
		-20	10.5686	18.7698	14.6946	-0.0122	-0.0028	-0.0300	44.08
	$T_t$	+20	16.7710	24.8354	23.6251	-0.0133	-0.0034	-0.0333	65.29
		-20	10.0236	19.4295	15.1119	-0.0120	-0.0026	-0.0288	44.61
	$T_{12}$	+20	12.1860	18.2585	19.4167	-0.0126	-0.0035	-0.0357	49.92
-20		11.0571	22.4558	17.7781	-0.0128	-0.0025	-0.0260	51.34	

Table 8. Cont.

Technique	Parameter Variation	Change %	$T_s$ (s)			$M_P$ (p.u.)			$J_1$
			$\Delta f_1$	$\Delta f_2$	$\Delta P_{tie}$	$\Delta f_1$	$\Delta f_2$	$\Delta P_{tie}$	
ILA	Nominal (case 1)		9.9360	15.8422	14.0597	-0.0126	-0.0049	-0.0302	39.90
	Loading condition	+20	9.9384	15.8419	14.0635	-0.0152	-0.0059	-0.0362	39.92
		-20	9.9375	15.8415	14.0646	-0.0101	-0.0039	-0.0241	39.89
	$T_g$	+20	15.1694	18.3797	16.9235	-0.0130	-0.0051	-0.0312	50.54
		-20	9.9998	15.5329	13.8243	-0.0122	-0.0047	-0.0290	39.42
	$T_t$	+20	15.8712	22.6582	17.5121	-0.0133	-0.0053	-0.0324	56.11
		-20	10.0556	15.3783	13.7813	-0.0119	-0.0045	-0.0278	39.27
	$T_{12}$	+20	11.5736	17.7338	16.2348	-0.0125	-0.0055	-0.0346	45.62
		-20	12.4240	16.4551	15.0944	-0.0128	-0.0042	-0.0253	44.03
	COA	Nominal (case 1)		10.0197	15.9110	14.1563	-0.0127	-0.0049	-0.0304
Loading condition		+20	10.0238	15.9098	14.1580	-0.0152	-0.0059	-0.0366	40.17
		-20	10.0231	15.9099	14.1572	-0.0102	-0.0039	-0.0244	40.14
$T_g$		+20	15.0578	18.4333	17.0247	-0.0131	-0.0051	-0.0316	50.58
		-20	10.1620	15.6305	13.9612	-0.0123	-0.0047	-0.0293	39.81
$T_t$		+20	15.7523	24.7266	17.5831	-0.0133	-0.0054	-0.0326	58.13
		-20	10.4963	15.4919	13.9324	-0.0120	-0.0045	-0.0281	39.98
$T_{12}$		+20	11.4851	17.8085	16.3403	-0.0126	-0.0055	-0.0349	45.71
		-20	12.4406	16.5491	15.2606	-0.0128	-0.0042	-0.0256	44.31
BOA		Nominal (case 1)		9.9692	15.8709	14.1367	-0.0127	-0.0049	-0.0303
	Loading condition	+20	9.9726	15.8696	14.1379	-0.0152	-0.0059	-0.0364	40.06
		-20	9.9718	15.8695	14.1385	-0.0101	-0.0039	-0.0242	40.03
	$T_g$	+20	15.1401	18.3479	16.9395	-0.0131	-0.0051	-0.0314	50.49
		-20	10.0700	15.6052	13.9305	-0.0123	-0.0047	-0.0292	39.67
	$T_t$	+20	15.8267	22.5841	17.5195	-0.0133	-0.0053	-0.0325	56.00
		-20	10.2489	15.4756	13.8893	-0.0120	-0.0045	-0.0279	39.67
	$T_{12}$	+20	11.5321	17.7349	16.2985	-0.0125	-0.0055	-0.0347	45.64
		-20	12.4816	16.5123	15.1977	-0.0128	-0.0042	-0.0254	44.25

Following the presentation of the sensitivity analysis in Table 8, it can be said that the different techniques offer a satisfactory level of robust and stable control even when operating loading conditions or system parameters fluctuate compared to the base system. So, the integral controller optimized by the proposed optimization techniques outperformed the base system controller in terms of adaptability to uncertainty. Furthermore, based on the value of  $J_1$ , we can say that ILA performed better than the other techniques when evaluating the robustness and stability of the system. Figure 23 below shows the frequency deviation in area 1 using ILA method with system parameter variation.

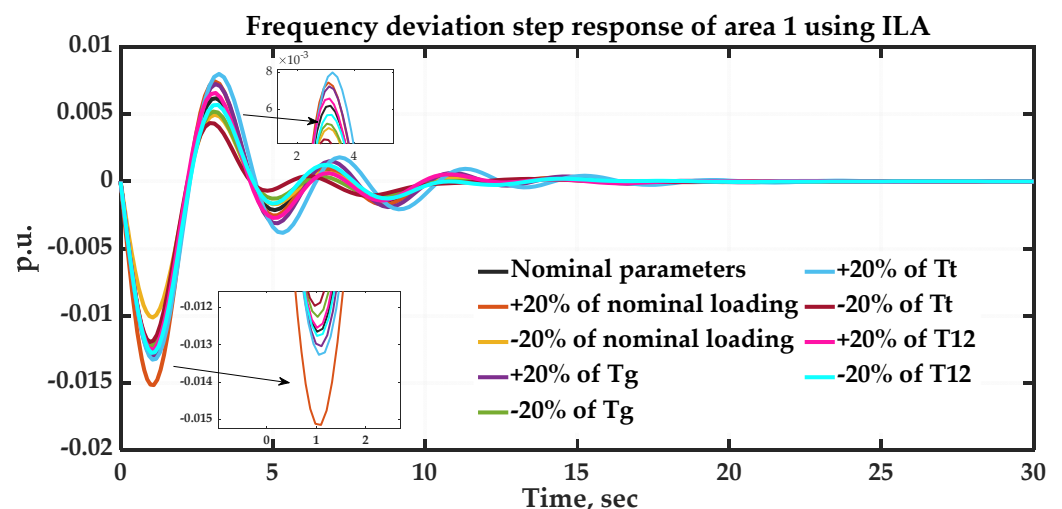
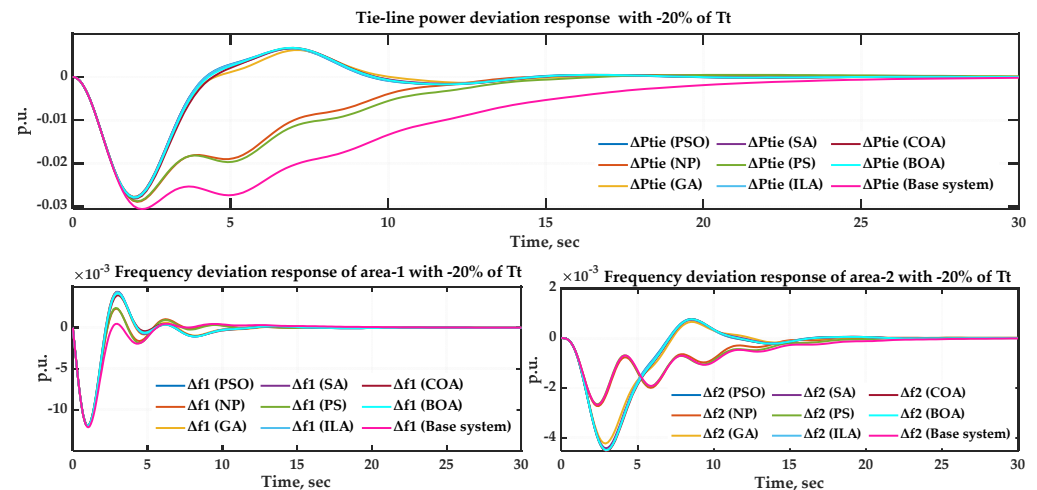


Figure 23. Frequency deviation in area-1 using ILA method with system parameter variation.

Figure 23 shows that the curves under different parameter variations are similar to some extent. The settling-max and the settling-min of the curves are fairly close as well

as the settling time. Therefore, it can be said that the suggested control approach offers a robust and stable control that is satisfactory under changes in operating loading conditions or system characteristics.

Figure 24 above shows the frequency and power deviation with  $-20\%$  of  $T_t$  using the eight techniques and base system. Figure 24 is an example of the robustness analysis which was presented in detail in Table 8. As shown in Figure 24, the responses of the frequency and power deviation with  $-20\%$  of  $T_t$  are close with the responses that were obtained when nominal  $T_t$  was used (Figure 12), which proves that the proposed approach provides stability and robustness for the system.



**Figure 24.** Frequency and power deviation with  $-20\%$  of  $T_t$  using the eight techniques and base system.

#### 7.4. Real-Time Simulation

Real-time simulation with OPAL-RT 4510 validates the effectiveness of the integral controller designed in Simulink for the LFC in a multi-area interconnected grid. The model and controller are developed in Simulink, and OPAL-RT takes over. It translates the Simulink model into a real-time executable program running on its hardware. This enables real-time simulation, meaning the simulation runs at the same pace as the actual power system (typically in microseconds). In order to validate the proposed approach, we performed the simulation of case 1 in real-time simulation form and Figure 25 shows the experimental setup. The dynamic response which was achieved with the eight techniques and the base system dynamic response are shown in Figure 26.

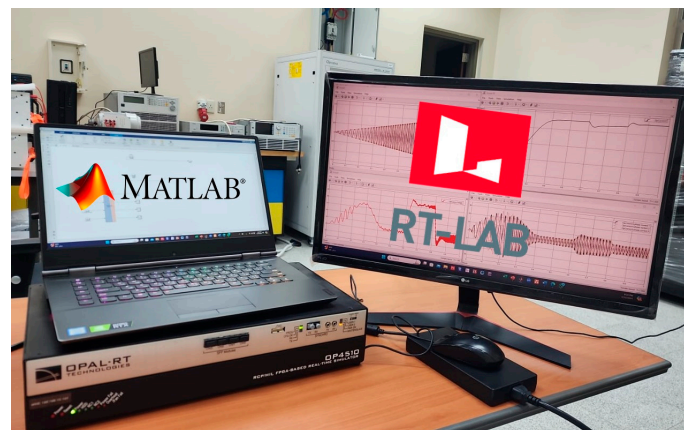


**Figure 25.** Experimental setup for case 1.

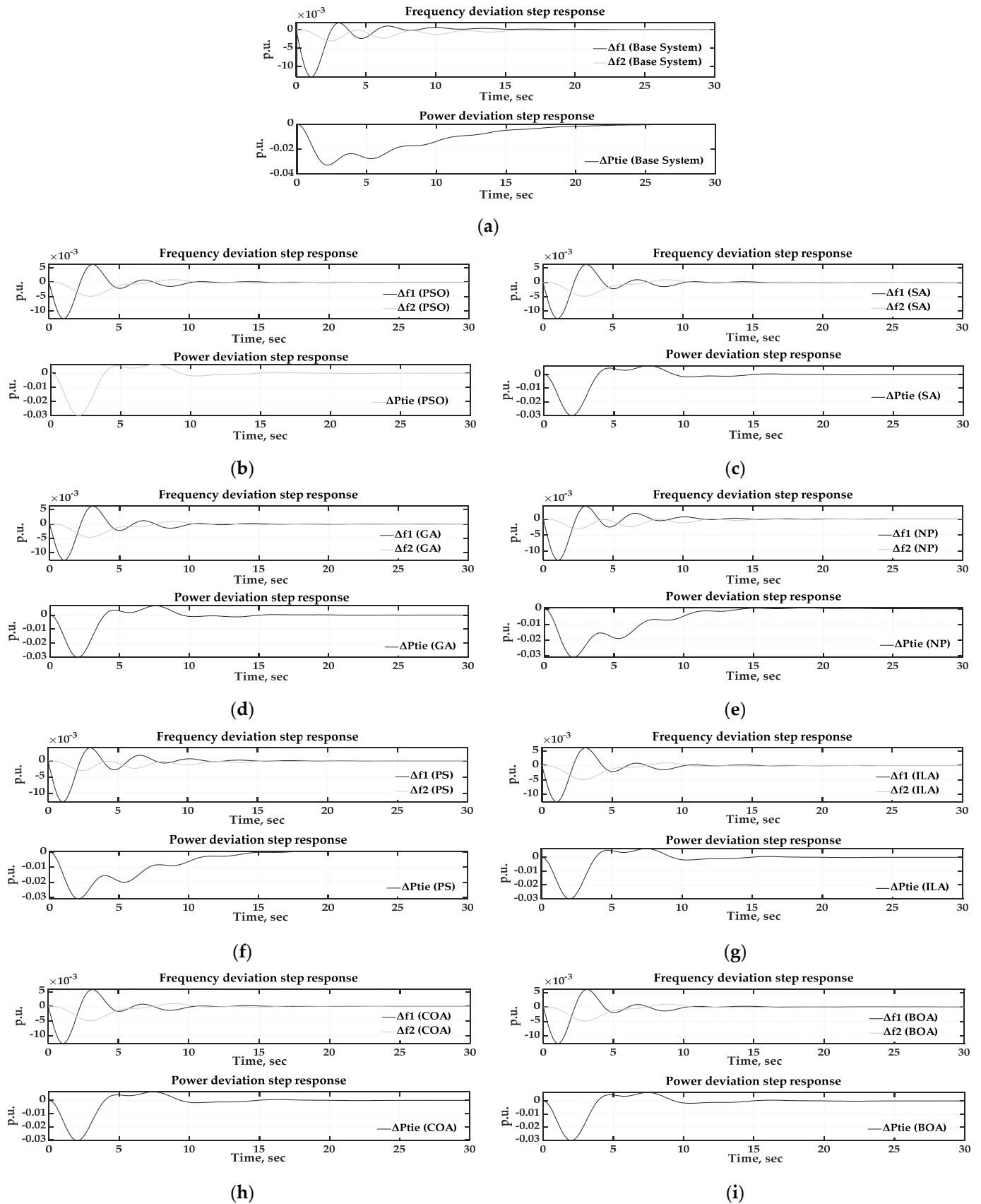


**Figure 26.** Frequency and tie-line power deviation response of the system using real-time simulation under case 1: (a) base system; (b) using PSO; (c) using SA; (d) using GA; (e) using NP; (f) using PS; (g) using ILA; (h) using COA; (i) using BOA.

As shown in Figure 26 above, the responses with used real-time simulation are identical with the responses that were obtained when MATLAB/Simulink only were used (Figure 12), which proves the effectiveness of the proposed approach.

### 7.5. Comparison Analysis

To show the effectiveness of the proposed approach, the performance of the eight techniques using  $J_1$  is compared with other published approaches for the same LFC model. The comparison performances are presented in Table 9. The comparative analysis is based on the scenario of a 20% step load change applied in area 1 at  $t = 0$  s. So, the optimization is repeated based on this scenario, and the parameters  $K_{I1}$ ,  $K_{I2}$ ,  $B_1$ , and  $B_2$  are tuned using the same procedure as described in Section 6.9. "Work Procedures using the Selected Techniques" using  $J_1$ . However, here, the maximum number of objective function evaluations allowed is set to 4100 for all algorithms, in order to shorten the algorithm's code elapsing time. It is worth noting that the performance of the techniques differs in each code's run due to the difference in the initial random values of ( $K_{I1}$ ,  $K_{I2}$ ,  $B_1$ , and  $B_2$ ) which are created by the techniques in each run. Therefore, the optimization process is repeated several times, and the best run is chosen. The new ( $K_{I1}$ ,  $K_{I2}$ ,  $B_1$ , and  $B_2$ ) obtained by the eight techniques are: PSO (1.7697, 1.7697, 4.7546, 3.3647), GA (1.7380, 1.7380, 4.9254, 3.2237), SA (1.7627, 1.7627, 4.7936, 3.3307), NP (0.3637, 0.3637, 16.2844, 10.7990), PS (0.4449, 0.4449, 16.9807, 10.4305), ILA (1.7582, 1.7582, 4.7596, 3.3465), COA (1.6756, 1.6756, 5.0596, 3.7506), and BOA (1.7453, 1.7453, 4.7118, and 3.3760).

**Table 9.** Dynamic performance characteristics under different approaches.

Approach	$T_S$ (s)			$M_P$ (p.u.)		
	$\Delta f_1$	$\Delta f_2$	$\Delta P_{tie}$	$\Delta f_1$	$\Delta f_2$	$\Delta P_{tie}$
PSO-(I)	9.9339	15.8398	14.0439	-0.0135	-0.0052	-0.0321
GA-(I)	9.9404	15.8417	14.1524	-0.0135	-0.0052	-0.0321
SA-(I)	9.9347	15.8368	14.0678	-0.0135	-0.0052	-0.0321
NP-(I)	10.9056	18.9035	14.8098	-0.0137	-0.0034	-0.0351
PS-(I)	10.9183	19.8930	13.7350	-0.0136	-0.0034	-0.0339
ILA-(I)	9.9457	15.8472	14.0854	-0.0135	-0.0050	-0.0322
COA-(I)	9.9068	15.9103	14.4053	-0.0135	-0.0050	-0.0322
BOA-(I)	9.9693	15.8702	14.1388	-0.0135	-0.0052	-0.0322
Classical-(I) [1]	14.36	22.93	24.64	-0.0137	-0.0033	-0.0350
PSO-(I) [2]	12.5	19.1	14.4	-0.0138	-0.0038	-0.0350
GA-(I) [2]	12.7	20.2	14.7	-0.0137	-0.0036	-0.0370
SA-(I) [2]	23.3	18.8	19.1	-0.0132	-0.0051	-0.0299
PSO-(Fuzzy + I) [52]	<u>5.30</u>	<u>8.80</u>	<u>6.60</u>	-0.0054	-0.0014	-0.0083
SA-(Fuzzy + I) [53]	<u>4.9699</u>	<u>8.7844</u>	<u>6.6326</u>	-0.0055	-0.0014	-0.0088
GA-(Fuzzy + I) [53]	<u>4.9660</u>	<u>8.7160</u>	<u>6.5738</u>	-0.0055	-0.0014	-0.0088
PS-(Fuzzy + I) [53]	<u>4.9639</u>	<b>8.7844</b>	<b>6.5597</b>	-0.0055	-0.0014	-0.0088
PSO-(FC FOPI-FOPD) [22]	<u>3.66</u> <sup>1</sup>	18.71	18.80	-0.04380	-0.00160	-0.00043
SA-(PID + Fuzzy) [11]	25.92	33.65	35.63	<b>-0.00078</b> <sup>2</sup>	-0.00135	-0.04921
SA-(PID) [11]	26.33	36.64	34.44	-0.00254	-0.00820	-0.13400
BA-(FC PI-PD) [54]	<u>2.19</u>	21.17	21.75	-0.04310	<b>-0.00099</b>	<b>-0.00027</b>
BA-(FPI + FPD) [54]	<u>7.06</u>	20.50	20.82	-0.03460	-0.00240	-0.00064
BA-(F-(PI + PD)) [54]	<u>2.14</u>	21.07	21.09	-0.07920	-0.00260	-0.00072
BA-(FPIDF) [55]	<u>6.94</u>	19.30	19.36	-0.04140	-0.00380	-0.00100
PSO-(FPIDF) [55]	<u>5.71</u>	19.10	19.15	-0.08900	-0.00360	-0.00100
TLBO-(FPIDF) [55]	<u>5.75</u>	19.33	18.89	-0.08680	-0.00360	-0.00099

<sup>1</sup> The underlined figures are better than all eight approaches. <sup>2</sup> The figures in bold are the best.

As seen in Table 9, no one approach showed its superiority over others. However, some approaches provided long settling times with low peak amplitude and vice versa. Also, some approaches provided short settling times for  $\Delta f_1$  and long for  $\Delta f_2$  and  $\Delta P_{tie}$ . But we can say that the approaches [52,53] provided a balanced performance. The proposed approach performed better than classic (I) [1] and optimized (I) [2]. Also, it performed better than SA-PID and SA-(PID + Fuzzy) [11] in terms of settling time. Moreover, the proposed approach performed satisfactorily when compared to the performance of intelligent and complex controllers used in other works, such as [22,54,55].

### 7.6. Extension to Two-Area Power System with GRC and GDB Nonlinearity

This work is expanded to a two-area power system with GRC and GDB nonlinearity to test the proposed approach's ability to deal with nonlinearity. The power change rate in a steam plant is constrained. If this rate is ignored, the LFC could face disturbances and significant transient variations. The settling time for a dynamic response with GRC characteristics is longer, and the peak overshoot is higher. Thus, the GRC has a significant impact on the dynamic efficiency of the LFC [56]. The range within which the LFC may permit the frequency to deviate without applying any controls is known as the dead band (backlash) [56]. The steam-turbine dead band is caused by backlash in the rod connecting the servo piston to the camshaft. Much of this appears to occur in the rack and pinion of the camshaft, which is utilized to move the control valve [10]. Appendix B depicts the system model with GRC and GDB nonlinearity, as well as the system parameters.

A 18.75% step load increase is applied in area 1 at  $t = 0$  s and the parameters  $K_{I1}$ ,  $K_{I2}$ ,  $B_1$ , and  $B_2$  are tuned using the same procedure as described in Section 6.9. "Work Procedures using the Selected Techniques" using  $J_1$ . The comparative performance for the power system with GRC and GDB nonlinearity results is shown in Table 10. The system dynamic responses are shown in Figures 27–29. It is noted from Table 10 that the proposed parameters of the eight techniques achieved better transient performances compared to the base system parameters. The PSO method achieved the minimum value of  $J_1$  and minimum ISE, which are 40.51 and 0.05504, respectively.

**Table 10.** Power system performance indices using GRC and GDB nonlinearity.

Parameters		Base System	PSO	SA	GA	NP	PS	ILA	COA	BOA
Controller parameters	$K_{I2}$	0.3	1.8860	1.7844	0.6432	0.6026	0.2931	1.8698	1.5361	1.8101
	$K_{I2}$	0.3	1.8860	1.7844	0.6432	0.6026	0.2931	1.8698	1.5361	1.8101
Frequency bias parameters	$B_1$	20.6	6.2518	6.6451	15.7887	12.9624	26.2597	6.3504	8.4208	6.2001
	$B_2$	16.9	4.2418	4.3802	7.8437	7.0519	11.6099	4.2987	4.8161	4.3092
ISE		0.10054	<b>0.05504</b>	0.05617	0.07044	0.07060	0.08177	0.05524	0.05858	0.05588
$J_1$		70.38	<b>40.51</b>	40.80	44.69	49.53	47.90	40.65	44.70	44.61
$T_s$ (s)	$\Delta f_1$	19.2756	13.2709	13.2310	12.6371	11.7070	<b>9.4935</b>	13.2578	16.2627	13.2518
	$\Delta f_2$	23.6847	<b>14.2634</b>	14.4524	16.9078	16.2390	20.5038	14.4045	15.0871	14.4121
	$\Delta P_{tie}$	27.1365	<b>12.7152</b>	12.8588	14.8887	21.3313	17.6410	12.7344	13.0982	16.6878
$M_p$ (p.u.)	$\Delta f_1$	<b>-0.0289</b>	-0.0290	-0.0290	<b>-0.0289</b>	<b>-0.0289</b>	<b>-0.0289</b>	-0.0290	<b>-0.0289</b>	-0.0290
	$\Delta f_2$	<b>-0.0211</b>	-0.0268	-0.0262	-0.0219	-0.0219	-0.0212	-0.0267	-0.0248	-0.0264
	$\Delta P_{tie}$	-0.1282	<b>-0.1160</b>	-0.1168	-0.1258	-0.1258	-0.1276	-0.1162	-0.1191	-0.1166

The figures in bold are the best.

It is observed from Table 10 that the value of ISE is high when the GRC and GDB are equipped in the system, because the peak amplitude for a dynamic response with GRC and GDB characteristics is higher, and a higher peak amplitude leads to higher ISE.

It can be seen from Figures 27–29 that the dynamic performance of the system is improved by the eight algorithms to optimize the parameters  $K_{I1}$ ,  $K_{I2}$ ,  $B_1$ , and  $B_2$  compared with the base system parameters in a case where GRC and GDB are connected. The settling time of  $\Delta f_1$ ,  $\Delta f_2$ , and  $\Delta P_{tie}$  are reduced when the eight optimization techniques are used. The minimum settling time of  $\Delta f_1$  was 9.4935 s, and it was obtained by PS. The lowest settling time of  $\Delta f_2$  was achieved by PSO and it equals to 14.2634 s. Also, PSO achieved the minimum settling time of  $\Delta P_{tie}$  which equals to 12.7152 s. The minimum peak amplitude of  $\Delta f_1$  is  $-0.0289$  (p.u.) and it is obtained by base system, COA, GA, NP, and PS. The minimum peak amplitude of  $\Delta f_2$  was  $-0.0211$  (p.u.) which was achieved by the base system. The minimum peak amplitude of  $\Delta P_{tie}$  was obtained by PSO and it is equal to  $-0.1160$  (p.u.).

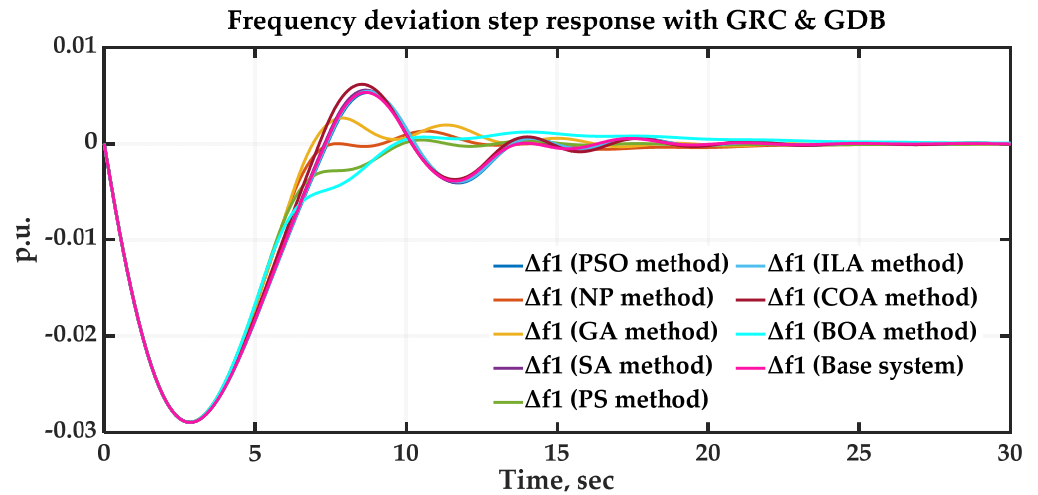


Figure 27. Area 1 frequency deviation response of the base system and using the eight techniques when GRC and GDB are connected.

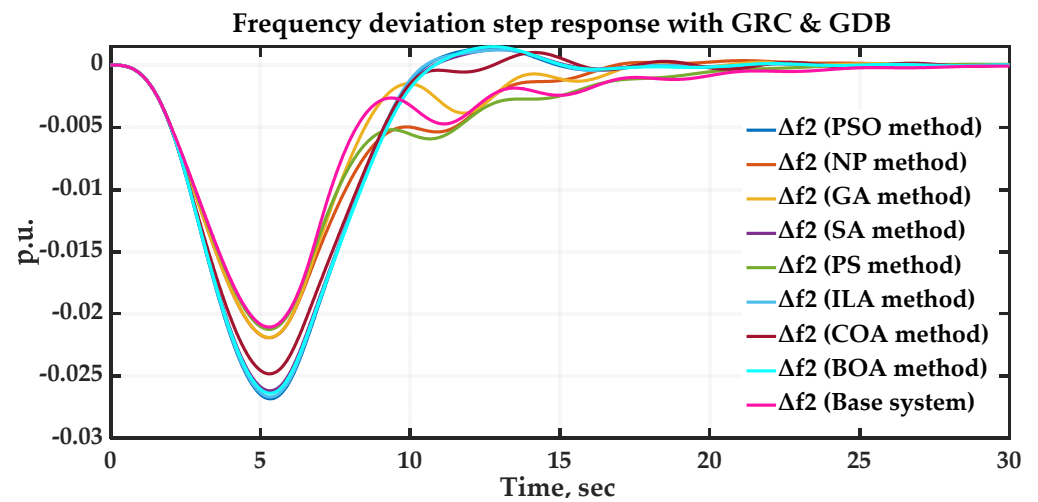


Figure 28. Area 2 frequency deviation response of the base system and using the eight techniques when GRC and GDB connected.

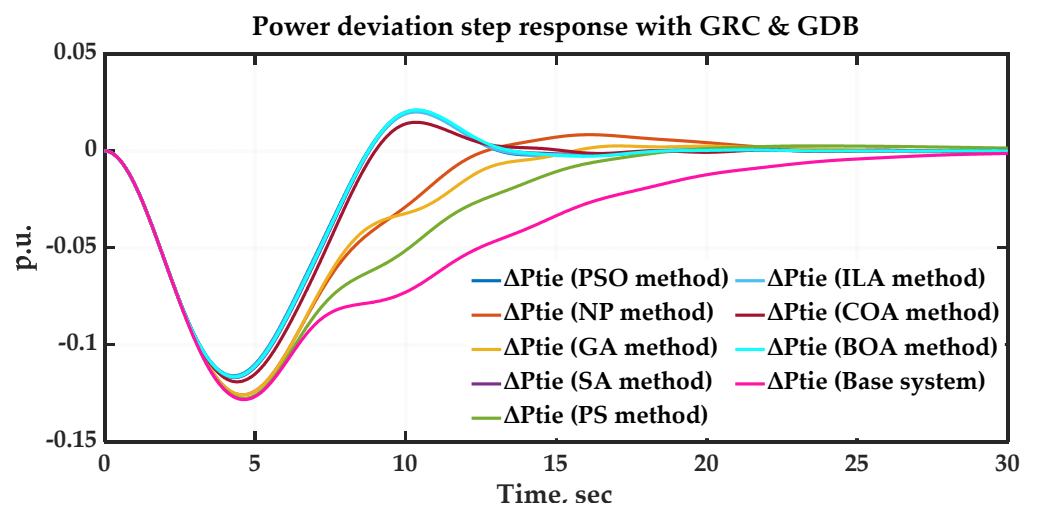


Figure 29. Tie-line power deviation response of the base system and using the eight techniques when GRC and GDB connected.

Three extra cases of the input disturbance are investigated to analyze the system's dynamic response using the suggested approach using the same values of  $K_{I1}$ ,  $K_{I2}$ ,  $B_1$ , and  $B_2$ , that are obtained in the case of a 18.75% input disturbance occurring in area 1. The four case results are listed in Table 11.  $J_1$  and ISE are used as the performance index to compare between the techniques.

**Table 11.**  $J_1$  and ISE results of various cases with GRC and GDB nonlinearity.

Technique	Case 1: $\Delta P_{D1} = 0.1875$ (p.u.) and $\Delta P_{D2} = 0.0$ (p.u.)		Case 2: $\Delta P_{D1} = 0.0$ (p.u.) and $\Delta P_{D2} = 0.1875$ (p.u.)		Case 3: $\Delta P_{D1} = 0.1875$ (p.u.) and $\Delta P_{D2} = 0.1875$ (p.u.)		Case 4: $\Delta P_{D1} = 0.1$ (p.u.) and $\Delta P_{D2} = -0.2$ (p.u.)	
	$J_1$	ISE	$J_1$	ISE	$J_1$	ISE	$J_1$	ISE
Base System	70.38	0.1005	68.50	0.1003	<b>65.84</b>	0.0384	75.11	0.1765
PSO	<b>40.51</b>	<b>0.0550</b>	69.29	0.0701	76.16	0.0390	84.07	0.1332
SA	40.80	0.0562	60.39	0.0711	75.63	0.0390	80.84	0.1299
GA	44.69	0.0704	61.90	0.0909	70.33	0.0398	61.63	0.1398
NP	49.53	0.0706	<b>59.56</b>	0.0851	67.08	0.0394	<b>61.38</b>	0.1384
PS	47.90	0.0818	73.25	0.1239	75.81	0.0502	76.26	0.1964
ILA	40.65	0.0552	69.31	0.0704	76.35	0.0389	83.97	0.1329
COA	44.70	0.0586	63.33	0.0774	75.77	0.0401	72.90	<b>0.1286</b>
BOA	44.61	0.05509	60.17	<b>0.0689</b>	71.27	<b>0.0383</b>	76.76	<b>0.1286</b>

The figures in bold are the best.

For case 1,  $J_1$  and ISE have the minimum value when PSO used. BOA obtained the minimum ISE for case 2, while the minimum  $J_1$  is obtained by NP. Unexpectedly, the eight techniques were not superior in performance than the base system in case 3, based on the value of  $J_1$ , but minimum ISE for case 3 was obtained by BOA. In case 4, NP obtained minimum  $J_1$ , while minimum ISE was obtained by COA and BOA. It is clear from the results of this investigation that the performance of the eight techniques was better in the case of GRC and GDB unconnected. So, it is better to reset the values of  $K_{I1}$ ,  $K_{I2}$ ,  $B_1$ , and  $B_2$  to obtain a high performance when the load circumstances change.

### 7.7. Extension to Three-Area Power System

This work is expanded to a three-area power system to test the proposed approach's ability to deal with multi-areas interconnected power systems. The system model of the three-area power system and the relevant parameters are shown in Appendix C.

In area 1, a 10% step load increase is performed at  $t = 0$  s, and the parameters  $K_{I1}$ ,  $K_{I2}$ ,  $K_{I3}$ ,  $B_1$ ,  $B_2$ , and  $B_3$  are adjusted using the same approach as stated in Section 6.9. "Work Procedures using the Selected Techniques" using  $J_1$ . The comparative performance for the system dynamic responses using the eight techniques is shown in Table 12.

**Table 12.** The optimization results of the eight techniques for three-area power system.

Technique	$K_{I1}$	$K_{I2}$	$K_{I3}$	$B_1$	$B_2$	$B_3$	ISE	$J_1$
PSO	1.1252	1.1252	1.1252	3.1316	3.6805	6.1879	0.001749	75.96
SA	1.6882	1.6882	1.6882	2.2675	3.0815	3.7792	0.001459	73.10
GA	0.6877	0.6877	0.6877	7.4116	14.9009	9.1471	0.001939	82.48
NP	1.1285	1.1285	1.1285	3.0091	3.5948	6.1789	0.001779	75.98
PS	0.6228	0.6228	0.6228	8.2767	5.9224	8.8687	0.001952	86.46
ILA	1.6372	1.6372	1.6372	2.4201	3.1168	3.8597	0.001448	<b>72.46</b>
COA	1.1738	1.1738	1.1738	3.6764	3.9310	5.4809	0.001543	76.83
BOA	1.7860	1.7860	1.7860	2.5605	2.7397	3.0952	<b>0.001401</b>	80.19

The figures in bold are the best.

As seen in Table 12, the ILA technique established its superiority over others based on  $J_1$ . ILA achieved the minimum value of  $J_1$  which is equal to 72.46 but the lowest ISE was

achieved by BOA with value equals to 0.001401. However, PS obtained the highest values of  $J_1$  and ISE. The system dynamic response curves are shown in Figure 30.

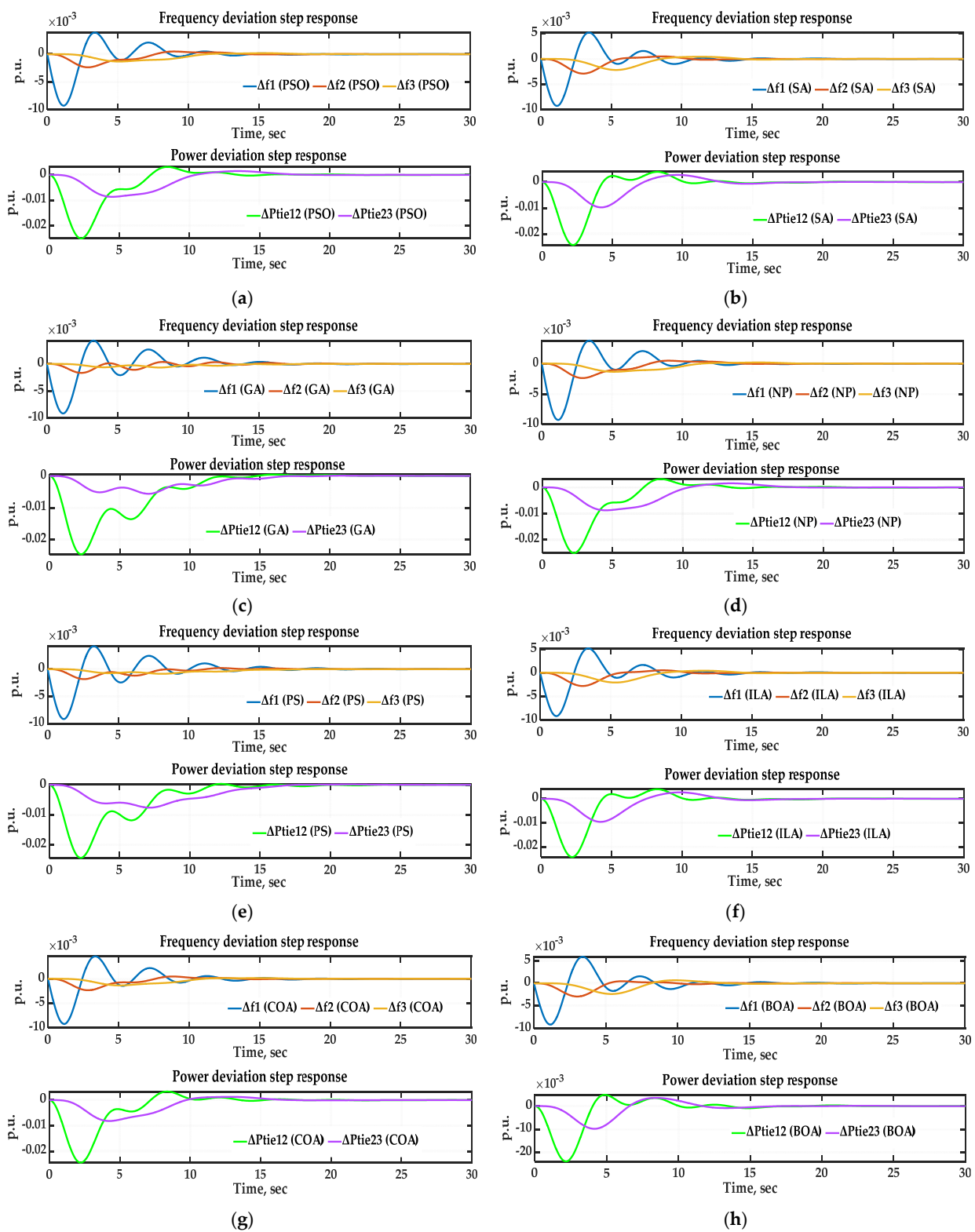


**Figure 30.** Frequency and tie-line power deviation response of the three-area power system: (a) using PSO; (b) using SA; (c) using GA; (d) using NP; (e) using PS; (f) using ILA; (g) using COA; (h) using BOA.

In Figure 30 above, no technique obtains the best values for all performance characteristics. Also, it is clear from Figure 30 that the values of the settling-max and the settling-min of  $\Delta P_{tie12}$  are bigger than the values of  $\Delta P_{tie23}$  because the load increase was applied in area 1 that also causes an increase in the values of the settling-max and the settling-min of  $\Delta f_1$ .

In the case of a 10% step load increase in area 1 at  $t = 0$  s, the performance of the proposed approach is compared with the previous LFC approaches for the same three-area power system published in the literature, as shown in Table 13.

**Table 13.** Performance indices under different approaches for three-area power system.

Approach	$T_s$ (s)					$ MP $ (p.u.)				
	$\Delta f_1$	$\Delta f_2$	$\Delta f_3$	$\Delta P_{tie12}$	$\Delta P_{tie23}$	$\Delta f_1$	$\Delta f_2$	$\Delta f_3$	$\Delta P_{tie12}$	$\Delta P_{tie23}$
PSO-I	13.72	13.83	18.05	12.85	17.45	0.0093	0.0024	0.0013	0.0249	0.0086
SA-I	14.28	13.50	17.54	10.80	16.93	<b>0.0092</b>	0.0029	0.0022	0.0243	0.0098
GA-I	15.94	20.31	17.90	11.67	16.61	<b>0.0092</b>	<b>0.0017</b>	<b>0.0007</b>	0.0245	<b>0.0056</b>
NP-I	<b>13.68</b>	13.87	18.10	12.83	17.46	0.0093	0.0024	0.0013	0.0250	0.0087
PS-I	19.09	17.33	18.26	14.85	16.88	<b>0.0092</b>	0.0018	0.0009	0.0245	0.0076
ILA-I	14.30	13.48	17.55	<b>9.89</b>	17.19	<b>0.0092</b>	0.0028	0.0021	0.0243	0.0096
COA-I	14.07	15.71	17.63	13.02	16.35	<b>0.0092</b>	0.0023	0.0013	0.0245	0.0082
BOA-I	16.33	13.94	17.69	15.98	<b>16.17</b>	<b>0.0092</b>	0.0029	0.0024	<b>0.0238</b>	0.0098
PI [57]	33	21	30	40	50	0.0900	0.0170	0.0050	0.2400	0.0700
PID [57]	28	20	27	35	35	0.0300	0.0060	0.0030	0.1350	0.0350
ANN [57]	14	<b>12</b>	<b>12</b>	17	37	0.0300	0.0020	0.0010	0.0400	0.0070

The figures in bold are the best.

The performance indices show that the performance of the proposed approach is better than the classic PI and PID controllers [57]. Also, the proposed approach outperformed an artificial neural network (ANN) controller [57] in some performance indices, as shown in Table 13, which proves the ability of the proposed approach to deal with multi-area interconnected power systems.

### 7.7.1. Investigation of Additional Cases

Two extra cases of the input disturbance are investigated to analyze the system's dynamic response using the suggested approach with the same values of  $K_{I1}$ ,  $K_{I2}$ ,  $K_{I3}$ ,  $B_1$ ,  $B_2$ , and  $B_3$  that are obtained in the case of a 10% step load increase in area 1 at  $t = 0$  s. The two scenarios of the change in load powers have been examined as:

1. Case 1: a 5% ramp load increase in area 2 from  $t = 0$  to  $t = 10$  s;
2. Case 2: a pulse load disturbance of 20% magnitude and 5 s duration in area 3 at  $t = 15$  s.

#### Case 1: Ramp Load

In this case, area 2 is subjected to a 5% ramp load increase from  $t = 0$  to  $t = 10$  s, with a slope equals to 0.02, so in  $t = 10$  s the load has increased by 25%, as shown in Figure 31. The system dynamic response curves in the case of area 2 subjected to a ramp load are shown in Figure 32.

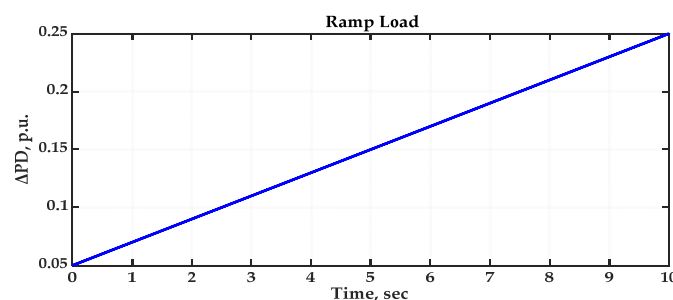


**Figure 31.** Ramp load pattern.

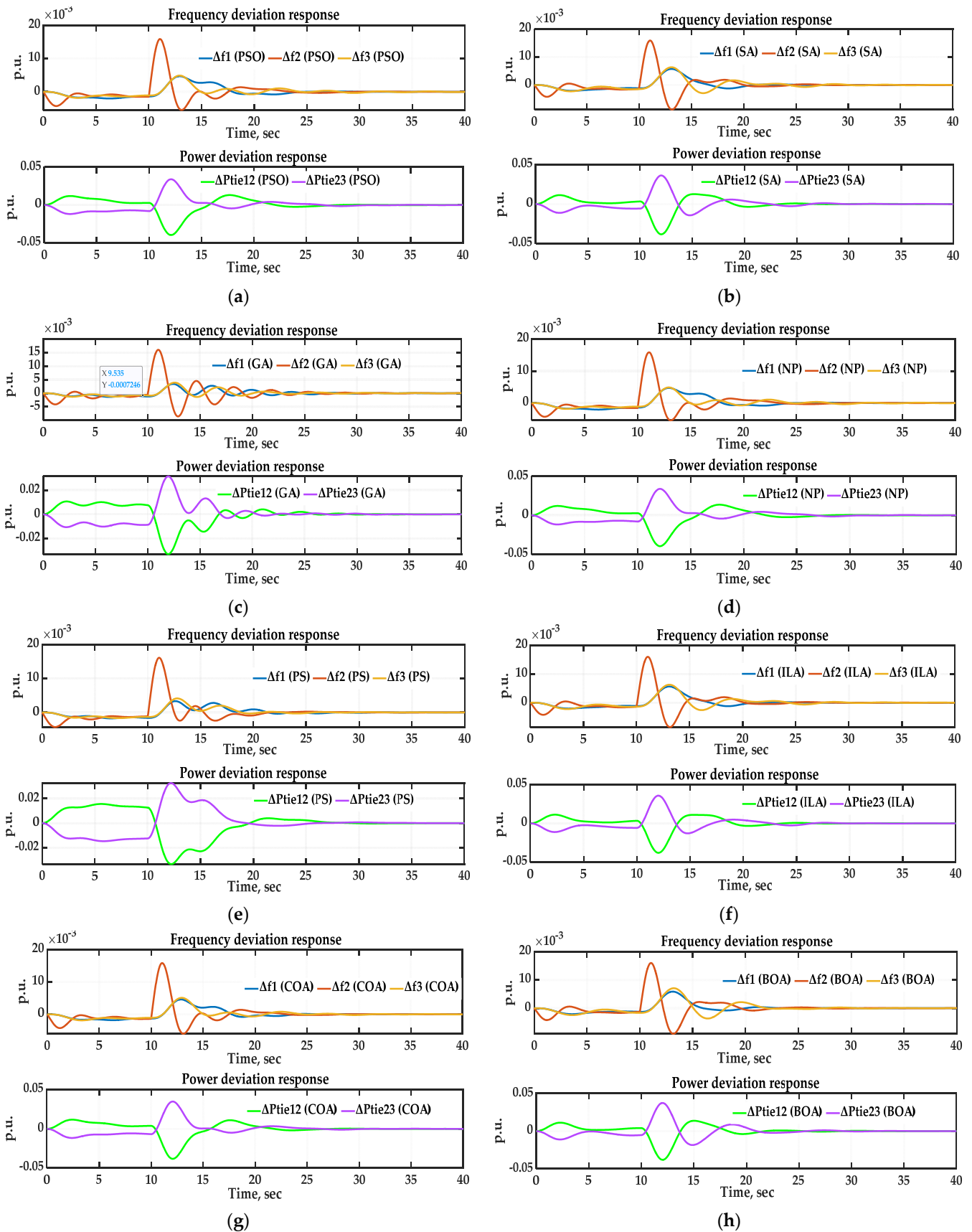


**Figure 32.** Frequency and power deviation responses for three-area system subjected to a ramp load: (a) using PSO; (b) using SA; (c) using GA; (d) using NP; (e) using PS; (f) using ILA; (g) using COA; (h) using BOA.

As seen in Figure 32 above, all system's responses were able to achieve stability in an acceptable span of time after the end of the ramp load. Also, the peak amplitudes of responses were reasonable. Furthermore, the frequency and power variations were acceptable during the period of increasing load from second 0 to second 10 and the drop in frequency was reasonable. Because the load was increasing and the period was extremely short, the frequency response that was obtained with various techniques was not able to reach the steady state during the period load, since the response time of an integral controller is not very fast, so if the period of the ramp load is longer than 10 s, the LFC's response will be able to reach the steady state. For instance, if area 2 is subjected to a 5% ramp load increase from  $t = 0$  to  $t = 20$  s, with a slope equal to 0.01, the dynamic response of LFC using BOA will be as shown in Figure 33.

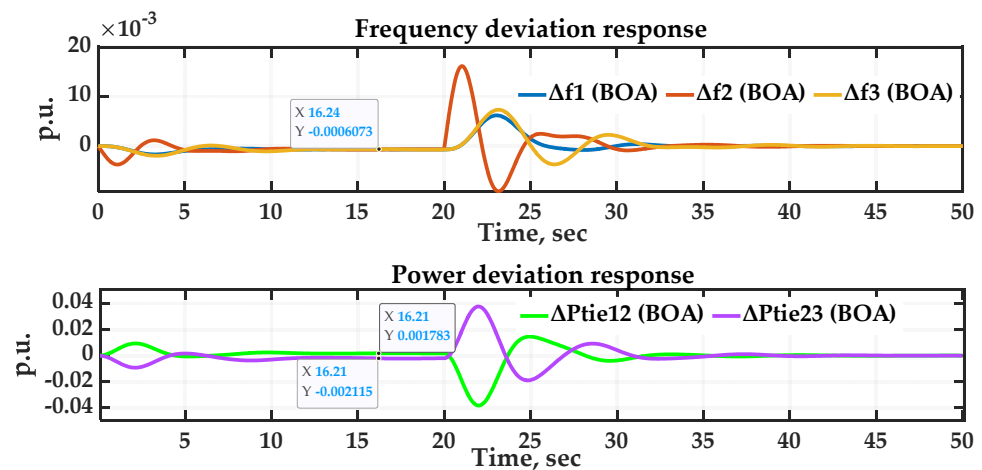


**Figure 33.** Frequency and power deviation responses using BOA for three-area system subjected to a ramp load.

As seen in Figure 33 above, the response during the period of increasing load from second 0 to second 20 reached the steady state with  $\Delta f_i$  equal to  $\sim(-0.00061$  p.u.), i.e., the steady state frequency of the system equals to  $\sim(59.96$  Hz). The steady state  $\Delta P_{tie12}$  equals  $\sim(0.0018$  p.u.), i.e., (1.8 MW) flows from area 1 to area 2. The steady state  $\Delta P_{tie23}$  equals  $\sim(-0.0021$  p.u.), i.e., (2.1 MW) flows from area 3 to area 2. In the end of the ramp load (in the  $t = 20$  s), the system's response entered a state of oscillation as a result of the sudden decrease in the load, then the system restored its normal state with  $\Delta f_i$  and  $\Delta P_{tieij}$  equal to  $\sim 0$ .

#### Case 2: Pulse Load

In this case, area 3 is subjected to a pulse load disturbance of 20% magnitude and 5 s duration in area 3 at  $t = 15$  s, as shown in Figure 34.

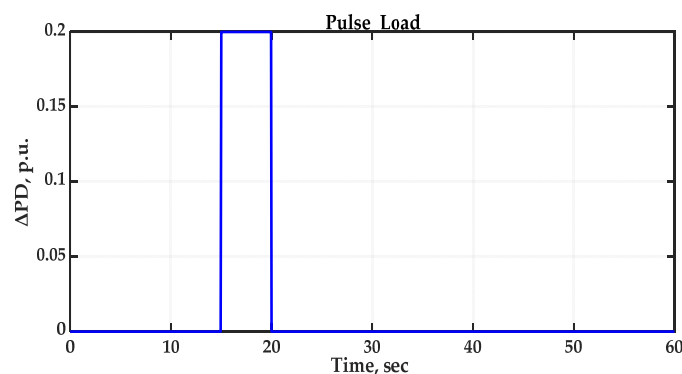


**Figure 34.** Pulse load pattern.

The system dynamic response curves of the eight techniques in the case of area 3 subjected to a pulse load using the same values of  $K_{I1}$ ,  $K_{I2}$ ,  $K_{I3}$ ,  $B_1$ ,  $B_2$ , and  $B_3$  that are obtained in the case of a 10% step load increase in area 1 at  $t = 0$  s are shown in Figure 35.

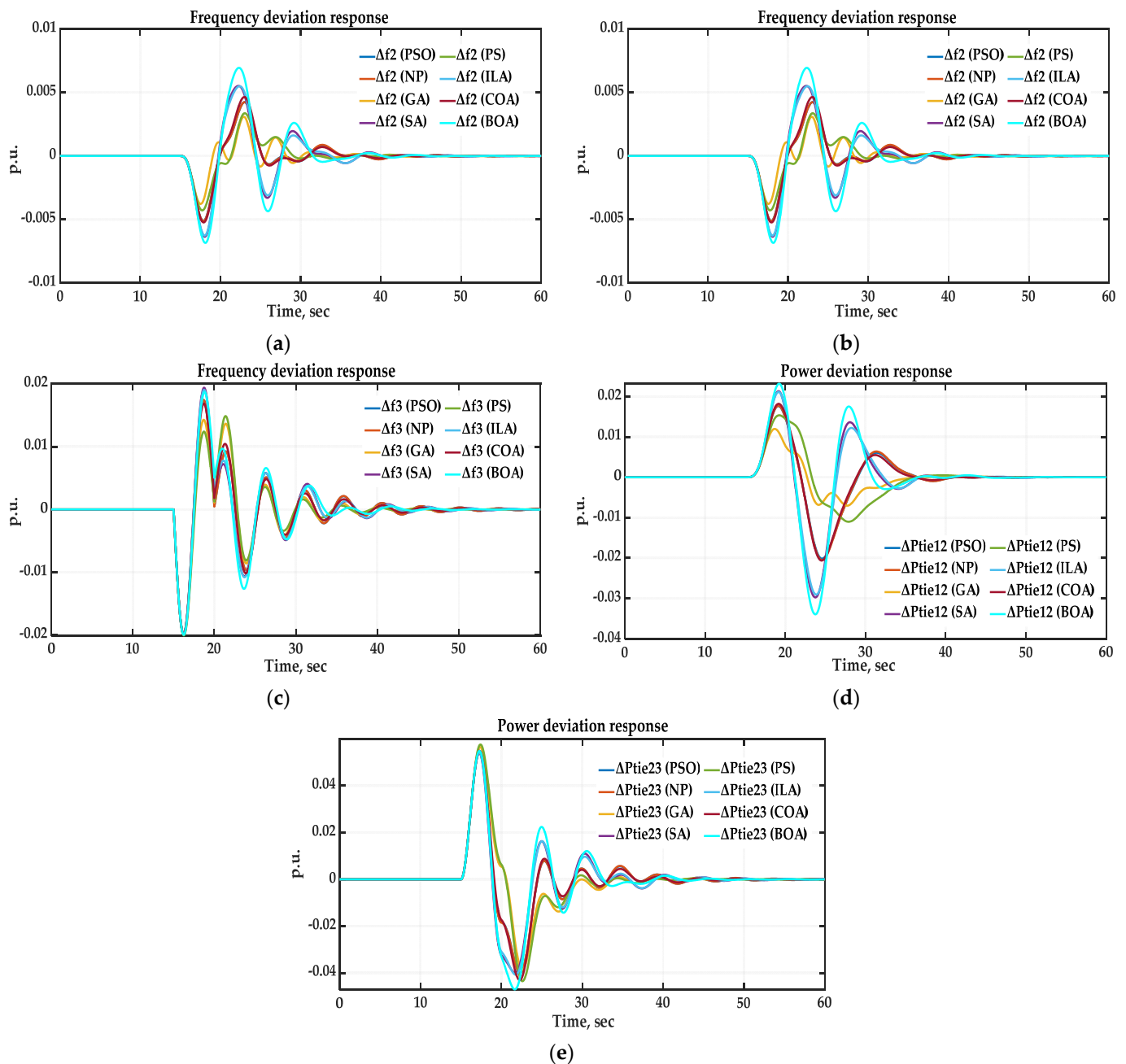


**Figure 35.** Dynamic response curves using various techniques for case 2: (a) frequency deviation of area 1; (b) frequency deviation of area 2; (c) frequency deviation of area 3; (d) tie-line 12 power deviation; (e) tie-line 23 power deviation.

As shown in Figure 35, the response obtained with the various techniques were not able to reach the steady state during the period load from 15 s to 20 s, because the load period was very short, so there was insufficient time for the integrated controller to restore the system to its normal state. Also, the system's response entered a state of oscillation as a result of the sudden increase and decrease in the load within 5 s with a large magnitude, then the system was restored to its normal state and oscillations vanished. In this situation, the GA approach obtained the minimum values of settling-max and settling-min of the

response. However, the PS approach obtained the minimum values of the settling time of the response. It is worth mentioning that if the load period is extended and the parameters  $K_{I1}$ ,  $K_{I2}$ ,  $K_{I3}$ ,  $B_1$ , and  $B_2$  are reset, then the response will be improved. Since the parameters  $K_{I1}$ ,  $K_{I2}$ ,  $K_{I3}$ ,  $B_1$ , and  $B_2$  are obtained in case of a 10% step load increase in area 1 at  $t = 0$  s, so they will give a better performance when the load changes occur in area 1. For instance, if area 1 was subjected to a periodic pulse load of 20% magnitude and 20 s duration at  $t = 15$ , the system dynamic response curves when using  $K_{I1}$ ,  $K_{I2}$ ,  $K_{I3}$ ,  $B_1$ , and  $B_2$  that ILA obtained will be as shown in Figure 36.

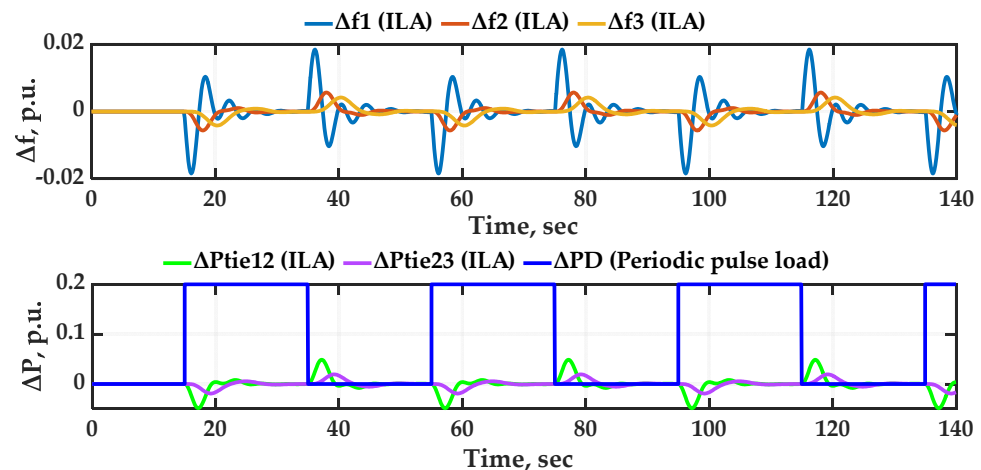


**Figure 36.** Frequency and power deviation responses using ILA for three-area system when area 1 subjected to a periodic pulse load.

As illustrated in Figure 36, the integral controller optimized by ILA restored the frequency and tie-line power deviations to zero every time the load change occurs. Also, the settling-min and the settling-max of the frequency and tie-line power deviations were reasonable. This demonstrates that the proposed approach enhanced LFC performance and stability.

### 7.8. Extension to Three-Area Power System with RESs, BESS, and EVs

According to the new international grid codes, ancillary services from RESs are critical [58]. Also, the ability to support ancillary services from EVs is checked here [59]. Furthermore, the energy storage system helps in enhancing the generated energy to minimize the time consumed by the system to be stable [29]. Hence, the power system's stability is increased when RESs, EVs, and BESS are connected to it. The work is expanded to a three-area multi sources power system comprising RESs such as PV and WT, BESS, and EVs to test the proposed approach's ability to deal with modern power systems. The architecture of the multi-interconnected system is shown in Figure 37 and Appendix D depicts the system Simulink model, as well as the system parameters.

In area 1, a 1% step load increase is performed at  $t = 0$  s, and the parameters  $K_{I1}$ ,  $K_{I2}$ ,  $K_{I3}$ ,  $B_1$ ,  $B_2$ , and  $B_3$  are adjusted using the same approach as stated in Section 6.9. "Work Procedures using the Selected Techniques" using  $J_1$ . However, here the maximum number of objective function evaluations allowed is set to 1500 for all algorithms, in order to shorten the algorithm's code's elapsing time and to demonstrate the power of the techniques in obtaining the optimal solutions in a short time. The comparative performance for the system dynamic responses using the eight techniques is shown in Table 14.

As seen in Table 14, the PSO technique established its superiority over others based on  $J_1$ . PSO achieved the minimum value of  $J_1$  which is equal to 100.96 but the lowest ISE achieved by NP with value equals  $6.87 \times 10^{-5}$ . The system dynamic response curves are shown in Figure 38.

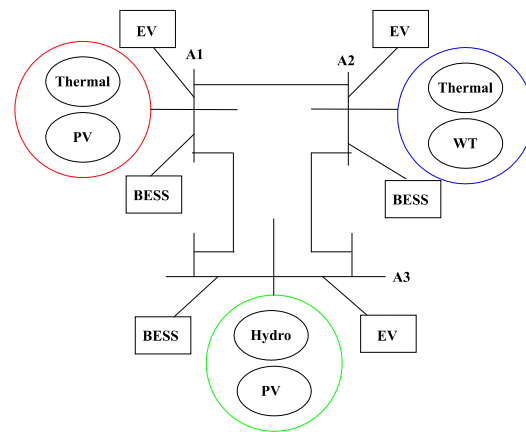


Figure 37. Architecture of the multi-interconnected system.

Table 14. The optimization results for the hybrid three-area multi sources power system.

Technique	$K_{I1}$	$K_{I2}$	$K_{I3}$	$B_1$	$B_2$	$B_3$	ISE	$J_1$
PSO	0.03384	1.94294	0.03384	0.850	0.2129	0.850	$8.9181 \times 10^{-5}$	<b>100.9638</b>
SA	0.0323	1.5551	0.0323	0.6296	0.4673	0.8212	$8.5452 \times 10^{-5}$	107.7549
GA	0.0333	1.9467	0.0333	0.8458	0.2394	0.8438	$8.8250 \times 10^{-5}$	101.9809
NP	0.0806	1.9610	0.0806	0.8471	0.2236	0.8469	<b><math>6.8667 \times 10^{-5}</math></b>	115.8080
PS	0.0239	2	0.0239	0.850	0.4721	0.850	$9.2679 \times 10^{-5}$	103.1253
ILA	0.03386	1.93533	0.03386	0.8467	0.2731	0.850	$8.5733 \times 10^{-5}$	101.5580
COA	0.0345	1.3613	0.0345	0.8480	0.3733	0.8486	$8.0483 \times 10^{-5}$	105.1183
BOA	0.0329	2	0.0329	0.850	0.3142	0.850	$8.4824 \times 10^{-5}$	103.5926

The figures in bold are the best.

To evaluate the role of RESs, EVs, and BESS in improving system stability, the performance of the proposed approach is compared with the previous LFC approaches for the same three-area power system that did not comprise RESs, BESS, and EVs. Table 15 shows the comparative analysis which is based on the scenario of a 1% step load change applied in area 1 at  $t = 0$  s.

Table 15. Performance indices under different approaches for the hybrid three-area multi sources power system.

Approach	$T_s$ (s)						$M_p$ (p.u.)					
	$\Delta f_1$	$\Delta f_2$	$\Delta f_3$	$\Delta P_{tie12}$	$\Delta P_{tie23}$	$\Delta P_{tie31}$	$\Delta f_1$	$\Delta f_2$	$\Delta f_3$	$\Delta P_{tie12}$	$\Delta P_{tie23}$	$\Delta P_{tie31}$
PSO-I	<b>3.8266</b>	<b>6.7898</b>	20.8501	18.9802	25.1381	25.3582	<b>-0.0086</b>	-0.0035	-0.0020	-0.0018	-0.0011	0.0021
SA-I	4.3288	8.8382	21.8485	19.6727	26.8208	26.2262	<b>-0.0086</b>	<b>-0.0027</b>	-0.0019	-0.0018	<b><math>-7.6 \times 10^{-4}</math></b>	0.0021
GA-I	3.8861	7.0237	20.9949	19.1257	25.4070	25.5229	<b>-0.0086</b>	-0.0034	-0.0020	-0.0018	-0.0011	0.0021
NP-I	13.1198	8.2079	22.7942	20.8550	25.3804	25.4282	<b>-0.0086</b>	-0.0032	<b>-0.0017</b>	<b>-0.0017</b>	$-9.4 \times 10^{-4}$	<b>0.0018</b>
PS-I	5.4319	12.2056	<b>17.0133</b>	22.0038	<b>23.4332</b>	<b>23.0181</b>	<b>-0.0086</b>	-0.0028	-0.0018	-0.0018	$-7.8 \times 10^{-4}$	0.0022
ILA-I	3.8326	7.0812	20.9126	18.9819	25.3708	25.3584	<b>-0.0086</b>	-0.0033	-0.0019	-0.0018	-0.0010	0.0021
COA-I	7.0692	7.5765	20.9911	<b>18.7657</b>	25.5157	25.1803	<b>-0.0086</b>	<b>-0.0027</b>	<b>-0.0017</b>	-0.0019	$-8.5 \times 10^{-4}$	0.0021
BOA-I	3.9082	7.9039	21.1257	19.2366	25.7833	25.6147	<b>-0.0086</b>	-0.0032	-0.0019	-0.0018	$-9.6 \times 10^{-4}$	0.0021
PSO-I (without RESs, EVs, and BESS)	22.3600	21.3068	23.0205	34.7416	35.1696	36.5877	-0.0241	-0.0246	-0.0235	-0.0054	0.0023	0.0048
Fuzzy [60] (without RESs, EVs, and BESS)	50	50	50	50	50	50	-0.071	-0.071	-0.080	0.033	-0.033	-0.033
ANN [60] (without RESs, EVs, and BESS)	35	35	45	45	45	45	-0.037	-0.037	-0.055	0.0065	-0.0065	-0.0065
ANFIS [60] (without RESs, EVs, and BESS)	30	30	27	40	40	40	-0.035	-0.035	-0.050	0.0060	-0.022	-0.022

The figures in bold are the best.

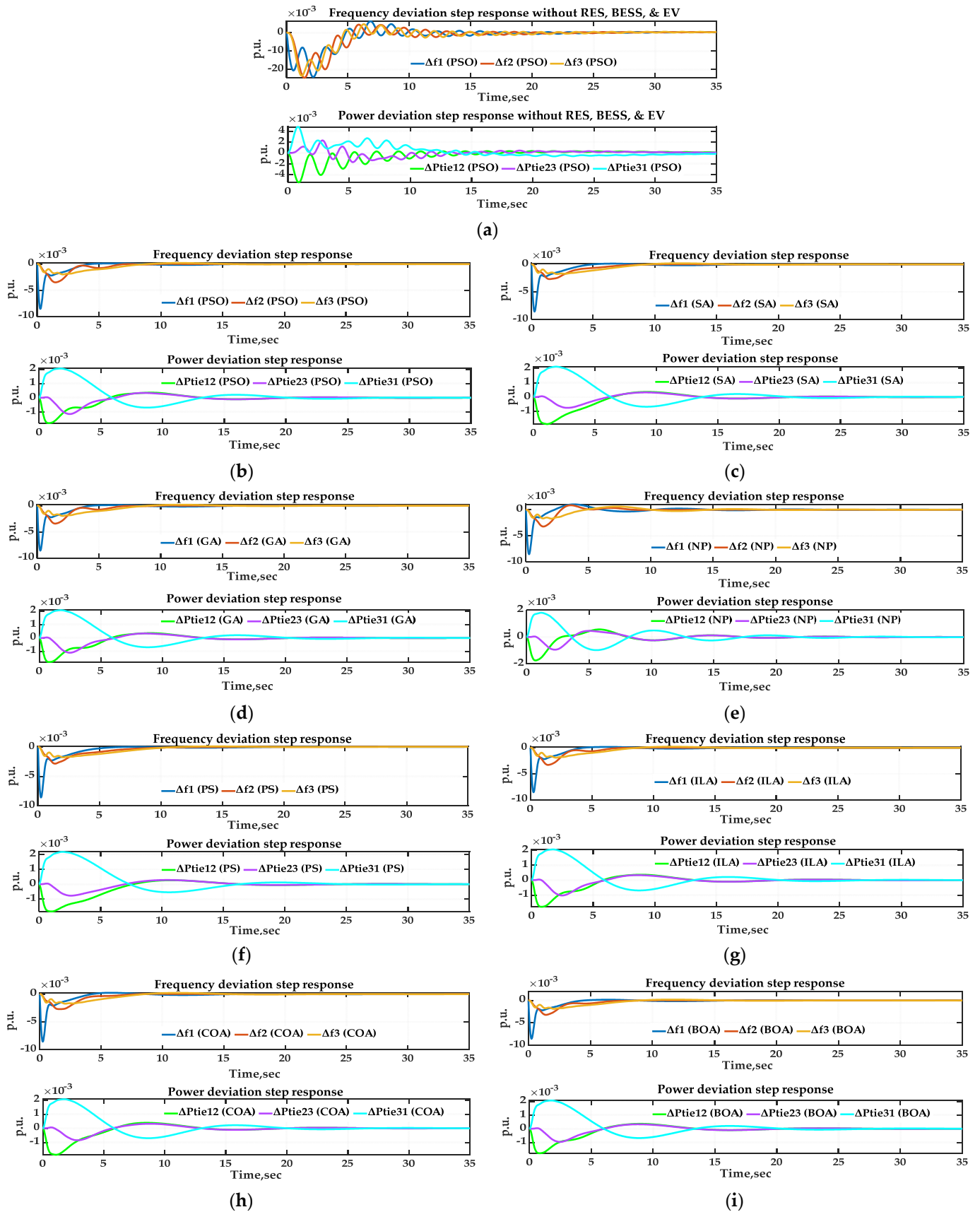


**Figure 38.** Frequency and tie-line power deviation response of the hybrid three-area multi sources power system: (a) using PSO (in the case of RESs, EVs, and BESS unconnected); (b) using PSO; (c) using SA; (d) using GA; (e) using NP; (f) using PS; (g) using ILA; (h) using COA; (i) using BOA.

It is clear from Table 15 that the RESs, EVs, and BESS contributed to a greater system stability. Also, in the case of RESs, EVs, and BESS unconnected, the performance of PSO-I is better than fuzzy, ANN, and fuzzy-based adaptive neuro-fuzzy inference system (ANFIS) controllers [60], which proves the ability of the proposed approach.

Figure 38 clearly shows that the RESs, EVs, and BESS all contributed to better system stability. The oscillations have diminished somewhat. Also, the settling time is reduced, allowing the response to reach a steady state in a shorter time. Furthermore, the values of the settling-max and the settling-min are improved.

### 7.9. Summary of the Results

The parameters of integral controller and frequency bias are selected by the eight optimization techniques and with the help of the proposed objective function improved the control effect. Also, different cases are used to describe the behavior of frequency and tie-line power flow deviations in the presence of the load perturbation as well as the system's robustness to changes in the loading conditions and system parameters is tested. Furthermore, real-time simulation is applied. This deep analysis proved that designing of an LFC for a two-area, non-reheat thermal system using an integral controller based on PSO, GA, SA, PS, NP, ILA, COA, and BOA approaches could provide an adequate LFC's response while reducing the implementation time and costs since integral controller available commercially and easily to impletion. Moreover, the proposed approach is implied in a two-area power system with GRC and GDB nonlinearity, in a three-area system power system, and the results are positive. It is capable of handling nonlinearity and could control a multi-area system. Finally, the comparative analysis for the eight optimization techniques is determined based on the value of  $J_1$  as follows:

- PSO proved its superiority for tuning the optimal parameters of integral controller and frequency bias by minimize the value of the objective function for two-area power system with/without GRC and GDB nonlinearity while NP showed its advantage with changing load powers. Moreover, ILA outperformed the other techniques with regard to the robustness analysis.
- For the three-area power system, ILA performs the best in dealing with tuning the optimal parameters of the integral controller and frequency bias by minimizing the value of the objective function.
- For hybrid three-area multi sources power system with RESs, BESS, and EVs, PSO performs the best in dealing with tuning the optimal parameters of the integral controller and frequency bias by minimizing the value of the objective function.

## 8. Conclusions

The purpose of this study is to identify the characteristics and optimal design of an LFC for a two-area, non-reheat thermal power system with an integrated controller. In this study, we have proposed a new objective function to determine the integral controller and frequency bias parameters of the secondary loop in LFC. Moreover, we have investigated eight optimization techniques to optimize these parameters, namely PSO, GA, SA, PS, NP, ILA, COA, and BOA. The proposed objective function in the presented paper outperformed the well-known integral time multiply absolute error. To the best of the authors' knowledge, no attempt has been made to use NP, ILA, COA, and BOA in designing LFCs. Moreover, unlike the literature, the design of the LFC using an integral controller with optimal tuning for integral and frequency bias was deeply analyzed.

To show the performance of the proposed controller, several cases have been tested under different scenarios of load disturbances. These scenarios are as follows: step load change in area 1; step load change in area 2; step load change in both areas; step load increment in area 1; and step load decrement in area 2. The dynamic performance of the proposed parameters is compared to the base system parameters' dynamic performance, and the proposed parameters achieved superiority. Consider the following scenario: a load change in area 1 by 0.1875 (p.u.) at  $t = 0$  s. The proposed controller achieved the lowest

ISE values. ISE values were: 0.005816, 0.001792, 0.001755, 0.001781, 0.003205, 0.003035, 0.001793, 0.001845, and 0.001814, with regard to classic I, PSO-I, GA-I, SA-I, PS-I, NP-I, ILA-I, COA-I, and BOA-I. Sensitivity analysis is used to demonstrate the robustness of the proposed parameters under varying load conditions and system parameters, and the outcomes were positive. Then, the proposed approach was extended to a two-area power system with the GRC and the GDB nonlinearity, and the results illustrated that the proposed approach is capable of handling nonlinearity. In the case of a load change in area 1 by 18.75% at  $t = 0$  s, PSO-I achieved the lowest ISE value equal to 0.0550 while classic I obtained 0.1005. After that, the proposed technique was tested in a three-area power system, and the results revealed that it sustains better performance than the standard PI and PID controllers. For example, ILA-I obtained settling times for  $(\Delta f_1, \Delta f_2, \Delta f_3, \Delta P_{tie12}, \Delta P_{tie23})$  equal to (14.30, 13.48, 17.55, 9.89, 17.19); however, PID obtained settling times for  $(\Delta f_1, \Delta f_2, \Delta f_3, \Delta P_{tie12}, \Delta P_{tie23})$  equal to (28, 20, 27, 35, 35). Finally, the work was expanded to a hybrid three-area multi source power system with comprising RESs such as PV and WT, BESS, and EVs, to evaluate the suggested method's suitability for handling contemporary power systems. The results showed that the RESs, EVs, and BESS contributed to greater system stability. In conclusion, the optimization model in this work provided a successful approach to solving the LFC issues.

In the future, potential extensions could include a powerful hybrid algorithm to optimize the integral controller gains. Furthermore, the proposed controller techniques will be tested in a large multi-area hybrid power system with consideration of the communication time delay issue in the design stage. Additionally, the performance of the integral controller can be further enhanced through combination with the intelligent or adaptive controllers.

**Author Contributions:** Conceptualization, A.B.W., A.A., A.A.A. and S.A.; methodology, A.B.W., A.A.A. and S.A.; software, A.B.W., M.V. and T.P.; validation, A.B.W., A.A. and A.A.A.; formal analysis, M.R. and T.P.; investigation, A.B.W., S.A. and M.V.; resources, A.A.A. and T.P.; data curation, M.V. and T.P.; writing—original draft preparation, A.B.W., A.A. and A.A.A.; writing—review and editing, S.A. and M.R.; visualization, M.V. and T.P.; supervision, S.A. and M.R.; project administration, M.R.; funding acquisition, M.R. and A.A.A. All authors have read and agreed to the published version of the manuscript.

**Funding:** This work was supported by Deanship of Scientific Research (DSR) at King Abdulaziz University, under grant no. RG-10-135-43.

**Institutional Review Board Statement:** Not applicable.

**Informed Consent Statement:** Not applicable.

**Data Availability Statement:** The data generated or analyzed to support findings of this study are included within the article.

**Acknowledgments:** The authors thank the Deanship of Scientific Research (DSR) at King Abdulaziz University, Jeddah, Saudi Arabia, for funding this project, under grant no. RG-10-135-43. The authors also acknowledge the support provided by King Abdullah City for Atomic and Renewable Energy (K.A. CARE) under the K.A. CARE-King Abdulaziz University Collaboration Program.

**Conflicts of Interest:** The authors declare that there are no conflicts of interest regarding the publication of this paper.

## Nomenclature

The following nomenclature are used in this manuscript:

LFC	Load frequency control
I	Integral
PSO	Particle swarm optimization
GA	Genetic algorithm
SA	Simulated annealing
PS	Pattern search
NP	Nonlinear programming

ILA	Incomprehensible but intelligible-in-time logics algorithm
COA	Coati optimization algorithm
BOA	Brown-bear optimization algorithm
GDB	Governor dead band
GRC	Generation rate constraint
RESs	Renewable energy sources
PV	Photovoltaic
WT	Wind turbine
BESS	Battery energy storage system
EV	Electric vehicle
$i$	Subscript referring to area ( $i = 1, 2, 3$ )
$ACE_i$	Area control error of area $i$
$\Delta f_i$	The change in frequency of area $i$ (Hz)
$\Delta P_{tie, ij}$	The change in tie-line real power of tie area $i$ –area $j$ (p.u)
$\Delta P_{Vi}$	The changes in steam valve position in area $i$ (p.u)
$\Delta P_{Ti}$	The change in turbine output powers in area $i$ (p.u)
$\Delta P_{ei}$	The change in the electrical power in area $i$ (p.u)
$\Delta P_{Di}$	The change in the load in area $i$ (p.u)
$\Delta P_{Gi}$	The governor output command in area $i$ (p.u)
$\Delta P_{refi}$	The change in the reference power setting in area $i$ (p.u)
$u_i$	The output of the integral controller of area $i$
$T_{ij}$	The synchronizing coefficient (p.u)
$T_{gi}$	Governor time constant of area $i$ (s)
$T_{ti}$	Turbine time constant of area $i$ (s)
$H_i$	The inertia constant of area $i$ (s)
$D_i$	Percent change in load divided by percent change in frequency in area $i$ (p.u/Hz)
$K_{psi}$	The generator and load gain of area $i$
$T_{psi}$	The generator and load time constant of area $i$ (s)
$B_i$	Frequency bias factor of area $i$ (p.u/Hz)
$\beta_i$	Area frequency response characteristic of area $i$ (p.u/Hz)
$R_i$	The speed regulation of the governor of area $i$ (Hz/p.u)
$K_{Ii}$	Gain of integral controller in area $i$ .
$J$	The proposed objective function
ISE	Integral of squared error
ITAE	Integral of time multiplied absolute error
$T_s$	Settling time of the response (s)
$S_{min}$	The minimum value of the response (Hz)—(p.u)
$S_{max}$	The maximum value of the response (Hz)—(p.u)
$M_P$	The peak amplitude of the response (Hz)—(p.u)
$t$	Simulation time (s)

## Appendix A

### Two Area Thermal System [1].

**Table A1.** Parameters of the two-area thermal system.

Area	1	2
Speed regulation	$R_1 = 0.05$	$R_2 = 0.0625$
Frequency dependency of load	$D_1 = 0.6$	$D_2 = 0.9$
Inertia constant	$H = 5$	$H = 4$
Base power	1000 MVA	1000 MVA
Governor time constant	$T_{g1} = 0.2$ s	$T_{g2} = 0.3$ s
Turbine Time constant	$T_{T1} = 0.5$ s	$T_{T2} = 0.6$ s
Integral controller gain	$K_{I1} = 0.3$	$K_{I2} = 0.3$
Frequency bias factor	$B_1 = 20.6$	$B_2 = 16.9$
Synchronizing power coefficient	$T_{12} = 2.0$ p.u.	
Nominal system frequency	$f = 60$ Hz	

### Appendix B

Two Area Thermal System with GRC and GDB Nonlinearity.

The nonlinear GRC and GDB limitations taken into consideration in this work are as below:

- GRC =  $\pm 0.03$  per minutes.
- GDB =  $\pm 0.0336$  Hz.

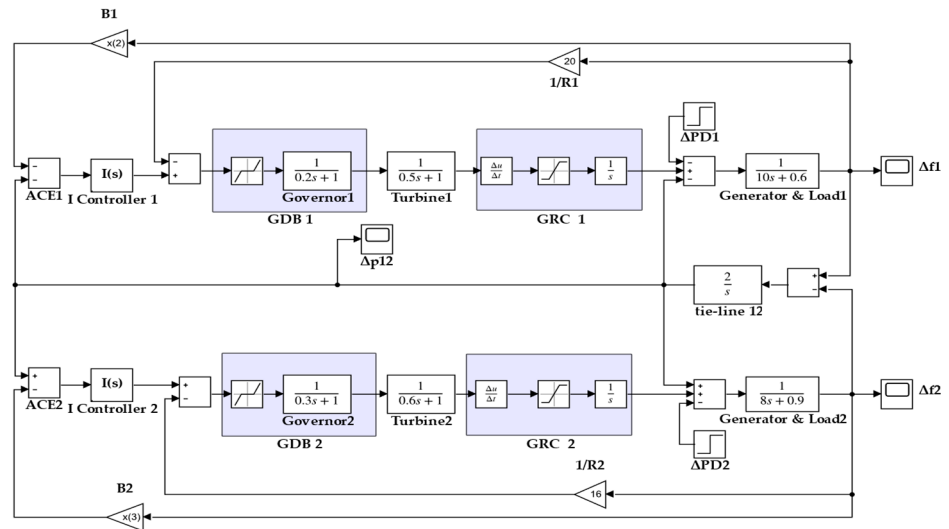


Figure A1. Block diagram of LFC model for two-area power system with GRC and GDB.

### Appendix C

Three Area Thermal System [57].

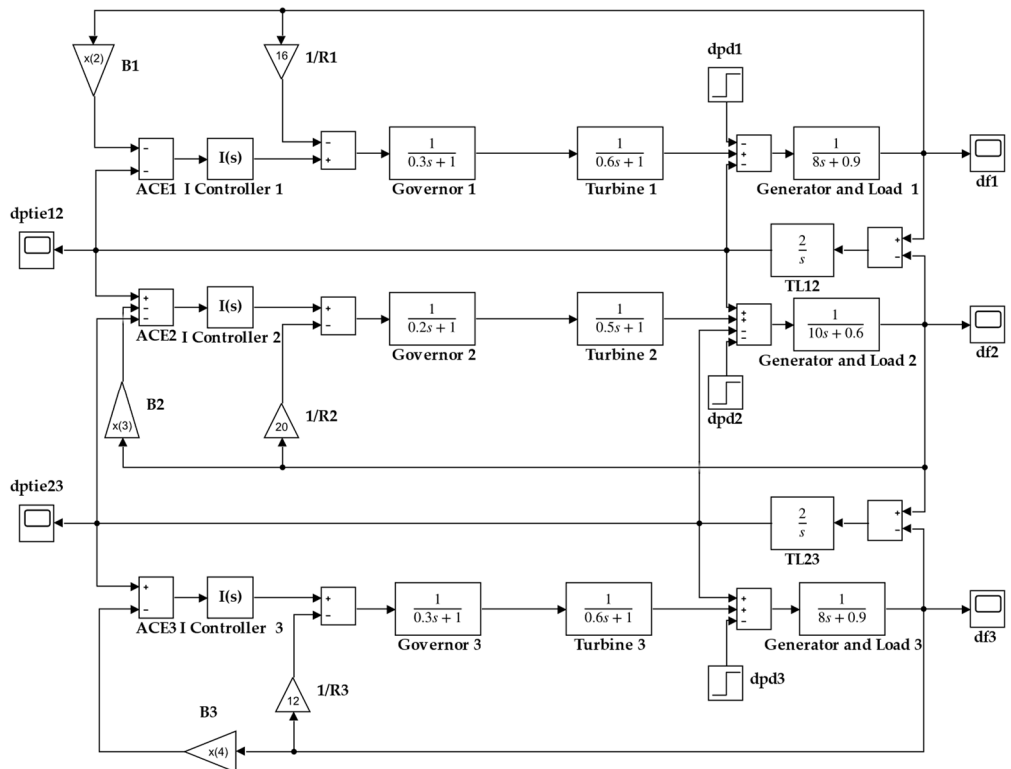


Figure A2. Block diagram of LFC model for three-area power system.

**Table A2.** Parameters of the three-area power system.

Area	1	2	3
Speed regulation	$R_1 = 1/16$	$R_2 = 1/20$	$R_3 = 1/12$
Frequency dependency of load	$D_1 = 0.9$	$D_2 = 0.6$	$D_3 = 0.9$
Inertia constant	$H = 4$	$H = 5$	$H = 4$
Governor time constant	$T_{g1} = 0.3$ s	$T_{g2} = 0.2$ s	$T_{g3} = 0.3$ s
Turbine Time constant	$T_{T1} = 0.6$ s	$T_{T2} = 0.5$ s	$T_{T3} = 0.6$ s
Frequency bias factor	$B_1 = 16.9$	$B_2 = 20.6$	$B_3 = 12.9$
Synchronizing power coefficient	$T_{12}$ and $T_{23} = 2.0$ per unit		

**Appendix D**

Hybrid three-area multi sources power system.

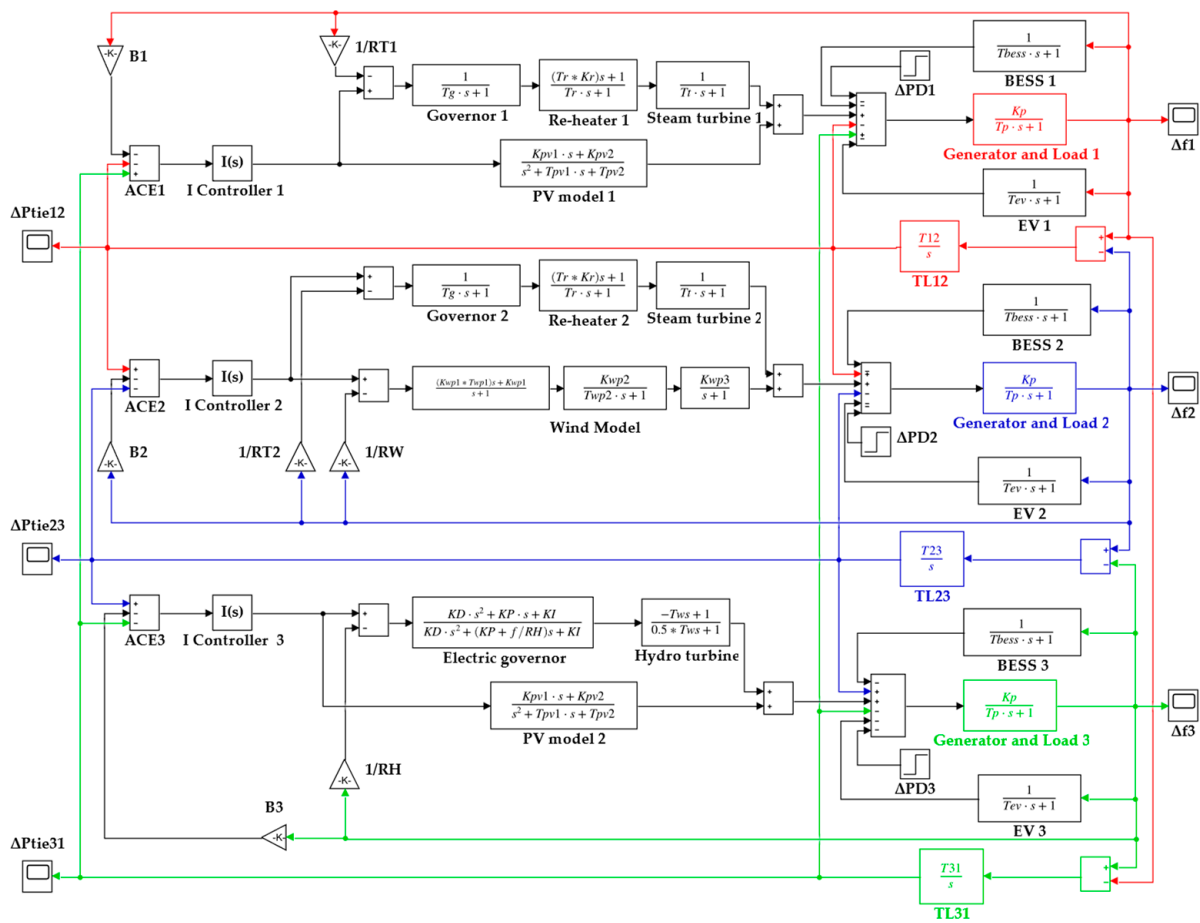


**Figure A3.** Block diagram of LFC model for the hybrid three-area multi sources power system.

**Table A3.** Parameters of the hybrid three-area multi sources power system.

Plant	Parameter	Nomenclature	Value
Thermal	Speed regulation	$R_{T1}$ and $R_{T2}$	2.4
	Governor time constant	$T_g$	0.08 s
	Steam turbine time constant	$T_t$	0.3 s
	Steam turbine reheat time constant	$T_r$	10 s
	Steam turbine reheat coefficient	$K_r$	0.5
Hydro	Speed regulation	$R_H$	2.4
	Water starting time	$T_w$	1 s
PV	Electric governor derivative, proportional, and integral gains	$KD, KP$ and $KI$	4, 1 and 5, respectively
	PV system's gains	$K_{pv1}$ and $K_{pv2}$	−18 and 900
WT	PV system's time constants	$T_{pv1}$ and $T_{pv2}$	100 and 50 s
	WT plant's gains	$K_{wp1}, K_{wp2}$ and $K_{wp3}$	1.25, 1 and 1.4, respectively
BESS	WT plant's time constants	$T_{wp1}$ and $T_{wp2}$	6 and 0.041 s
	BESS time constant	$T_{bess}$	0.1 s
EV	EV time constant	$T_{ev}$	1 s
	Frequency bias factor	$B_1, B_2$ and $B_3$	0.425
	Synchronizing power coefficient	$T_{12}, T_{23}$ and $T_{31}$	0.545 p.u.
	Frequency dependency of load	$D$	0.00833
	Inertia constant	$H$	5 s
	The generator and load gain	$K_p = \frac{1}{D}$	120
	The generator and load time constant	$T_p = \frac{2H}{fD}$	20 s
	Nominal system frequency	$f$	60 Hz

## References

- Saadat, H. *Power System Analysis*, 3rd ed.; PSA Publishing LLC: New York, NY, USA, 2010; pp. 566–593.
- Ahmed, M.O.; Magzoub, M.A.; Salem, A. Load Frequency Control in Two Area Power System using GA, SA and PSO Algorithms: A Comparative Study. In Proceedings of the 2021 31st Australasian Universities Power Engineering Conference (AUPEC), Perth, Australia, 26–30 September 2021. [\[CrossRef\]](#)
- Zhu, Q.; Bolzoni, A.; Forsyth, A.; Todd, R.; Smith, M.; Gladwin, D.T.; John, T.; Patsios, C.; Jones, G.; Rogers, D.J. Delay compensation amongst aggregated storage assets providing fast frequency regulation. In Proceedings of the 2020 IEEE 9th International Power Electronics and Motion Control Conference (IPEMC2020-ECCE Asia), Nanjing, China, 29 November–2 December 2020. [\[CrossRef\]](#)
- Prasad, S.; Purwar, S.; Kishor, N.  $H$ -infinity based non-linear sliding mode controller for frequency regulation in interconnected power systems with constant and time-varying delays. *IET Gener. Transm. Distrib.* **2016**, *10*, 2771–2784. [\[CrossRef\]](#)
- Lai, H.B.; Tran, A.-T.; Huynh, V.; Amaefule, E.N.; Tran, P.T.; Phan, V.-D. Optimal linear quadratic Gaussian control based frequency regulation with communication delays in power system. *Int. J. Electr. Comput. Eng. (IJECE)* **2022**, *12*, 157. [\[CrossRef\]](#)
- Pradhan, S.K.; Das, D.K.  $H_\infty$  load frequency control design based on delay discretization approach for interconnected power systems with time delay. *J. Mod. Power Syst. Clean Energy* **2021**, *9*, 1468–1477. [\[CrossRef\]](#)
- Ranjan, M.; Shankar, R. A literature survey on load frequency control considering renewable energy integration in power system: Recent trends and future prospects. *J. Energy Storage* **2022**, *45*, 103717. [\[CrossRef\]](#)
- Shouran, M.; Anayi, F.; Packianather, M. A State-of-the-Art Review on LFC Strategies in Conventional and Modern Power Systems. In Proceedings of the 2021 International Conference on Advance Computing and Innovative Technologies in Engineering (ICACITE), Greater Noida, India, 4–5 March 2021. [\[CrossRef\]](#)
- Mansour, S.; Badr, A.O.; Attia, M.A.; Sameh, M.A.; Kotb, H.; Elgamli, E.; Shouran, M. Fuzzy Logic Controller Equilibrium Base to Enhance AGC System Performance with Renewable Energy Disturbances. *Energies* **2022**, *15*, 6709. [\[CrossRef\]](#)
- Chen, G.; Li, Z.; Zhang, Z.; Li, S. An Improved ACO Algorithm Optimized Fuzzy PID Controller for Load Frequency Control in Multi Area Interconnected Power Systems. *IEEE Access* **2020**, *8*, 6429–6447. [\[CrossRef\]](#)
- Magzoub, M.A.; Alquthami, T. Optimal Design of Automatic Generation Control Based on Simulated Annealing in Interconnected Two-Area Power System Using Hybrid PID—Fuzzy Control. *Energies* **2022**, *15*, 1540. [\[CrossRef\]](#)
- Rout, U.K.; Sahu, R.K.; Panda, S. Design and analysis of differential evolution algorithm based automatic generation control for interconnected power system. *Ain Shams Eng. J.* **2013**, *4*, 409–421. [\[CrossRef\]](#)
- Rathor, S.; Acharya, D.S.; Gude, S.; Mishra, P. Application of artificial bee colony optimization for load frequency control. In Proceedings of the World Congress on Information and Communication Technologies, Mumbai, India, 11–14 December 2011. [\[CrossRef\]](#)
- Ali, E.S.; Abd-Elazim, S.M. Bacteria foraging optimization algorithm based load frequency controller for interconnected power system. *Int. J. Electr. Power Energy Syst.* **2011**, *33*, 633–638. [\[CrossRef\]](#)

15. Padhan, S.; Kumar, S.; Panda, S. Application of Firefly Algorithm for Load Frequency Control of Multi-area Interconnected Power System. *Electr. Power Compon. Syst.* **2014**, *42*, 1419–1430. [CrossRef]
16. Nahas, N.; Abouheaf, M.; Sharaf, A.; Gueaieb, W. A Self-Adjusting Adaptive AVR-LFC Scheme for Synchronous Generators. *IEEE Trans. Power Syst.* **2019**, *34*, 5073–5075. [CrossRef]
17. El-Sehiemy, R.; Shaheen, A.; Ginidi, A.; Al-Gahtani, S.F. Proportional-Integral-Derivative Controller Based-Artificial Rabbits Algorithm for Load Frequency Control in Multi-Area Power Systems. *Fractal Fract.* **2023**, *7*, 97. [CrossRef]
18. Sahu, R.K.; Panda, S.; Padhan, S. A novel hybrid gravitational search and pattern search algorithm for load frequency control of nonlinear power system. *Appl. Soft Comput.* **2015**, *29*, 310–327. [CrossRef]
19. Panwar, A.; Sharma, G.; Bansal, R.C. Optimal AGC Design for a Hybrid Power System Using Hybrid Bacteria Foraging Optimization Algorithm. *Electr. Power Compon. Syst.* **2019**, *47*, 955–965. [CrossRef]
20. Gupta, D.K.; Soni, A.K.; Jha, A.V.; Mishra, S.K.; Appasani, B.; Srinivasulu, A.; Bizon, N.; Thounthong, P. Hybrid Gravitational-Firefly Algorithm-Based Load Frequency Control for Hydrothermal Two-Area System. *Mathematics* **2021**, *9*, 712. [CrossRef]
21. Shouran, M.; Anayi, F. TLBO Tuned a Novel Robust Fuzzy Control Structure for LFC of a Hybrid Power System with Photovoltaic Source. *Eng. Proc.* **2022**, *19*, 1. [CrossRef]
22. Shouran, M.; Alseid, A. Particle Swarm Optimization Algorithm-Tuned Fuzzy Cascade Fractional Order PI-Fractional Order PD for Frequency Regulation of Dual-Area Power System. *Processes* **2022**, *10*, 477. [CrossRef]
23. Bhuyan, M.; Das, D.C.; Barik, A.K. Proficient Power Control Strategy for Combined Solar Gas Turbine-wind Turbine Generator-biodiesel Generator Based Two Area Interconnected Microgrid Employed with Dc Link Using Harris's Hawk Optimization Optimised Tilt-integral-derivative Controller. *Int. J. Numer. Model. Electron. Netw. Devices Fields* **2022**, *35*, e2991. [CrossRef]
24. Alharbi, M.; Ragab, M.; AboRas, K.M.; Kotb, H.; Dashtdar, M.; Shouran, M.; Elgamli, E. Innovative AVR-LFC Design for a Multi-Area Power System Using Hybrid Fractional-Order PI and PIDD<sup>2</sup> Controllers Based on Dandelion Optimizer. *Mathematics* **2023**, *11*, 1387. [CrossRef]
25. Mokhtar, M.; Marei, M.I.; Sameh, M.A.; Attia, M.A. An Adaptive Load Frequency Control for Power Systems with Renewable Energy Sources. *Energies* **2022**, *15*, 573. [CrossRef]
26. Razmi, P.; Rahimi, T.; Sabahi, K.; Gheisarnejad, M.; Khooban, M. Adaptive fuzzy gain scheduling PID controller for Frequency Regulation in modern power system. *IET Renew. Power Gener.* **2022**, 1–16. [CrossRef]
27. Kullapadayachi Govindaraju, S.; Sivalingam, R.; Panda, S.; Sahu, P.R.; Padmanaban, S. Frequency control of power system with distributed sources by adaptive type 2 fuzzy PID Controller. *Electr. Power Compon. Syst.* **2023**, *52*, 487–508. [CrossRef]
28. Gulzar, M.M.; Sibtain, D.; Ahmad, A.; Javed, I.; Murawwat, S.; Rasool, I.; Hayat, A. An Efficient Design of Adaptive Model Predictive Controller for Load Frequency Control in Hybrid Power System. *Int. Trans. Electr. Energy Syst.* **2022**, *2022*, 7894264. [CrossRef]
29. Ali, H.H.; Kassem, A.M.; Al-Dhaifallah, M.; Fathy, A. Multi-Verse Optimizer for Model Predictive Load Frequency Control of Hybrid Multi-Interconnected Plants Comprising Renewable Energy. *IEEE Access* **2020**, *8*, 114623–114642. [CrossRef]
30. Ersdal, A.M.; Imsland, L.; Uhlen, K. Model Predictive Load-Frequency Control. *IEEE Trans. Power Syst.* **2016**, *31*, 777–785. [CrossRef]
31. Oshnoei, S.; Oshnoei, A.; Mosallanejad, A.; Haghjoo, F. Novel Load Frequency Control Scheme for an Interconnected Two-Area Power System Including Wind Turbine Generation and Redox Flow Battery. *Int. J. Electr. Power Energy Syst.* **2021**, *130*, 107033. [CrossRef]
32. Zaid, S.A.; Bakeer, A.; Magdy, G.; Albalawi, H.; Kassem, A.M.; El-Shimy, M.E.; AbdelMeguid, H.; Manqarah, B. A New Intelligent Fractional-Order Load Frequency Control for Interconnected Modern Power Systems with Virtual Inertia Control. *Fractal Fract.* **2023**, *7*, 62. [CrossRef]
33. Gheisarnejad, M. An effective hybrid harmony search and cuckoo optimization algorithm based fuzzy PID controller for load frequency control. *Appl. Soft Comput.* **2018**, *65*, 121–138. [CrossRef]
34. Ranjitha, K.; Sivakumar, P.; Monica, M.; Elavarasu, R. Swarm Intelligence based Load Frequency Control of Two Area Thermal System—Comparative Analysis. In Proceedings of the 4th International Conference on Electronics, Communication and Aerospace Technology (ICECA), Coimbatore, India, 5–7 November 2020. [CrossRef]
35. Fun. Available online: <https://www.mathworks.com/help/optim/ug/fmincon.html> (accessed on 21 February 2024).
36. Wächter, A.; Biegler, L.T. On the implementation of an interior-point filter line-search algorithm for large-scale nonlinear programming. *Math. Program.* **2005**, *106*, 25–57. [CrossRef]
37. Azaroual, M.; Ouassaid, M.; Maaroufi, M. Optimum Energy Flow Management of a Grid-Tied Photovoltaic-Wind-Battery System Considering Cost, Reliability, and CO<sub>2</sub> Emission. *Int. J. Photoenergy* **2021**, *2021*, 1–20. [CrossRef]
38. Kouba, N.E.Y.; Mena, M.; Hasni, M.; Boudour, M. Optimal load frequency control based on artificial bee colony optimization applied to single, two and multi-area interconnected power systems. In Proceedings of the 2015 3rd International Conference on Control, Engineering & Information Technology (CEIT), Tlemcen, Algeria, 25–27 May 2015. [CrossRef]
39. Aibangbee, J.O. Automatic Load Frequency Control of Two Area Power System Using Proportional Integral Derivative Tuning Through Internal Model Control. *IORS J. Electr. Electron. Eng.* **2016**, *11*, 13–17. [CrossRef]
40. Mahboob Ul Hassan, S.; Ramli, M.A.; Milyani, A.H. Robust Load Frequency Control of Hybrid Solar Power Systems Using Optimization Techniques. *Front. Energy Res.* **2022**, *10*, 902776. [CrossRef]

41. Alghamdi, S.; Wazir, A.B.; Awaji, H.H.; Alhussainy, A.A.; Sindi, H.F.; Rawa, M. Tuning PID Controller Parameters of Automatic Voltage Regulator (AVR) Using Particle Swarm Optimization: A Comparative Study. In Proceedings of the 2023 IEEE PES Conference on Innovative Smart Grid Technologies-Middle East (ISGT Middle East), Abu Dhabi, United Arab Emirates, 12–15 March 2023. [CrossRef]
42. Qu, P.; Du, F. Improved Particle Swarm Optimization for Laser Cutting Path Planning. *IEEE Access* **2023**, *11*, 4574–4588. [CrossRef]
43. Bertsimas, D.; Tsitsiklis, J. Simulated annealing. *Statist. Sci.* **1993**, *8*, 10–15. [CrossRef]
44. Dolan, E.D.; Lewis, R.M.; Torczon, V. On the Local Convergence of Pattern Search. *SIAM J. Optim.* **2003**, *14*, 567–583. [CrossRef]
45. Yin, S.; Cagan, J. An Extended Pattern Search Algorithm for Three-Dimensional Component Layout. *ASME J. Mech. Des.* **2000**, *122*, 102–108. [CrossRef]
46. Mirrashid, M.; Naderpour, H. Incomprehensible but Intelligible-in-Time Logics: Theory and Optimization Algorithm. *Knowl.-Based Syst.* **2023**, *264*, 110305. [CrossRef]
47. Dehghani, M.; Montazeri, Z.; Trojovská, E.; Trojovský, P. Coati Optimization Algorithm: A New Bio-Inspired Metaheuristic Algorithm for Solving Optimization Problems. *Knowl.-Based Syst.* **2023**, *259*, 110011. [CrossRef]
48. Prakash, T.; Singh, P.P.; Singh, V.P.; Singh, S.N. A Novel Brown-Bear Optimization Algorithm for Solving Economic Dispatch Problem. In *Advanced Control and Optimization Paradigms for Energy System Operation and Management*; River Publishers: Gistrup, Denmark, 2022.
49. Mirrashid, M.; Naderpour, H. Ibi Logics Optimization Algorithm (2023): MATLAB Codes. Available online: [https://www.mathworks.com/matlabcentral/fileexchange/124390-ibi-logics-optimization-algorithm-2023-matlab-codes?s\\_tid=FX\\_rc2\\_behav](https://www.mathworks.com/matlabcentral/fileexchange/124390-ibi-logics-optimization-algorithm-2023-matlab-codes?s_tid=FX_rc2_behav) (accessed on 24 January 2024).
50. Dehghani, M.; Montazeri, Z.; Trojovský, P. COA: Coati Optimization Algorithm. Available online: [https://www.mathworks.com/matlabcentral/fileexchange/116965-coa-coati-optimization-algorithm?s\\_tid=srchtitle](https://www.mathworks.com/matlabcentral/fileexchange/116965-coa-coati-optimization-algorithm?s_tid=srchtitle) (accessed on 24 January 2024).
51. Prakash, T. Release v.1.0.0. TPRAKASH05/Brown-Bear-Optimization-Algorithm. Available online: <https://github.com/TPRakash05/Brown-bear-optimization-algorithm/releases/tag/v1.1.0> (accessed on 24 January 2024).
52. Wazir, A.B.; Alhussainy, A.A.; Alghamdi, S.; Rawa, M.; Sindi, H.F. Robust load frequency control of two-area interconnected power system using fuzzy-I controller. In Proceedings of the 2023 IEEE IAS Global Conference on Emerging Technologies (GlobConET), London, UK, 19–21 May 2023. [CrossRef]
53. Wazir, A.B.; Alhussainy, A.A.; Alobaidi, A.H.; Altaf, A.; Kumar, A.; Kumar, M.; Alghamdi, S. Robust frequency regulation for dual-area interconnected grids using hybrid controller: A comparative study. In Proceedings of the 2023 IEEE 3rd International Conference on Smart Technologies for Power, Energy and Control (STPEC), Bhubaneswar, India, 10–13 December 2023. [CrossRef]
54. Shouran, M.; Anayi, F.; Packianather, M.; Habil, M. Different Fuzzy Control Configurations Tuned by the Bees Algorithm for LFC of Two-Area Power System. *Energies* **2022**, *15*, 657. [CrossRef]
55. Shouran, M.; Anayi, F.; Packianather, M.; Habil, M. Load Frequency Control Based on the Bees Algorithm for the Great Britain Power System. *Designs* **2021**, *5*, 50. [CrossRef]
56. Jaber, H.H.; Miry, A.H.; Al-Anbarri, K. Automatic Generation Control of a Multi-Area Power System Based on Grey Wolf Optimization Algorithm. *J. Eng. Sustain. Dev.* **2021**, *25*, 138–151. [CrossRef]
57. Alzaareer, K.; Al-Shetwi, A.Q.; El-bayeh, C.Z.; Taha, M.B. Automatic Generation Control of Multi-Area Interconnected Power Systems Using Ann Controller. *Rev. d'Intell. Artif.* **2020**, *34*, 1–10. [CrossRef]
58. Kamel, O.M.; Abdelaziz, A.Y.; Zaki Diab, A.A. Damping Oscillation Techniques for Wind Farm DFIG Integrated into Inter-Connected Power System. *Electr. Power Compon. Syst.* **2020**, *48*, 1551–1570. [CrossRef]
59. Kamel, O.M.; Diab, A.A.Z.; Mahmoud, M.M.; Al-Sumaiti, A.S.; Sultan, H.M. Performance Enhancement of an Islanded Microgrid with the Support of Electrical Vehicle and STATCOM Systems. *Energies* **2023**, *16*, 1577. [CrossRef]
60. Prakash, S.; Sinha, S.K. Load Frequency Control of Multi-Area Power Systems Using Neuro-Fuzzy Hybrid Intelligent Controllers. *IETE J. Res.* **2015**, *61*, 526–532. [CrossRef]

**Disclaimer/Publisher's Note:** The statements, opinions and data contained in all publications are solely those of the individual author(s) and contributor(s) and not of MDPI and/or the editor(s). MDPI and/or the editor(s) disclaim responsibility for any injury to people or property resulting from any ideas, methods, instructions or products referred to in the content.